공학박사 학위논문

A NANOFIBER-STRUCTURED BIOPOLYMER FOR ADVANCED DRUG DELIVERY SYSTEMS

차세대 약물 전달 시스템을 위한 나노섬유 구조의 생체 고분자 연구

2014 년 8 월

서울대학교 대학원

협동과정 바이오엔지니어링 전공

박 천 권

A NANOFIBER-STRUCTURED BIOPOLYMER FOR ADVANCED DRUG DELIVERY SYSTEMS

차세대 약물 전달 시스템을 위한 나노섬유 구조의 생체 고분자 연구

지도 교수 최 영 빈

이 논문을 공학박사 학위논문으로 제출함

2014 년 8 월

서울대학교 대학원

협동과정 바이오엔지니어링 전공

박 천 권

박천권의 공학박사 학위논문을 인준함

2014 년 7 월

위 원 장 김 희 찬 (인)

부위원장 최 영 빈 (인)

위 원 박 기 호 (인)

위 원 이 정 찬 (인)

위 원 박 지 호 (인)

Ph. D. Dissertation

A NANOFIBER-STRUCTURED BIOPOLYMER FOR ADVANCED DRUG DELIVERY SYSTEMS

BY

CHUN GWON PARK

AUGUST 2014

INTERDISCIPLINARY PROGRAM IN BIOENGINEERING

THE GRADUATE SCHOOL

SEOUL NATIONAL UNIVERSITY

A NANOFIBER-STRUCTURED BIOPOLYMER FOR ADVANCED DRUG DELIVERY SYSTEMS

BY

CHUN GWON PARK

INTERDISCIPLINARY PROGRAM IN BIOENGINEERING

THE GRADUATE SCHOOL

SEOUL NATIONAL UNIVERSITY

THIS DISSERTATION IS APPROVED FOR THE DEGREE OF DOCTOR OF PHILOSOPHY

JULY 2014

DOCTORAL COMMITTEE:

Chairman	*Hee Chan Kim, Ph. D.*
Vice Chairman	*Young Bin Choy, Ph. D.*
Member	*Ki Ho Park, MD, Ph. D.*
Member	*Jung Chan Lee, Ph. D.*
Member	*Ji Ho Park, Ph.D.*

Abstract

A NANOFIBER-STRUCTURED BIOPOLYMER FOR ADVANCED DRUG DELIVERY SYSTEMS

By

Chun Gwon Park

Interdisciplinary Program in Bioengineering

The Graduate School

Seoul National University

This dissertation is focused on the design, fabrication and evaluation of novel drug-delivery devices based on nanofiber-structured biopolymers. Two advantageous features of nanofiber-structured biopolymers (i.e., high specific surface area and micro-porosity) are utilized to obtain effective delivery of drugs at the desired sites, hence enhanced disease treatments.

Firstly, we fabricated nanostructured microparticles (NMs) to utilize the feature of their large specific surface area. The NMs contained a mucoadhesive polymer as drug carrier to achieve

prolonged retention of microparticles in the preocular surface and, thus, to obtain higher bioavailability of ocular drugs. To prepare the NMs, nanofibrous sheets were first prepared with poly (lactic-co-glycolic acid) (PLGA) and polyethylene glycol (PEG) as a diffusion-wall material and a mucoadhesion promoter, respectively. The sheet was then freeze-milled to obtain the NMs. The NMs containing brimonidine as a model drug were formulated in a rapidly dissolving dry tablet of poly vinyl alcohol (PVA). For the *in vivo* evaluation, the tablet of drug-loaded NMs was administered into the lower cul-de-sac of the rabbit eye, where the intraocular pressure (IOP) was measured at the scheduled times. The NMs appeared to be composed of randomly oriented nanofibers to give a rough surface, resulting in a 13-fold increase in specific surface area, as compared with conventional spherical microparticles. Thus, the NMs better adhered to the eye surface when incorporated with a mucoadhesive material, PEG, while releasing the drug to the eye surface in a sustained manner. Hence, the IOP-lowering effect of brimonidine improved more than two-fold, as compared with Alphagan-P, the medication already approved in clinical use.

Secondly, we developed a nanofibrous sheet-based system to utilize its feature of micro-porosity and eventually to achieve the linear release of the oral drug, nifedipine. The nanofibrous sheets of micro-porosity were first fabricated by the electrospinning method, using PLGA, a biocompatible polymer. The sheets were then used as a drug-diffusion barrier by capping and sealing a compressed table

that consisted of nifedipine and a solubility enhancer, polyvinylpyrrolidone. In this work, nanofibrous sheets of different thicknesses were prepared in order to vary the rate of drug diffusion. An *in vitro* drug-release study revealed that as the sheet thickness increased, drug release became more retarded, and a lag phase of drug release became more evident. We realized linear drug release by combining two distinctly capped tablets, each showing a different drug release, which exhibited an almost linear release of nifedipine during 24 h ($R^2 > 0.986$). Therefore, we concluded that combining two tablets, each capped with nanofibrous sheets of different thicknesses, is a promising method of linear delivery for oral drugs.

We also developed an esophageal stent coated with a nanostructured polymer of micro-porosity for sustained delivery of an anticancer drug, fluorouracil (5-FU). The stents were coated with drug-loaded PLGA nanofibers (DPN) using the electrospinning method, which exhibited a sustained drug-release pattern for up to 6 days. To extend drug release, we also added the nanofiber layers composed of PLGA alone (PN), surrounding the DPN layer, as a more resistive diffusion barrier. In this way, the period of drug release could be extended to 21 days with the DPN layer topped with another 192-μm thick PN layer. Therefore, we envisioned longer periods of drug-release with the thicker PN layers, obtained simply with a longer collection time of PLGA nanofibers using electrospinning. Overall, we concluded that the drug-delivery esophageal stent prepared in this study is beneficial in the long-term treatment of

dysphagia due to esophageal cancer.

Keywords : biopolymer, drug delivery system, electrospinning, micro-porosity, nanofibers, specific surface area

Student Number : 2009-23194

Contents

List of Tables

List of Figures

Chapter 1

Introduction

1.1 Biopolymers

Biopolymers are a class of polymers that function in contact with living tissues without any complications or adverse side effects, and thus can be used *in vivo* for medical and pharmaceutical purposes (Table 1.1 and Table 1.2) [1, 2]. Biopolymers can be either synthetic or natural polymers, and they can also be classified into degradable or non-degradable polymers (Table 1.1) [1]. In many cases, natural polymers are biodegradable and biocompatible, but they are often limited in batch-to-batch variation due to difficulties in purification. Synthetic polymers, on the other hand, are easily modifiable and can be prepared with a wide range of compositions. For this reason,

synthetic polymers are preferred to natural polymers in the biomedical field (e.g., for drug–delivery systems and tissue engineering). Biodegradable polymers naturally degrade in the body in response to biological conditions, and they yield degradation products that also need to be bio–inert in the body. The biodegradation time of materials can be controlled by varying the ingredients and terminal groups of the materials, depending on their usage. Biodegradation can result from enzymatic, chemical, or microbial reactions, and it is often affected by various factors (Table 1.3).

Table 1.1. Representative list of biopolymers[1].

Classification	Parameters
Natural polymers	
Protein-based polymers	Collagen, albumin, gelatin
Polysaccharides	Agarose, alginate, carrageenan, hyaluronic acid, dextran, chitosan cyclodextrins
Synthetic polymers	
Biodegradable	
Polyesters	Poly (lactic acid), poly (glycolic acid) Poly (hydroxyl butyrate), poly (ε-caprolactone), poly (β-malic acid) Poly (dioxanones)
Polyanhydrides	Poly(sebacic acid), poly (adipic acid)
Polyamides	Poly (imino carbonates), polyamino acids
Phosphorous-based polymers	Polyphosphates, polyphosphonates, polyphosphazenes
Others	Poly(cyanoacrylates), polyurethanes Poly (ortho esters), polydihydropyrans polyacetals
Non-biodegradable	
Cellulose derivatives	Carboxymethyl cellulose, ethyl cellulose, cellulose acetate, cellulose acetate propionate, hydroxypropyl methyl cellulose
Silicones	Polydimethylsiloxane, colloidal silica
Acrylic polymers	Polymethacrylates, poly (methyl methacrylate), poly hydro (ethyl-methacrylate)
Others	Polyvinyl pyrrolidone, ethyl vinyl Acetate, poloxamers, poloxamines

Table 1.2. Different biopolymers and their biomedical applications [2].

Biopolymers	Biomedical Applications
Poly (methyl methacrylate)	Intraocular lens, bone cement, dentures
Poly (dimethylsiloxane)	Breast prostheses
Polyethylene	Hip joint replacement
Polyurethane	Facial prostheses, blood/device interfaces

Table 1.3. Factors affecting biodegradation of polymers [1].

Chemical structure and composition
Physico-chemical factors (ion exchange, ionic strength, pH)
Physical factors (shape, size, chain defects)
Morphology (amorphous, semicrystalline, crystalline, microstructure, residual stress)
Mechanism of degradation (enzymatic, hydrolysis, microbial)
Molecular-weight distribution
Processing conditions and sterilization process
Annealing and storage history
Route of administration and site of action

1.2 Nanofiber-structured Biopolymers

Despite the advances in fiber fabrication techniques, including melt-blowing and multicomponent processes, increasing attention has been paid to electrospinning in recent years for the production of continuous nanofibers with dimensions down to the nanometer range, using various materials, due to its flexibility, versatility, and ease of fiber production [3, 4]. For this reason, there has been a dramatic increase in the number of publications associated with electrospinning in the past few years (Figure 1.1).

Four major elements are required for a typical electrospinning process: a high-voltage direct-current power supply, a metallic needle with a blunt tip, a syringe for ejecting the polymer solution, and a grounded conductive collector (Figure 1.2) [4]. A polymeric solution or melt is ejected through a thin metallic needle at a controlled rate by a syringe pump and a droplet forms due to the confinement of surface tension. When a high electric field of 100–500 kV/m is applied between the metallic needle and the grounded conductive collector (typically 10–25 cm in laboratory systems), electric charges are built on the surface of the droplet at the spinneret. A cone-shaped deformation of polymer solution, called a Taylor cone, then appears once the repulsion among the surface charges is strong enough to overcome the surface tension. When a higher electric field is applied, the jet is stretched by electrostatic repulsion, the solvent is evaporated rapidly, and solidified fibers are

deposited on the grounded conductive collector.

Generally, almost all polymers can be processed into nanofibers by electrospinning, regardless of their source (natural or synthetic) or degradability (degradable or non-degradable). However, in order to successfully prepare nanofibers of interest, experimental parameters must be carefully optimized (Table 1.4).

Table 1.4. Parameters affecting electrospinning procedure.

Classification	Parameters
Properties of the polymer	Mean molecular weight
	Molecular-weight distribution
	Solubility
	Melting point
	Glass-transition temperature
Properties of the polymer solution	Viscosity
	Concentration
	Solution conductivity
	Surface tension
Electrospinning process	Electric field
	Feed rate
	Tip-to-collector distance
	Collector composition and geometry
	Relative humidity
	Temperature

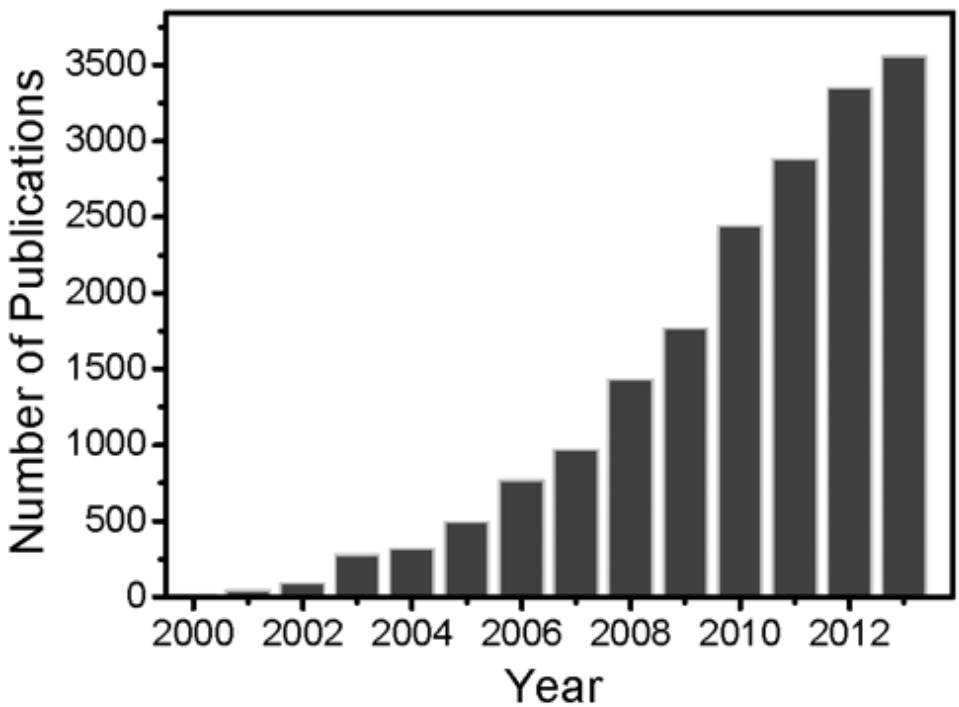

Figure 1.1. Schematic representation of the number of publications per year on electrospinning over the last 14 years following the SciFinder Scholar [4].

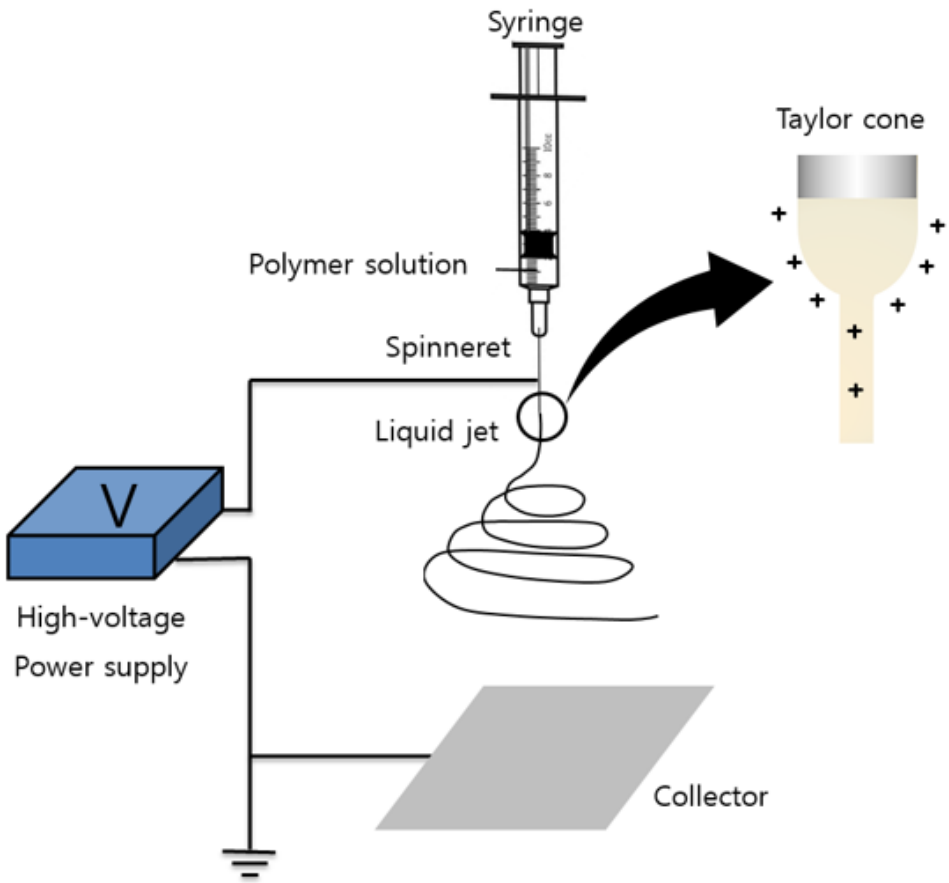

Figure 1.2. Schematic representation of the electrospinning process [5].

1.3 Features of Nanofiber-structured Biopolymers

Nanofiber-structured biopolymers prepared by electrospinning possess various advantages over other conventionally prepared biopolymers. Among them, two features are highlighted in this chapter: high specific surface area and micro-porosity.

As the name implies, nanofiber-structured biopolymers are composed of nanofibers with diameters ranging from a few nanometers to a few hundred nanometers; hence, theoretically, they possess a larger specific surface area than in other conventionally prepared fibers. The specific surface area of nanofibers can be manipulated by altering the fiber diameter. Larger specific surface areas could lead to enhanced interactions with surroundings and hence are often advantageous in biomedical fields, including wound-dressing applications for fluid absorption and dermal delivery, and tissue engineering for better interaction with cells.

Nanofiber-structured biopolymers often exhibit high porosity due to their nano-size diameter, allowing for high gas or liquid permeation. In addition, the pore size could be controlled by varying the thickness of the nanofibrous sheets or the diameter of the fibers. In this way, a flow of gas or liquid can also be controlled by altering the sheet thickness, thereby varying resistive diffusion barriers depending on their usage.

1.4 Research Aims

The major objective of this dissertation is to develop new drug-delivery systems using nanofiber-structured biopolymers. For this purpose, two features of nanofiber-structured biopolymers—high specific surface area and micro-porosity—are used in drug delivery systems to obtain sustained delivery of drugs of interest, thus, to enhance the treatment of diseases. Nanofibers with high specific surface area is used as drug-delivery carriers to topical drug delivery to the eye, while micro-porosity is used as diffusion-barriers to control drug-release for oral route and through esophageal stents.

In Chapter 2, we present rationales for material selection and the optimization process for nanofiber-structured biopolymers. Among a variety of biopolymers, a suitable biopolymer is selected by taking biocompatibility and biodegradability into consideration, and some of its applications are discussed. In addition, we have varied many parameters in the electrospinning process to optimize the nanofibers for use in drug-delivery systems.

In Chapter 3, we provide nanostructured microparticles (NMs) to better interact with preocular mucosal layers, hence prolonging the retention of microparticles. The nanofibrous sheets of high specific surface area can be freeze-milled to prepare the NMs while retaining their large specific surface area. Once a drug of interest is encapsulated in the microparticles, the extent and period of activity

of the drug can be enhanced compared with a market product of the same kind.

In Chapter 4, we present a novel method of linear delivery of the oral drug, nifedipine, using nanofibrous sheets of micro-porosity. Compressed drug tablets were covered and sealed by nanofibrous sheets, and various drug-release profiles were expected depending on the thickness of the nanofibrous sheets. With the proper combination of the two differently capped tablets, we obtained linear delivery of the drug, which, in some cases, is highly desirable.

In Chapter 5, we attempt to coat and provide drug-delivery functionality to medical devices. We chose an esophageal stent to be coated by the electrospinning method and an anti-cancer agent to be released from the stent for the prevention of re-occlusion. To better control drug release, we also coated the drug-free protective layers and varied the thickness of the layers by altering the electrospinning collection time.

Chapter 2

Preparation of Nanofiber-structured Biopolymers

2.1 Polymer Selection

As we mentioned in Chapter 1.1, synthetic biopolymers are preferable to natural biopolymers due to the ease of purification; thus, quality control and reproducibility are easier. Among the many different types of synthetic biopolymers, the polyester-based polymers such as poly (ε-caprolactone) (PCL), poly (lactic acid) (PLA), poly (glycolic acid) (PGA) and their copolymer, poly (lactic-co-glycolic acid) (PLGA) have attracted a great deal of interest in the biomedical area due to their excellent biocompatibility and

tunability [5].

In particular, PLGA is one of the most attractive and widely used polymers due to its desirable properties (Figure 2.1): (i) Excellent biocompatibility and tunable biodegradability; (ii) FDA and European Medicine Agency (EMA) approval in drug delivery systems; (iii) easily tunable mechanical properties; (iv) various formulations and fabrication methods for the encapsulation of drugs; (v) the possibility of sustained and targeted drug release; and (vi) easily modifiable surface properties for stealthness or an enhanced interaction with living tissues. Thus, it is generally accepted as the "gold standard" of biodegradable polymers [6].

The name PLGA normally refers to the ratios of the two monomers used. For instance, PLGA 50:50 is a copolymer of 50 % lactic acid and 50 % glycolic acid. PLGA undergoes hydrolysis in the body and produces endogenous materials such as lactic acid and glycolic acid; hence, it is extremely biocompatible. In addition, the biodegradation time of PLGA can be easily adjusted from a few weeks to several years, depending on the molecular weight and copolymer compositions. PLGA is commercially available with different molecular weights, copolymer ratios (lactic acid: glycolic acid) and purity grades.

PLGA can be present in almost any shape and size, depending on the fabrication method, and can encapsulate virtually any molecules of interest, regardless of their molecular weights or properties. In addition, PLGA is soluble in a variety of organic

solvents, including chlorinated solvents, tetrahydrofuran, acetone and ethyl acetate [7]. Due to this versatility, PLGA has been a common choice for the development of medical devices, including grafts, absorbable sutures, drug delivery systems, and implantable and prosthetic devices [6-9]. One example of a commercially available drug-delivery device using PLGA is Lupron Depot, which is now used for the treatment of advanced prostate cancer.

In this study, PLGA is chosen as a biopolymer to be processed to possess a nanofiber structure, which is then applied in drug delivery systems. We use PLGA as a drug-delivery carrier for ocular drug delivery, and a drug-capping material for oral delivery, where the retention of the nanofiber-structured PLGA is within one week in preocular surface and gastrointestinal tract. In addition, PLGA is used for drug-delivery coating materials for an esophageal stent, where the drug release is terminated within one month. For all cases used in this study, the nanofiber-structured PLGA was seen to maintain its two features (i.e., high specific surface area and micro-porosity), since we use the PLGA of the known degradation period of more than two months (PLGA; 50:50; i.v. 0.36 dl/g, lot number = LX00111-68, Lakeshore Biomaterials, AL, USA). Furthermore, even if the nanofiber-structured PLGA is left in the body, such as preocular surface or gastrointestinal tract, due to unexpected circumstances, PLGA eventually degrades in the body, assuring the complete elimination after use [10]. In addition, PLGA is highly biocompatible and soluble in a wide range of organic solvents, which

facilitates its easy-to-vary electrospinning condition, hence enabling the fabrication of various nanofiber-structured PLGA.

However, the applications for nanostructured biopolymers are not just possible with PLGA. Once other biomaterials such as PCL, PLA, PGA, polyethylene and polyurethane possess the same profiles of specific surface area or micro-porosity, they could also be used for the same purposes herein, such as enhanced preocular retention, linear delivery of oral drugs and sustained delivery of anti-cancer agent from esophageal stent. When a drug of interest is encapsulated in the nanofiber-structured biopolymer of different kinds, the drug-loading amount and release profiles of the drug may need to be re-optimized. However, with the increase in specific surface area due to nanofiber structures, the preocular retention of microparticles can be improved by addition of mucoadhesive polymer. When used for oral drug delivery or drug-delivery coating, drug release can also be controlled by changing the degree of porosity of the nanostructure of the polymers. Hence, theoretically, it can be envisioned that any types of biomaterials be used for the purposes described in this dissertation.

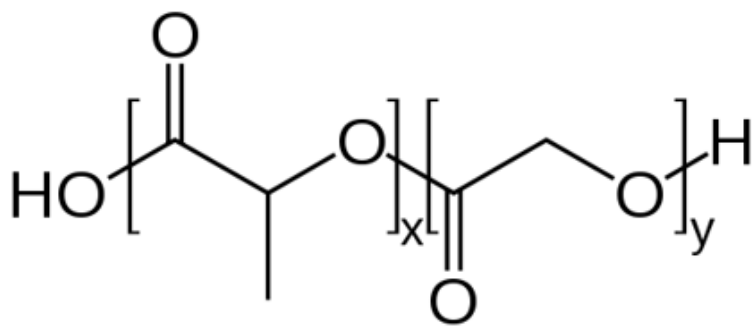

Figure 2.1. Structure of poly(lactic-co-glycolic acid) (x is the number of lactic acid units and y is the number of glycolic acid units) [7].

2.2 Optimization Process for Nanofiber-structured Biopolymers

As shown in Table 1.4, many parameters affect the electrospinning procedure, and they can be classified into three main factors: Polymer, polymer solution and electrospinning condition. In this dissertation, PLGA is used as an example biopolymer and is electrospun to give a nanofiber structure. In this chapter, we changed the properties of the polymer solution and conditions for electrospinning to obtain nanofiber-structured PLGA and to change the specific surface area and micro-porosity of nanofibers, as shown in Table 2.1.

2.2.1 Variations in Polymer Solution Concentration

Fixed Conditions: Applied voltage, 30 kV; tip-to-collector distance, 10 cm; polymer-solution flow rate, 0.6 ml/h; polymer molecular weight, 39 kDa; rotation speed, 100 rpm.
Variable Conditions: Solvent = Dichloromethane (DCM) only or solvent mixture (DCM: Tetrahydrofuran (THF): Dimethylformamide (DMF) = 3:1:1, v/v/v), polymer concentration = 5-30 %.

- The PLGA concentration should be more than 30 % w/v to make the nanofiber structure, regardless of solvents used (i.e., DCM

only or solvent mixture) (Figure 2.2).

- When only DCM was used as solvent, not nanofibers but particle formation was shown with 5% and 10% PLGA solutions, as shown in Figure 2.2 (a, b).
- Nanofiber structure started to appear with a 20 % PLGA solution, but bead formations also appeared on nanofibers (Figure 2.2c).
- Clear nanofiber structures were obtained with a 30 % PLGA solution.
- However, the use of only DCM as solvent did not produce nanofibers with homogenous diameters, possibly due to high vapor pressure of DCM.
- When the solvent mixture was used as solvent, particle formation or nanofibers with beads were obtained with 5–20% PLGA solutions.
- An increase in polymer concentration leads to a decrease in bead formation, and clear and homogeneous nanofibers were obtained with a 30% PLGA solution.

Table 2.1. Variable parameters for electrospinning.

Parameters	Range
PLGA molecular weight	25-58 kDa
PLGA solution concentration	5-30 % (w/v)
Polymer solution flow rate	0.2-4.0 ml/h
Applied voltage	10-25 kV
Tip-to-collector distance	5-15 cm
Collector drum rotation speed	100-3000 rpm

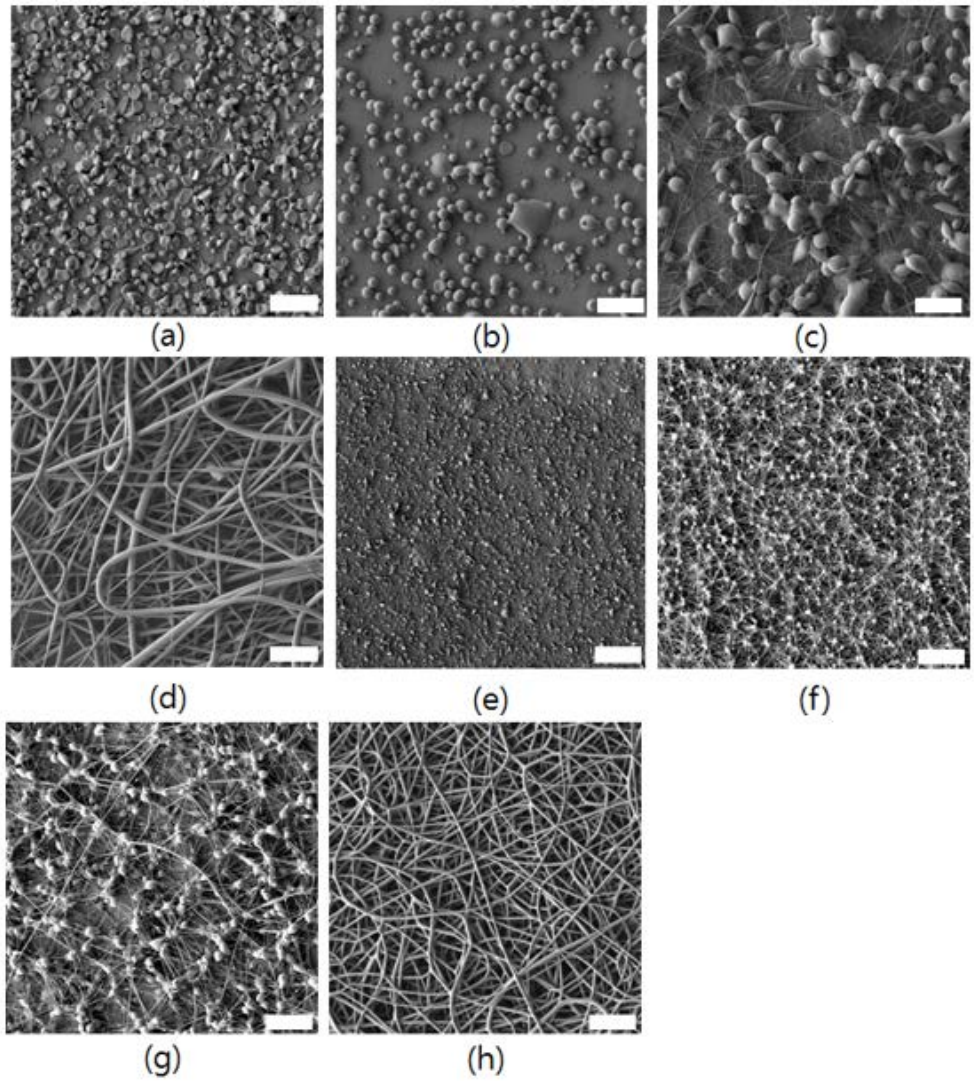

Figure 2.2. SEM images for change in PLGA solution concentration (solvent used, polymer concentration): (a) DCM, 5%; (b) DCM, 10%; (c) DCM, 20%; (d) DCM, 30%; (e) solvent mixture, 5%; (f) solvent mixture, 10%; (g) solvent mixture, 20%; (h) solvent mixture, 30%. Scale bars = 20 μm.

2.2.2 Variations in Polymer Molecular Weight

Fixed Conditions: Applied voltage, 15 kV; tip–to–collector distance, 10 cm; polymer solution flow rate, 0.6 ml/h; polymer solution concentration, 30%; rotation speed, 100 rpm.

Variable Conditions: Solvent = Dichloromethane (DCM) only, or solvent mixture (DCM: THF: DMF = 3:1:1, v/v/v), polymer molecular weight= 25–58 kDa.

- Varying the molecular weight of PLGA showed that at least 25 kDa of PLGA should be used to produce the homogenous nanofibers, as shown in Figure 2.3.
- When PLGA with molecular weight of 25 kDa was used for electrospinning, nanofibers with bead strings appeared, as obtained with the low–concentration polymer in Chapter 2.2.1, regardless of the solvents used.
- An increase in the molecular weight of PLGA resulted in nanofibers with thicker diameters, which could be ascribed to the increased viscosity of the polymer solution.
- We obtained more homogenous nanofibers with the solvent mixture than with only the DCM when we used the same molecular weight of PLGA.

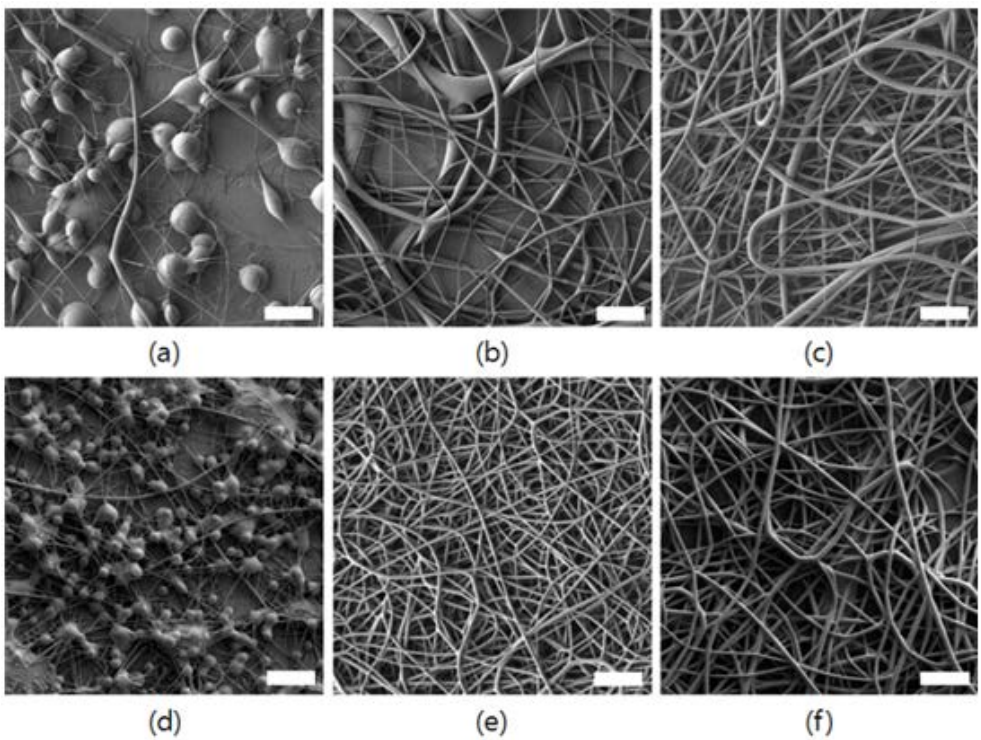

Figure 2.3. SEM images for change in polymer molecular weight (PLGA) (solvent used, polymer molecular weight): (a) DCM, 25 kDa; (b) DCM, 33 kDa; (c) DCM, 56 kDa; (d) solvent mixture, 25 kDa; (e) solvent mixture, 39 kDa; (f) solvent mixture, 58 kDa. Scale bars = 20 μm.

2.2.3 Variations in Tip–to–collector Distance

Fixed Conditions: Solvent, solvent mixture (DCM: THF: DMF = 3:1:1, v/v/v); applied voltage, 15 kV; polymer–solution flow rate, 0.6 ml/h; polymer solution concentration, 30%; rotation speed, 100 rpm; polymer molecular–weight, 39 kDa.

Variable Conditions: Tip–to–collector distance = 5–15 cm.

- When the tip–to–collector distance was 5 cm or less, the solvent did not evaporate and the PLGA solution was deposited on the collector before it formed the nanofiber structure (Figure 2.4(a)).
- When the tip–to–collector distance was 10 cm, the organic solvent completely evaporated and homogeneous nanofibers were deposited on the collector (Figure 2.4(b)).
- When the distance was maintained for 15 cm or more, we could obtain clear nanofibers with homogeneous diameters. However, due to the long distance, the quantity of nanofibers deposited on the collector decreased (Figure 2.4(c)).

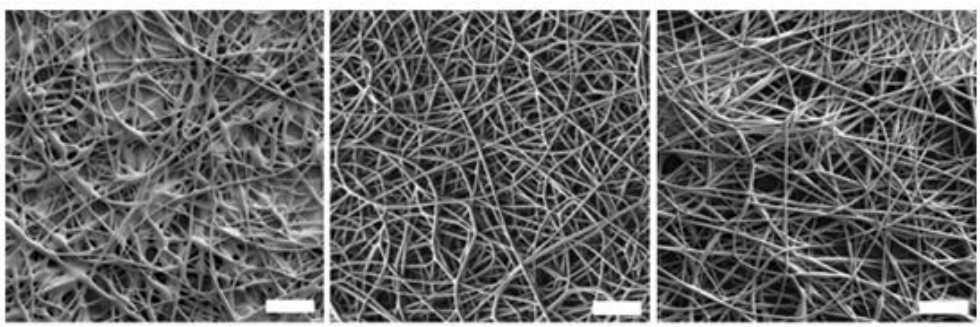

Figure 2.4. SEM images for the change in tip-to-collector distance: (a) 5 cm, (b) 10 cm and (c) 15 cm. Scale bars = 20 μm.

2.2.4 Variations in Applied Voltage

Fixed Conditions: Polymer solution concentration, 30 %; polymer solution flow rate, 0.6 ml/h; tip–to–collector distance, 10 cm; polymer molecular weight, 39 kDa; rotation speed, 100rpm.

Variable Condition: Solvent = Dichloromethane (DCM) only or solvent mixture (DCM: THF: DMF = 3:1:1, v/v/v); applied voltage = 10–25 kV.

- Basically, the higher the applied voltage, the more homogenous the nanofibers that were formed (Figure 2.5).
- When only DCM was used as solvent, non–uniform nanofibers and bead formation on the nanofibers were formed with an applied voltage of 15 kV (Figure 2.5(a)), and more uniform nanofibers without bead formation were observed with an applied voltage of 20 kV (Figure 2.5(b)).
- However, when 25 kV was applied, the solvent evaporated almost instantly; thus, the polymer often blocked the needle (Figure 2.5(c)).
- When the solvent mixture was used as a solvent, bead formation on the nanofibers was sporadically observed with an applied voltage of 10 kV (Figure 2.5 (d)) and clearly uniform nanofibers were formed with an applied voltage of 15 kV (Figure 2.5 (e)).
- As shown in Figure 2.5(f), when 20 kV was applied in electrospinning, nanofibers were observed with thinner

diameters than those with an applied voltage of 15 kV.

- When 20 kV was applied, the end of the needle was often blocked with polymers due to the fast evaporation of the organic solvent, as was observed with DCM only.

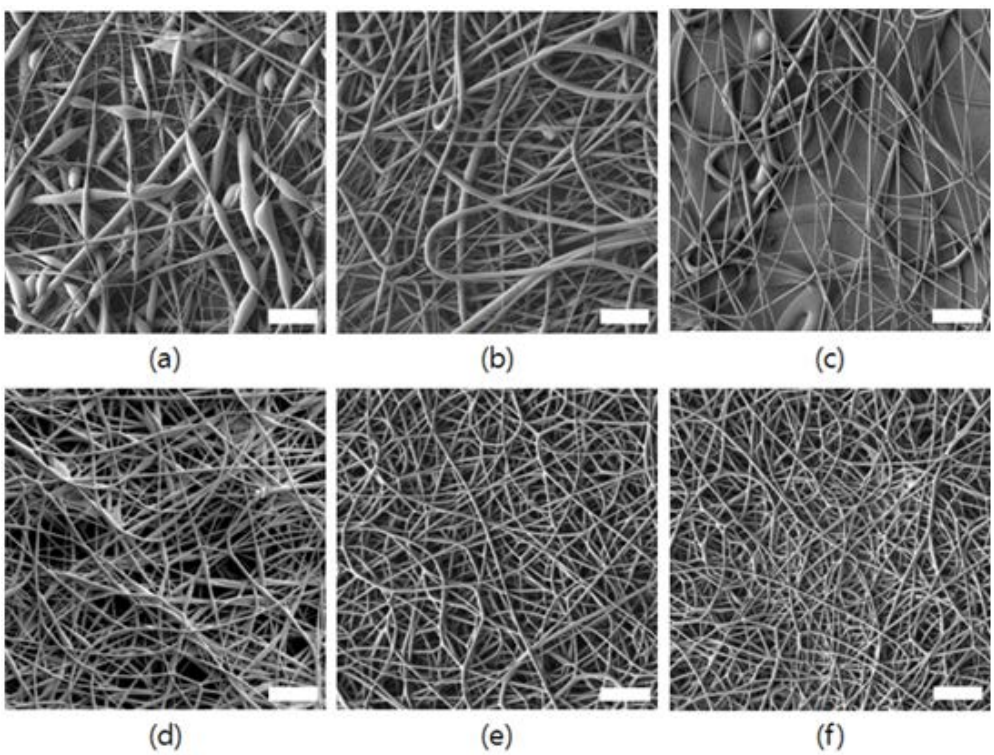

Figure 2.5. SEM images for the change in applied voltage (Solvent used, applied voltage): (a) DCM, 15 kV; (b) DCM, 20 kV; (c) DCM, 25 kV; (d) solvent mixture, 10 kV; (e) solvent mixture, 15 kV; (f) solvent mixture, 20 kV. Scale bars = 20 μm.

2.2.5 Variations in Polymer Solution Flow Rate

Fixed Conditions: Applied voltage, 15 kV; tip–to–collector distance, 10 cm; polymer solution concentration, 30 %; polymer molecular weight, 39 kDa; rotation speed, 100 rpm.

Variable Conditions: Solvent = Dichloromethane (DCM) only or solvent mixture (DCM: THF: DMF = 3:1:1, v/v/v); flow rate = 0.2–4.0 ml/h.

- When the PLGA solution was fed at 0.2 ml/h, the supply of polymer solution to the needle tip was unstable and the production of nanofibers was irregular (Figure 2.6(a), 2.6(e)).
- As shown in Figure 2.6 (b, f), the best nanofibers were obtained with a flow rate of 0.6 ml/h.
- When the PLGA solution was fed at more than 0.6 ml/h, bead formation was observed with the nanofibers, hence the non–uniform nanofibers (Figure 2.6 (c, d, g, h)).

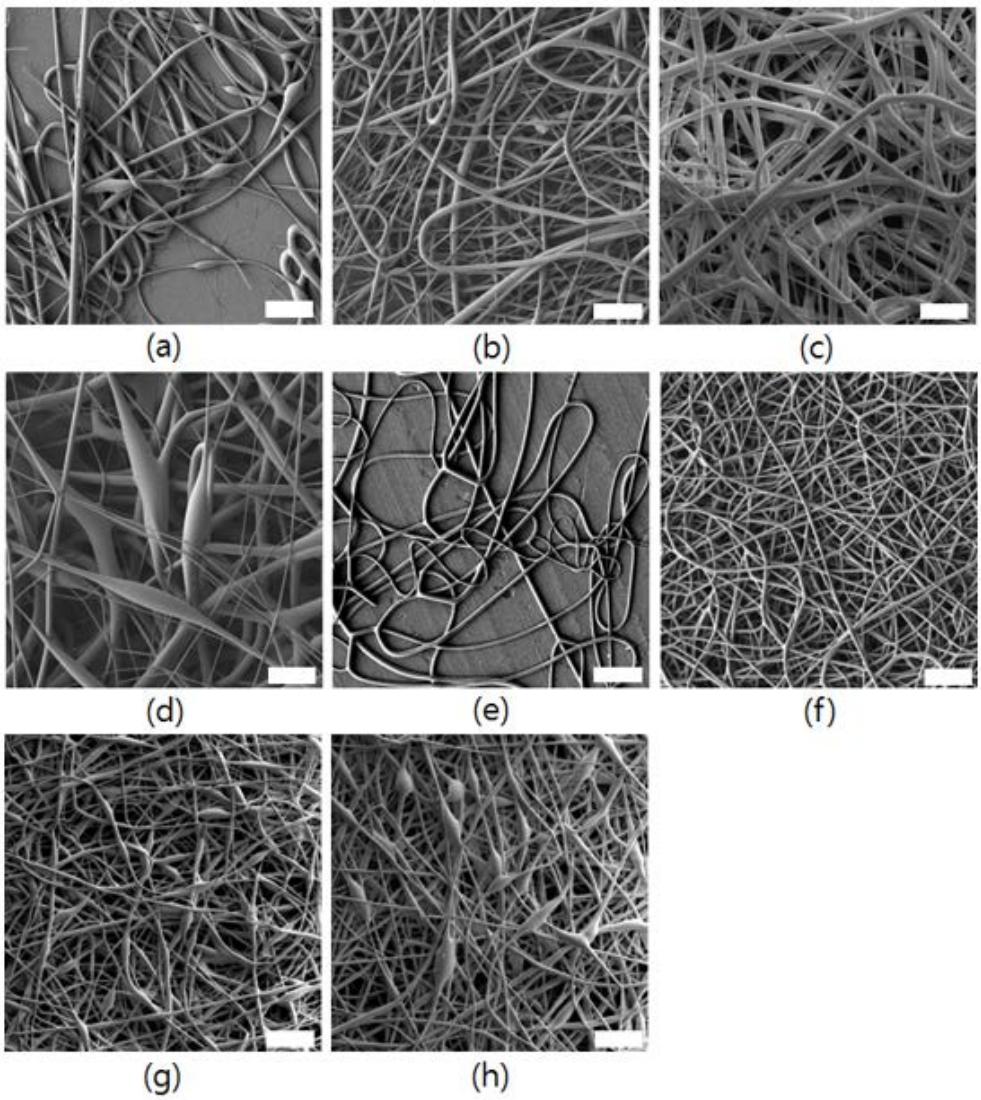

Figure 2.6. SEM images for the change in flow rate (Solvent used, flow rate): (a) DCM, 0.2 ml/h; (b) DCM, 0.6 ml/h; (c) DCM, 1.5 ml/h; (d) DCM, 4 ml/h; (e) solvent mixture, 0.2 ml/h; (f) solvent mixture, 0.6 ml/h; (g) solvent mixture, 1.2ml/h; and (h) solvent mixture, 2.4 ml/h. Scale bars = 20 μm.

2.2.6 Variations in Rotation Speed

Fixed Conditions: Applied voltage, 15 kV; tip–to–collector distance, 10 cm; polymer–solution flow rate, 0.6 ml/h; polymer–solution concentration, 30 %; polymer molecular weight, 39 kDa.

Variable Conditions: Solvent = Dichloromethane (DCM) only or solvent mixture (DCM: THF: DMF = 3:1:1, v/v/v); rotation speed = 100–3000 rpm.

- Figure 2.7 shows the change of the nanofiber–structure with a change in rotation speed from 100 rpm to 3000 rpm.
- Regardless of the solvent type, the most entangled and random structures were observed at 100 rpm (Figure 2.7 (a, e)).
- As the rotation speed increased, more aligned nanofibers were obtained (Figure 2.7 (b, c, d, f, g, h)).
- The most aligned and homogeneous nanofibers were fabricated with a rotation speed of 2000 rpm (Figure 2.7 (c, g)).

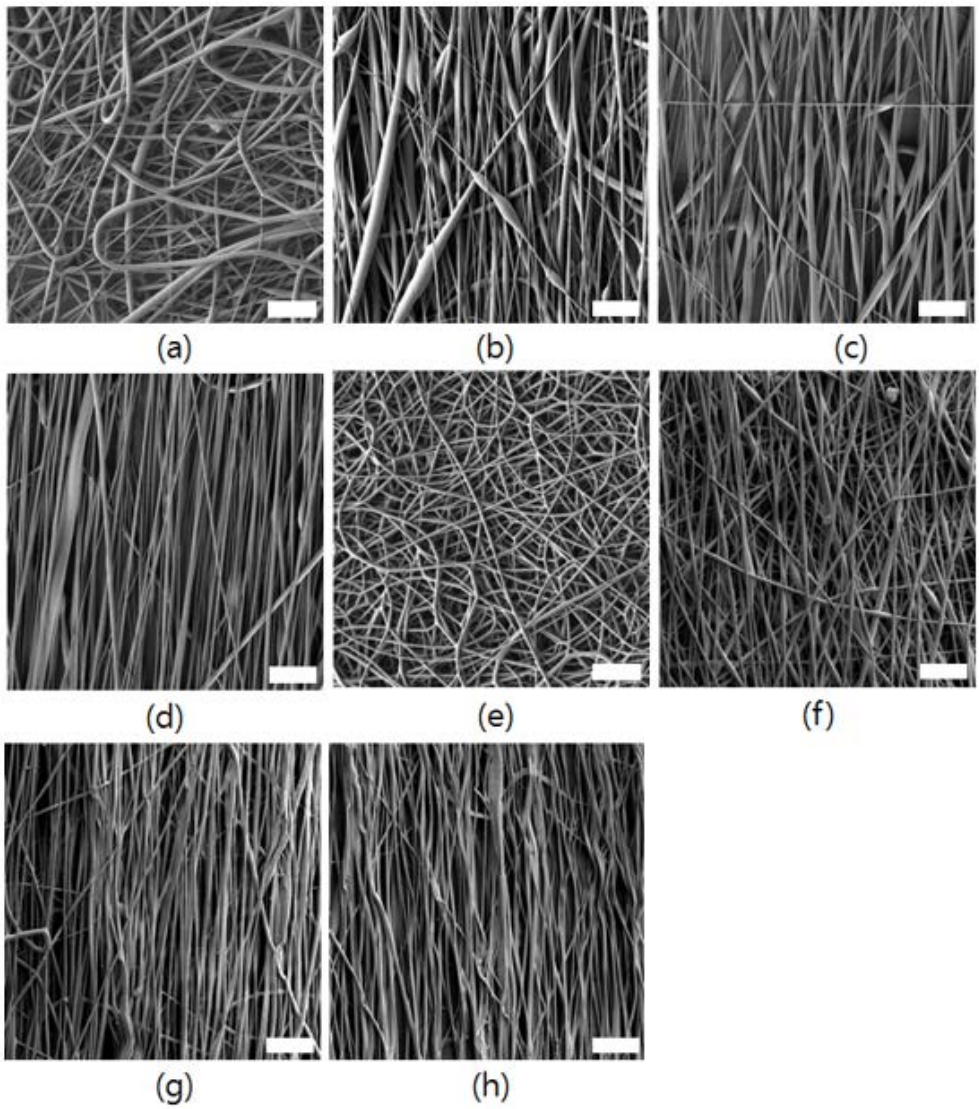

Figure 2.7. SEM images for the change in rotation speed (solvent used, rotation speed): (a) DCM, 100 rpm; (b) DCM, 1000 rpm; (c) DCM, 2000 rpm; (d) DCM, 3000 rpm; (e) solvent mixture, 100 rpm; (f) solvent mixture, 1000 rpm; (g) solvent mixture, 2000 rpm; and (h) solvent mixture, 3000 rpm. Scale bars = 20 μm.

2.2.7 Optimized Condition for Nanofiber-structured Biopolymers

We have varied the polymer-solution concentration, polymer molecular weight, tip-to-collector distance, applied voltage, polymer solution flow rate, and rotation speed in electrospinning to vary nanofiber structures and, eventually, to find the best nanofiber structures to be used in drug-delivery applications.

Due to the high vapor pressure of DCM, we have had many restrictions on the production of nanofiber-structured biopolymers using only DCM as solvent. For example, bead formation on nanofibers and the non-uniform diameters of nanofibers were often observed and the needle tip was frequently blocked due to the fast evaporation of DCM.

On the other hand, when the solvent mixture (DCM: DMF: THF = 3:1:1, v/v/v) was used as solvent, clearly uniform nanofibers with homogenous diameters were fabricated [11]. Overall, the optimized conditions for electrospinning to fabricate the best nanofiber-structured biopolymers are shown in Table 2.2, and the resultant nanofiber-structured biopolymers were shown in Figure 2.8.

Table 2.2. Optimized parameters for electrospinning used in this study.

Parameters	Value
PLGA molecular weight	39 kDa
Polymer solution concentration	30 %
Polymer solution flow rate	0.6-3.0 ml/h
Applied voltage	15-20 kV
Tip-to-collector distance	10 cm
Collector drum rotation speed	100 rpm
Solvent used	Solvent mixture (DCM: DMF: THF = 3:1:1, v/v/v)

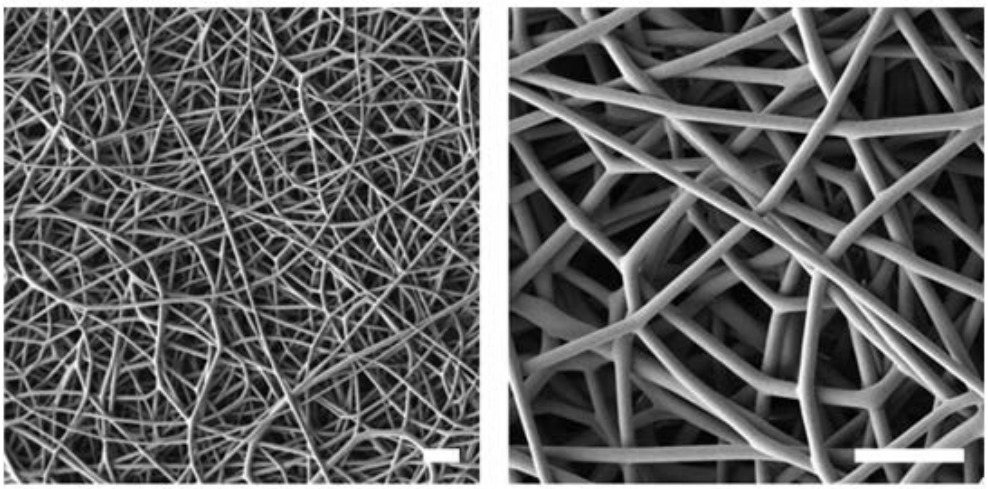

Figure 2.8. Representative SEM images of the nanofiber-structured PLGA used in this study. Scale bars = 10 μm.

Chapter 3

Nanostructured Mucoadhesive Microparticles for Enhanced Ocular Bioavailability of Brimonidine

3.1 Introduction

Topical drug administration to the eye has been widely accepted to treat eye disorders due to ease of administration and high patients' acceptance [12]. However, extensive drug loss from the preocular surface, mostly caused by tear clearance and blinking, has been problematic, thereby very low drug bioavailability [13]. Therefore, numerous approaches, employing the viscosifying formulations with

polymers[14, 15] or gels[16, 17] or a macroscopic device as drug depot[18, 19], have been suggested to increase the drug residence time at the preocular surface[20, 21]; however, the patients' acceptance of those systems was not satisfactory due to discomfort on the sensitive eye surface[13]. Microparticles of biocompatible materials could be easily prepared small enough to minimize eye irritation[22] and as carrier, they could deliver drug in a sustained manner with slower preocular clearance than drug solutes in eye drops[13, 23-25]. Microparticles were also made of mucoadhesive polymers to allow adherence to the mucus layer on the eye surface [26, 27]. However, the best retention would be obtained when the microparticles were made of an adhesive material as a whole, which would limit the use of wall material for diffusion, thereby difficulty in microparticle variation needed for controlled drug release.

To resolve this, for the first time to our knowledge, we demonstrate the nanostructured microparticles containing mucoadhesive polymer and evaluate their *in vivo* preocular retention property. In this work, we suggest the following strategy for microparticle design: 1) microparticles are made mainly of wall material as potential drug carrier, 2) a mucoadhesion promoter is employed as additive material and 3) mucoadhesiveness of microparticles is improved by a physical means, i.e., an enlarged specific surface area of microparticles originated from the nanostructure. In this way, microparticles could better interact with the mucus layer on the eye without a major change in wall material

composition. To synergistically improve this effect, we formulated the microparticles in a dry-tablet dosage form, i.e., a tablet of water-soluble polymer embedded with the nanostructured microparticles. Thus, the tablet medium dissolved in tear to release only the microparticles on the preocular surface, while increasing the tear viscosity and thus, allowing more time for microparticle interaction with the mucus layer on the eye. In this way, the microparticles could deliver drug to the surface of the eye in a sustained manner, hence higher drug bioavailability.

In this work, the microparticles were made mainly of poly (lactic-co-glycolic acid) (PLGA) [28], where polyethylene glycol (PEG) was added to give a mucoadhesion property [29, 30].

PEG is a highly biocompatible polymer without any known immunogenicity, antigenicity, or toxicity, and it is also approved by the FDA for injectable, topical, rectal, and nasal pharmaceutical formulations. Hence, it is widely accepted as safe for various biomedical applications [31, 32]. Mucoadhesion between PEG and preocular mucosal layers is generally known to be created by mainly hydrogen bonds [33]. For this reason, PEG has been widely used for applications of ocular drug delivery [30, 34].

To obtain the microparticles of nanostructured morphology (NM), we freeze-milled a nanofibrous sheet, composed of PLGA and PEG, that was prepared by the electrospinning method (Figure 3.1(a)). In this way, the nanofibrous structure could be well retained in the resulting microparticles, hence an enlarged surface area, as

compared with the spherical particles. Unlike the conventional fabrication method of spherical microparticles, such as emulsification[35, 36] or spray drying[37], the process introduced herein was not necessarily involved with an exposure of aqueous phase or high temperature needed for solvent evaporation, which we anticipate that be advantageous for retaining the stability of entrapped drug[38-40]. Moreover, the electrospinning method for nanostructure formation can be adapted for numerous different biomaterials [41], thereby ease of wall-material variation beneficial for controlled drug delivery. In this work, the NM were embedded in a dry tablet medium of polyvinyl alcohol (PVA), a biocompatible, viscosifying agent, already widely used in an ophthalmic formulation (Figure 3.1(b)) [42]. Considering the patients' compliance, the tablet was prepared to be small and suitable for topical administration to the eye and also highly porous to facilitate the water absorption, thereby rapid dissolution of the tablet medium.

In this study, Brimonidine tartrate (BRT), which has been used for the management of open-angle glaucoma [43], was chosen as a model drug and loaded in NM. BRT is a potent and relatively selective alpha-2 adrenergic receptor that reduces intraocular pressure (IOP) by decreasing the synthesis of Aqueous Humor (AH) and by increasing uveoscleral outflow [43]. BRT has also been known to have a neuroprotective effect that can prevent further injuries of the damaged neurons in animal models of ocular hypertension and glaucoma and restore damaged retinal ganglion cells [43]. Due to this

dual functionality, BRT is among the most promising therapeutic agents for the treatment of glaucoma, and it is therefore being studied extensively [44].

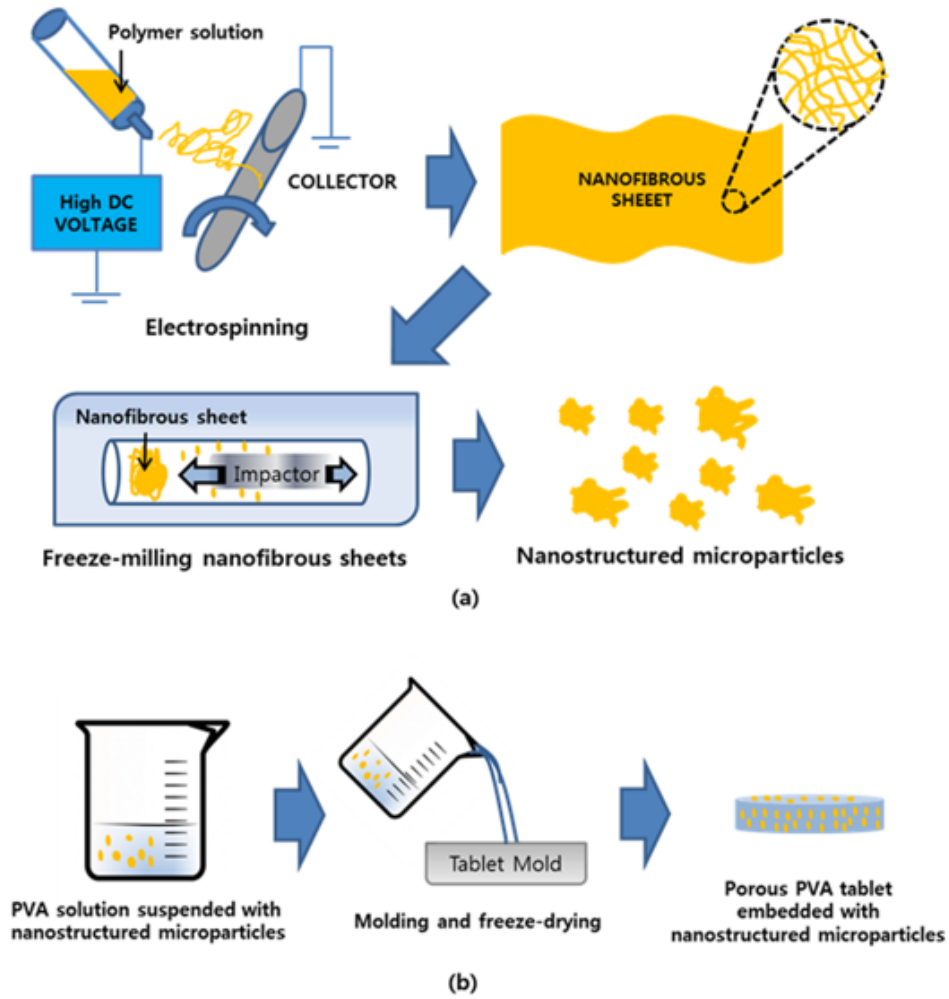

Figure 3.1. Schematic procedure for preparation of (a) nanostructured microparticles (NM) and (b) their tablet formulation.

3.2 Materials and Methods

3.2.1 Materials

Poly (lactic-co-glycolic acid) (PLGA; 50:50; i.v. = 0.43 dl/g), polyethylene glycol (PEG; average MW = 6kDa) and Brimonidine tartrate (BRT, assay > 99.8%) were purchased from Lakeshore Biomaterials (AL, USA), Acros Organics (NJ, USA) and Nanjing Yuance Industry & Trade Co., Ltd. (China), respectively. Polyvinyl alcohol (PVA; average MW = 31 - 50 kDa, 87%-89% hydrolyzed) and Nile Red were obtained from Sigma (MO, USA). Dichloromethane (DCM) and acetone were supplied from JT Baker (NJ, USA). Dimethylformamide (DMF), trahydrofurane (THF) and phosphate-buffered saline (PBS; pH 7.4) were obtained from Mallinckrodt (MO, USA), Daejung (Korea) and Seoul National University Hospital Biomedical Research Institute (Seoul, Korea), respectively. Proparacaine hydrochloride (Alcaine; 0.5% ophthalmic solution) was purchased from Alcon-Couvreur (Puurs, Belgium). Ketamine hydrochloride (Ketamine), xylazine (Rompun) and acepromazine maleate (Sedaject) were obtained from Yuhan (Seoul, Korea), Bayer (Leverkusen, Germany) and Samu Median (Yesan, Korea), respectively. Alphagan P was a kind gift from Samil Allergan (Korea).

3.2.2 Preparation of Microparticles

To prepare the spherical microparticles (MS), the classic emulsion method was employed in this work. To produce microparticles containing Nile Red, either 500 mg PLGA or a blend of 500 mg PLGA and 100 mg PEG was dissolved in 5 ml DCM, where 5 mg Nile Red was also dissolved as a marker. The resulting solution was then dispersed in an aqueous solution of PVA (20 ml; 1% w/v) and sonicated at 100 W for 5 s (Model 5 Digital Sonic Dismembrator, Fisher Scientific, PA, USA). The emulsion was then added in 80 ml of an aqueous solution of 1% w/v PVA and stirred at 100 rpm under vacuum (−12.5 psi) for 30 min to evaporate the solvent[30]. The suspension was filtered (nylon net filter, 11−μm pore, Millipore, Billerica, MA) to obtain the MS smaller than 10 μm, which were washed thoroughly with DI water and freeze−dried. To fabricate microparticles containing BRT, a blend of 500 mg PLGA and 625 mg PEG were first dissolved in 5 ml DCM, where 50 mg BRT were added to such solution. The polymer solution was dispersed in 50 ml phosphate buffer (20 mM, pH=12) containing 1% PVA, which was sonicated at 100W for 30 s. The resulting emulsion was added to 50 ml phosphate buffer of the same kind and stirred at 150 rpm under vacuum (−12.5 psi) for 40 min to evaporate the solvent. The resultant microparticles were washed thoroughly with DI water and freeze−dried.

To fabricate the nanostructured microparticles (NM), containing Nile Red, either 90 mg PLGA and or a blend of 90 mg PLGA and 18 mg PEG was dissolved in 0.3 ml of the solvent mixture of DCM, DMF and THF (3:1:1 = v/v/v), where 0.9 mg Nile Red was also dissolved as a marker. The resulting solution was then electrospun for 30 min under the following conditions (Nano NC, Korea) to obtain the nanofibrous sheets: applied voltage, 20 kV; collector distance, 10 cm; flow rate; 0.6 ml/h [45]. The sheets were then freeze-milled (6770 Freezer Mill, Spex, Metuchen, NJ, USA) at -196℃ for 60 min [46]. The resulting particles were suspended in an aqueous solution of PVA (100 ml; 1% w/v) and stirred at 100 rpm under vacuum (-12.5 psi) for 30 min, which was intentionally conducted to have the NM exposed to the same condition as with the MS in emulsion. The suspension was then filtered (nylon net filter, 11-μm pore, Millipore, Billerica, MA) to obtain the NM smaller than 10 μm. The particles were then washed thoroughly with DI water and freeze-dried. To make NM containing BRT, either 1000 mg PLGA or a blend of 1000 mg PLGA and 60 mg PEG were dissolved in a solvent mixture of DCM, THF and DMF (3:1:1, v/v/v). This made a 30% polymer solution, in which 30 mg BRT was dissolved as a model drug. The polymer solution was then electrospun for 1 h under the following conditions: applied voltage, 20 kV; tip-to-collector distance, 10 cm; collector rotation speed, 100 rpm; needle gauge, 26 G; feeding rate, 3.0 ml/h. The obtained nanofibrous sheets were freeze-milled, as described above, and filtered with a certified

standard sieve (mesh size, 20 μm; 60 mm X 18 mm, Cisa, Barcelona, Spain).

3.2.3 Preparation of Microparticle Formulations

The microparticles, containing Nile Red, were formulated into two distinct dosage forms, aqueous suspension and a dry tablet. To prepare a suspension, 0.5 mg microparticles were homogeneously dispersed in 30 μl PBS (pH 7.4).

To prepare a dry tablet, a 30 μl drop of 2% w/v PVA in pH 7.4 PBS was suspended with 0.5 mg microparticles, which was then added into a mold (6.5 mm in width, 3.5 mm in length, and 2.5 mm in height) and freeze-dried for 1 day.

To prepare a BRT-loaded dry tablet formulations, microparticles of calculated amounts (2.32-2.61 mg as shown in Table 3.1; equivalent amount of BRT = 52.5 μg) were suspended in 40 μl of 2% w/v PVA, which was poured into the same mold and then freeze-dried for 1 day. For comparison, we also prepared a dry tablet formulation without microparticles by dissolving 52.5 μg BRT powder in 40 μl of an aqueous solution of 2% w/v PVA, which was poured into the same mold and then freeze-dried for 1 day.

3.2.4 Characterization of Microparticles

The size and morphology of microparticles were examined using a

scanning electron microscope (SEM; 7401F, Jeol, Japan). A droplet of an aqueous suspension containing microparticles was placed on a silicon wafer, which was attached on top of a SEM sample mount. The sample was dried in a desiccator to evaporate water, which was then sputter-coated with platinum for 10 min (208HR, Cressington Scientific, England) before imaging.

To determine the size distribution of microparticles, the microparticles were suspended in an electrolyte diluent (Isoton II, Beckman Coulter, CA, USA), which was assessed with a Coulter counter (Multisizer 4, Beckman Coulter, CA, USA) equipped with a 50-μm aperture. At least 30,000 microparticles were counted for each sample.

To examine the increase in surface area of the NM, both MS and NM were examined with a surface area and porosity analyzer, using TriStar II 3020 (Micromeritics, GA, USA) and Autosorb-iQ 2ST/MP (Quantachrome Instruments, FL, USA) for Nile Red-loaded microparticles and BRT-loaded microparticles, respectively. For Nile Red-loaded microparticles, the surface area of about 100 mg microparticles were measured with the CO_2 adsorption/desorption method over a relative pressure range of P/P_0 = 0.01 - 0.025 at 0℃ and calculated, using the Dubinin-Astakhov model[47, 48]. For microparticles including BRT, the surface area of microparticles (>500 mg) were measured with the N_2 adsorption/desorption method at a relative pressure range of P/P_0 = 0.01-0.25 at -196℃, where the surface area was calculated with the Brunauer-Emmett-Teller

(BET) method [49]. The microparticle samples were degassed for > 24 h at room temperature before measurement.

Gel permeation chromatography (GPC) was performed to determine the presence of PEG in the Nile Red-loaded microparticles [50, 51]. Thus, the microparticles were dissolved in THF and filtered through a 0.2 μm-pore membrane filter (Whatman, Clifton, NJ, USA), which was then analyzed by high performance liquid chromatograph (HPLC; Waters 515, Waters, MA, USA) at a flow rate of 1.0 ml/min through three columns in series (PLgel 5.0 guard; 50 mm X 7.5 mm, MIXED-C; 300 mm X 7.5 mm and MIXED-D; 300 mm X 7.5 mm, Polymer Laboratories, Shrewbury, UK) with THF as eluent at 35℃. The GPC system was calibrated with polystyrene standards before use.

Thermogravimetric analysis (TGA; TGA-Q50, TA Instruments, DE, USA) was performed to further confirm the presence of PEG in the Nile Red-loaded microparticles. A known amount of the microparticles (20 - 30 mg) was placed in a platinum pan under nitrogen gas flow, where the temperature was increased from 40℃ to 600℃ at a rate of 10℃/min. A powder of intact PLGA and PEG was also measured for comparison.

To quantify the actual PEG amount left in BRT-loaded microparticles after preparation, nuclear magnetic resonance (NMR) spectroscopy was utilized. Microparticles weighing approximately 10 mg were dissolved in 1 ml of deuterated chloroform (Sigma, MO, USA) containing 0.1% v/v tetramethylsilane. The proton NMR spectra were

obtained on an NMR spectrometer (Varian Unity-Inova 500 MHz, Varian Inc., Palo Alto, CA, USA). The hydrogen of the methane group of the lactic acid unit and the methylene group of the glycolic acid unit of the PLGA copolymer resonated at 4.8 and 5.2 ppm, respectively, while that of the methylene group of the PEG homopolymer appeared at 3.6 ppm. The areas under the peaks were integrated to determine the PEG content of microparticles [52].

In this work, Nile Red was loaded in the microparticles as a tracer to examine the *in vivo* retention of microparticles on the rabbit eye. For quantitative analysis, the actual loading amount of Nile Red in the microparticles was measured. Thus, a known amount of microparticles (4 - 5 mg) was dissolved in 50 ml acetone for 1 h with strong agitation, which was measured with fluorescence spectroscopy (FS2, Scinco, Korea) [53].

To assess the drug stability and determine the BRT content after preparation of MSs and NMs, microparticles weighing 5-10 mg were first completely dissolved in 1ml DCM. Then, 15 ml phosphate buffered saline (PBS) (pH 7.4) were added to the resulting solution, which was sonicated at 160 W for 5 min (Model 500 Digital Sonic Dismembrator, Fisher Scientific, PA, USA) and centrifuged at 3,500 rpm for 10 min at 15℃ (Heraeus Megafuge 40R, Thermo Scientific, PA, USA). The supernatant was analyzed with high performance liquid chromatography (HPLC, Agilent 1260 series, Agilent Technologies, CA, USA) using Poroshell (120 EC-C18, 4.6 X 100 mm, 2.7 μm, Agilent Technologies, CA, USA). The mobile phase

was prepared by mixing a 20 mM phosphate buffer at pH 2.5 and methanol (8:2, v/v). The flow rate and injection volume were 1 ml/min and 10 μl, respectively. The column was maintained at 40℃, and the UV absorbance was measured at 248 nm[54].

To determine the presence of PLGA and BRT in microparticles, Fourier transform infrared spectroscopy (FTIR) spectra of the intact PLGA, intact PEG, BRT, PLGA MS, PLGA/PEG MS, PLGA NM, and PLGA/PEG NM were collected with a JASCO 6100 spectrophotometer (JASCO, Inc., Japan) in a range of 500–4000^{-1} using the KBr disk method[55, 56].

3.2.5 *In vitro* Drug Release Experiments

To examine the *in vitro* drug-release profiles, each dry tablet was placed in 10 mL PBS (pH=7.4) and incubated in a shaking incubator (SI-600R, Jeio Tech, Seoul, Korea) while being continuously stirred at 125 rpm at 37℃. At scheduled intervals, an aliquot of the release media was taken, and the same amount of fresh buffer was filled again to maintain the sink condition. The aliquot was assayed with HPLC as described above. At least three samples for each tablet were tested for statistics.

3.2.6 *In vivo* Evaluation of Preocular Microparticle Retention

In vivo study was performed with male New Zealand White rabbits (Cheonan Yonam College, Chungcheongnam-do, Korea), weighing 2.5 - 4.5 kg, without any known ocular abnormality. The experiment procedure was approved by the Institutional Animal Care and Use Committee (IACUC No. 10-0304 and 13-0101) at Seoul National University Hospital Biomedical Research Institute. The animals were housed singly in a standard cage at controlled temperature (21 ± 1℃) and humidity (55 ± 1%) with a 12/12-h light-dark cycle without any restriction of food and water.

In vivo preocular retention was tested with the eight different microparticle formulations prepared in this work, following the protocol as previously proposed [29]. Briefly, for administration of the microparticle formulation, either aqueous suspension or a dry tablet, each rabbit was taken out from the cage and positioned in a restrict bag with only the head exposed. Then, the formulation, containing 0.5 mg microparticles, was administered into the lower fornix of the rabbit eye without anesthesia and the eye was manually closed for 3 min. After that, the rabbit was placed back in the cage before sample collection.

The microparticles remaining at the preocular surface were collected at predetermined times. The eye surface was wiped thoroughly with a surgical sponge (PVA Spears, Network Medical Products, Ripon, UK) 10 min, 30 min, 60 min, 90 min and 120 min

after administration of the formulation. To ensure almost no microparticles left on the eye surface, the whole preocular region was wiped at least 5 times at each time of collections. Then, the surgical sponge was immersed in acetone and agitated strongly for 1 h to completely extract Nile Red, which was analyzed with fluorescence spectroscopy (FS2, Scinco, Korea) to determine the amount of collected microparticles [53]. While the sample was collected, the eye was locally anesthetized with topical administration of 30 μl of a 0.5% proparacaine eye drop (Alcaine; Alcon-Couvreurm, Puurs, Belgium). More than four eyes were tested for each of the formulations and at each time after administration for statistics.

We also obtained the images of the preocular surface of the rabbit after administration of the microparticle formulations [29]. Before imaging, the rabbit was anesthetized with a subcutaneous injection of a cocktail of 17.5 mg · kg^{-1} ketamine, 5 mg · kg^{-1} xylazine and 0.2 mg · kg^{-1} acepromazine. One additional booster (a half dose of the first injection) was used if necessary. Each of the eight microparticle formulations was administrated as stated above and the fluorescent images of Nile Red-loaded microparticles left on the rabbit eye were obtained 10 min, 30 min, 60 min, 90 min and 120 min after administration. For this, the eye surface was imaged with a camera (HTC raider, HTC, Taiwan) equipped with a Tetramethylrhodamine Isothiocyanate (TRITC) emission filter with transmission wavelengths of 594 - 646 nm (MF620-52, Thorlabs,

NJ, USA) while the eye was illuminated with a LED lamp (AM-R5 mini, Aimai, Korea) equipped with a TRITC excitation filter with transmission wavelengths of 532 - 552 nm (MF542-20, Thorlabs, NJ, USA). The image included the whole anterior surface of the eyeball and the lower fornix while the upper fornix was not imaged (Figure 3.2) since almost no microparticles were observed. The rabbit lay on its side during imaging and on its stomach between the intervals of imaging.

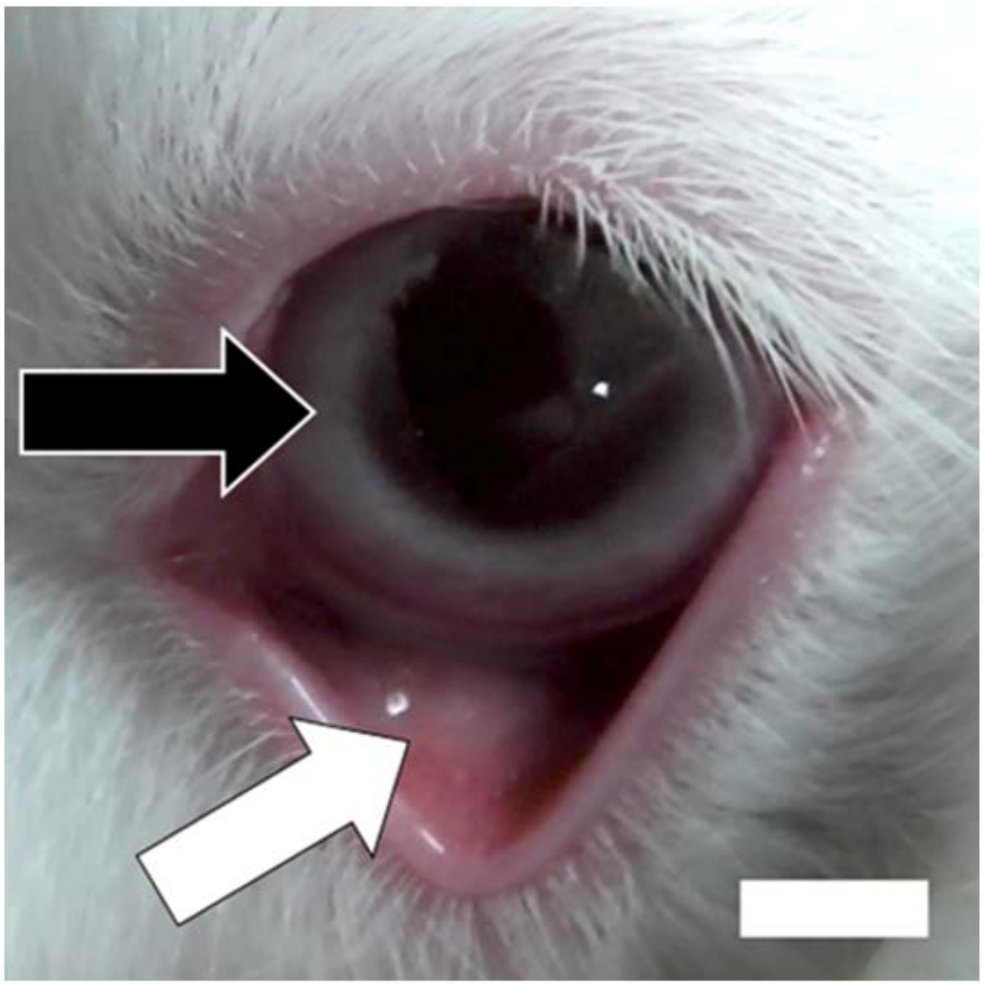

Figure 3.2. Anterior surface of the eyeball and lower fornix of the rabbit eye exposed for fluorescence imaging. The black and white arrows indicate the locations of the eyeball and exposed lower fornix of the rabbit eye, respectively. Scale bar = 5 mm.

3.2.7 *In vivo* Evaluation of IOP-lowering Effect

To evaluate the IOP-lowering effect on rabbits, each rabbit was first placed in a restriction bag and the IOP of the left eye was measured using a tonometer (Tono-Pen AVIA, Reichert, NY, USA) as a control. Then, each rabbit eye was treated with each formulation containing 52.5 μg BRT and closed manually for 1 min, and then the rabbit was moved back to the cage until the IOP measurement. At scheduled time points, the IOP of the left eye was measured and calibrated as suggested in literature, where a decrease in IOP was calculated according to the following equation:

$$\% \text{ Decrease in IOP} = \frac{\text{IOP control} - \text{IOP dosed eye}}{\text{IOP control}} \text{ X } 100$$

Before measuring the IOP, the rabbit's left eye was locally anesthetized with 35 μl of 0.5% proparacaine. At least five eyes were measured for each formulation at each time for statistical analysis.

3.2.8 *In vivo* BRT Concentration in Aqueous Humor (AH)

To determine the BRT concentration in rabbits' AH over time, each type of BRT formulation containing 52.5 μg BRT was administered as stated above. Before sampling at 20 min, 40 min, 1 h, 2 h, 3h, 5 h,

7 h, and 9 h post-dose, the rabbit was anesthetized systemically with an intramuscular injection of a cocktail of 17.5 mg/kg ketamine, 5 mg/kg xylazine, and 0.2 mg/kg acepromazine, and the rabbit eye was locally anesthetized with a drop of 0.5% proparacaine. After that, approximately 100 ㎕ of AH was aspirated using a 1-ml syringe fitted with a 30-gauge disposable needle and stored below -15℃ before analysis. Terramycin eye ointment (Pfizer, NY, USA) was applied to the eye surface prior to returning the animal to its cage to prevent infection. The concentration of BRT in AH was analyzed with HPLC as stated above with only a small difference. Since AH is a transparent material with very little protein, 50 ㎕ AH were injected directly into HPLC after filtering (syringe filter, 0.2 ㎛, 4 mm, Whatman, UK). The mobile phase was a mixture of 20 mM phosphate buffer (pH 2.5) and methanol (9:1, v/v).

3.2.9 Safety Evaluation

3.2.9.1 *In vitro* Cytotoxicity

The cytotoxicity of the PLGA/PEG NM tablet was evaluated by the lactate dehydrogenase (LDH) assay, following the supplier's instruction (TOX7, Sigma-Aldrich, MO, USA). In brief, L929 fibroblast cells (Korean Cell Line Bank, Seoul, Korea) were seeded in 6-well culture plates at the initial density of 5×10^5 cells/well, where the PLGA/PEG NM tablets were added. In each well, we added

two tablets since the medium volume in each well (2 ml) is twice as much as that of daily tear production of the rabbit (ca. 1 ml/day) [57], i.e., envisioning one-tablet administration per day. Nile Red was not loaded in microparticles for cytotoxicity evaluation to rule out the effect of a tracer agent. After 24 h incubation, the medium was centrifuged at 250 g for 4 min, where 50 μl of supernatant was collected. The resulting supernatant was then transferred to a 96-well plate, mixed with 100 μl of the reagent (TOX7, Sigma-Aldrich, MO, USA) and incubated for 30 min in dark room at room temperature. The absorbance of the reaction mixture was measured at 490 nm, using a microplate reader (VersaMax ELISA Microplate Reader, Molecular Devices, CA, USA) with reference wavelength at 690 nm. Intact, untreated cells and cells treated with 1% Triton-X100 (Sigma, MO, USA) were used for background release and as positive control, respectively. The cytotoxicity (%) of the PLGA/PEG NM tablet was calculated by the following equation [58].

$$\text{Cytotoxicity (\%)} = \frac{(\text{tablet sample} - \text{background release})}{(\text{positive control} - \text{background release})} X\ 100\ \%$$

At least four independent experiments were performed for each cytotoxicity value.

3.2.9.2 *In vivo* Safety Evaluation

Either an increase or decrease in pH in the rabbit's tears after the installation of microparticles may adversely affect the rabbit eye. Thus, we measured pH levels in the rabbit's tears before and after 10, 30 and 60 min of administration of BRT-loaded PLGA/PEG NM tablet by placing the pH test paper (Macherey-Nagel, Germany) into the lower cul-de-sac of the rabbit eye for 30 s. Then, the color of the pH test paper was compared with the reference colors provided by the manufacturer. To assess the *in vivo* safety, after topical administration of a PLGA/PEG NM tablet, the rabbit eye was examined with microscopy and external ophthalmic photography by a professional ophthalmologist. The intraocular pressure was also monitored, using a tonometer (Tonopen AVIA, Reichert, NY, USA). For each of the animals, the left eye was treated with a PLGA/PEG NM tablet and evaluated 1 h, 2 h and 24 h after administration while the right eye remained intact. Four rabbits were tested for safety evaluation in this work.

3.2.10 Statistical Analysis

The percentage of the microparticles remaining on the preocular surface of the rabbit was calculated based on the amount of the microparticles initially applied to the eye (i.e., 0.5 mg microparticles per dose). Mean percentages of remaining microparticles among the

eight different microparticle formulations and decrease in IOP with the seven different formulations were each analyzed for statistical significance with ANOVA with $\alpha = 0.05$, followed by pairwise comparisons using a Tukey's post hoc test. The AH concentrations for Alphagan P and the PLGA/PEG NM tablet were analyzed for statistical significance using a paired t-test for each time point.

3.3 Results and Discussion

3.3.1 Characterization of Microparticles and Tablet Formulations

We prepared four different types of microparticles in this work: spherical microparticles without mucoadhesion (PLGA MS; smooth surface with PLGA only), spherical ones with mucoadhesion (PLGA/PEG MS; smooth surface with a blend of PLGA and PEG), nanostructured ones without mucoadhesion (PLGA NM; rough surface with PLGA only) and nanostructured ones with mucoadhesion (PLGA/PEG NM; rough surface with a blend of PLGA and PEG). The spherical microparticles (MS) were prepared by the classic emulsion method in this work [35, 36]. Thus, we could compare the preocular retention property and drug bioavailability of the mucoadhesive microparticles of nanostructure (i.e., PLGA/PEG NM) with those of the other different kinds of the microparticles (i.e., PLGA MS, PLGA/PEG MS and PLGA NM). All microparticles were loaded with either a tracer, Nile Red, or an anti-glaucoma drug, BRT (Table 3.1 and Table 3.2), for both quantitative and qualitative analyses of their preocular retention and drug bioavailability, respectively. Nile Red is almost insoluble in water (< 1 μg/ml) [59] and thus, almost no release was expected during a period of preocular retention study in this work.

Figures 3.3 and Figures 3.4 show the scanning electron micrographs (SEM) of the microparticles, each containing Nile Red

and BRT, respectively. The MS exhibited a smooth surface (Figures 3.3(a-b) and Figures 3.4 (a-b)) while the NM showed a rough surface, composed of the agglomerated pieces of the nanofibers (Figures 3.3(c-d) and Figures 3.4(c-d)). The initially added amount of PEG did not appear to influence the microparticle morphology in this work. We controlled the size and size distribution of the microparticles similar in range to rule out the effect of the particle size on overall surface area. The mean diameters were measured to be 1.8 - 2.2 μm for microparticles containing Nile Red(Table 3.1) and 1.59-1.66 μm for microparticles including BRT (Table 3.2), also showing similar size distributions (Figure 3.5). The microparticles in this size range (< 10 μm) were expected to minimize possible eye irritation [12] and allow particle clearance through the lacrimal canals, 300 - 500 μm in diameter[22]. As we analyzed the microparticles with a surface area and porosity analyzer [47-49], the increase in specific surface area of the NM was apparent, showing a more than 10-fold increase, as compared with that of the MS (Table 3.1 and Table 3.2). This result was ascribed to the nanostructured, rough surface of the microparticles, originated from randomly-oriented electrospun nanofibers (Figure 3.6) [46].

We performed the gel permeation chromatography (GPC) analyses to validate the presence of PEG in the microparticles containing Nile Red, as shown in Figure 3.7 and Table 3.3[50, 51]. As we measured the intact PLGA and PEG powders, the peak retention volumes were observed around at 13.6 ml and 15.3 ml,

respectively, due to their difference in molecular weight. For the microparticles made of PLGA only (i.e., PLGA MS and PLGA NM), a single peak retention volume was observed, as with intact PLGA. On the other hand, the microparticles made of a blend of PLGA and PEG (i.e., PLGA/PEG MS and PLGA/PEG NM) exhibited two distinct peak retention volumes, each originated from PLGA and PEG, respectively. The result from thermogravimetric analyses (TGA) further confirmed the presence of PEG in PLGA/PEG MS and PLGA/PEG NM, both containing Nile Red, as shown in Figures 3.8. For intact PLGA and PEG, the weight losses by decomposition were observed at 130 – 370℃ and 305 – 415℃, respectively (Figure 3.8(a)) [60–62]. The microparticles composed of PLGA only (i.e., PLGA MS and PLGA NM) exhibited a single weight loss in the same temperature range, as with intact PLGA. However, PLGA/PEG MS and PLGA/PEG NM exhibited two consecutive weight losses due to the presence of both PLGA and PEG. According to the second weight loss at 355 – 410℃, both PLGA/PEG MS and PLGA/PEG NM were suggested to contain a similar amount of PEG of about 10 wt. %(Figure 3.8(b)) [63]. In addition, for microparticles containing BRT, the PEG content in PLGA/PEG MSs was measured to be similar to that in PLGA/PEG NMs. The actual PEG amounts in BRT–loaded microparticles were determined to be 5.91 and 5.93 wt. % for PLGA MSs and PLGA NMs, respectively (Table 3.2) [52].

To assess the composition of microparticles, the Fourier transform infrared spectroscopy (FTIR) spectra of intact PLGA,

intact PEG, BRT, PLGA MS, PLGA/PEG MS, PLGA NM, and PLGA/PEG NM were obtained, as shown in Figure 3.9. The intact PLGA exhibited a strong and sharp band at about 1750 cm^{-1} and double bands near 2960 and 3000 cm^{-1} for the C=O stretch and C-H stretch in methane groups[55], respectively, while BRT showed a double band near 3224 cm^{-1} for the -NH stretch[56]. For all microparticles, the characteristic bands from PLGA and BRT were observed, indicating that both PLGA and BRT were present in microparticles.

The drug-stability results from the high performance liquid chromatography (HPLC) analysis revealed that the drug-retention time remained unchanged for all microparticles, as compared with the BRT powder[64] (Figure 3.10). We also confirmed the amounts of BRT content encapsulated in all types of microparticles, which were 20.1-23.5 μg/mg (Table 3.2).

In this work, we formulated the microparticles into two dosage forms, i.e., aqueous suspension and a dry tablet to examine the effect of the formulation design on preocular microparticle retention. A single administration is designed to contain the same dose of 0.5 mg microparticles in a 30 μl-drop suspension of phosphate buffered saline (pH 7.4) and a tablet, respectively. A dry tablet of porous medium was prepared by freeze-drying a PVA solution suspended with the microparticles in a mold (Figure 3.1(b)). Thus, eight different formulations were prepared in this work: PLGA MS suspension, PLGA/PEG MS suspension, PLGA NM suspension,

PLGA/PEG NM suspension, PLGA MS tablet, PLGA/PEG MS tablet, PLGA NM tablet and PLGA/PEG NM tablet. For administration of BRT-loaded microparticles, only a dry table was formulated, each containing no microparticle or one of four different types of microparticles (2.32-2.51 mg, depending on BRT content; equivalent BRT amount = 52.5 μg).

Figures 3.11 (a-b) show the fluorescence images of a tablet, where the bright signals indicated the presence of Nile Red loaded microparticles. The tablet was 3 mm in width, 6 mm in length and 2 mm in height with an equivalent volume of approximately 30 μl, which was similar to the volume of a single-dose eye drop[65].

For a tablet of microparticles containing BRT, the height increased to 2.5 mm, hence equivalent volume of approximately 40 μl. Figures 3.11(c-d) show the SEM images of the tablet surfaces, where the microparticles were seen to be bound with the polymeric medium, PVA. When immersed in pH 7.4 phosphate buffered saline (PBS), a porous tablet medium dissolved away rapidly (< 1 min), freeing the fluorescent microparticles in the media, as shown in Figures 3.11(e-f). The distinctive shapes of the microparticles, i.e., spherical and nanostructured ones, were discernible, depending on their own geometry. The agglomerated nanofibers in each of the NM were not seen to be disassembled in aqueous media.

Table 3.1. Mean diameters, Nile Red contents and specific surface areas of the microparticles prepared in this work. Four different types of the microparticles were prepared in this work, which were each formulated into two different formulations, suspension and tablet, to give eight different microparticle formulations for *in vivo* evaluation of preocular retention.

Particle type	Mean diameter (μm)	Nile Red content (μg mg^{-1})	Specific surface area ($m^2 g^{-1}$)
PLGA MS	1.89 ± 0.37	8.59 ± 0.46	NA
PLGA/PEG MS	1.95 ± 0.35	7.72 ± 0.55	8.13
PLGA NM	1.98 ± 0.35	8.30 ± 0.33	NA
PLGA/PEG NM	2.14 ± 0.32	7.48 ± 0.37	108.78

Values are mean ± SD. NA, not available.

Table 3.2. Mean size, weight percent of PEG, amounts of Brimonidine of microparticles, amounts of microparticle needed for tablet formulation and specific surface area of PLGA/PEG MS and PLGA/PEG NM measured with N_2 adsorption/desorption method.

Microparticle Type	Mean size (μm)	Specific surface area (m^2/g)	PEG weight percent (wt%)	Brimonidine amount (μm/mg)	Microparticle amount in tablet (mg)
PLGA MS	1.59	N/A	0%	21.6	2.43
PLGA/PEG MS	1.60	3.211	5.91%	20.1	2.61
PLGANM	1.60	N/A	0%	22.6	2.32
PLGA/PEG NM	1.66	44.216	5.93%	23.5	2.34

N/A (not available)

Table 3.3. Peak retention volumes and molecular weights of PLGA, PEG and the microparticles measured with gel permeation chromatography.

Particle Type	Peak Retention Volume (ml)	Mw (Daltons)
Intact PLGA	13.62	45,568
Intact PEG	15.36	7,509
PLGA MS	13.60	45,386
PLGA/PEG MS	13.64	45,278
	15.26	8,167
PLGA NM	13.62	44,700
PLGA/PEG NM	13.66	44,721
	15.30	7372

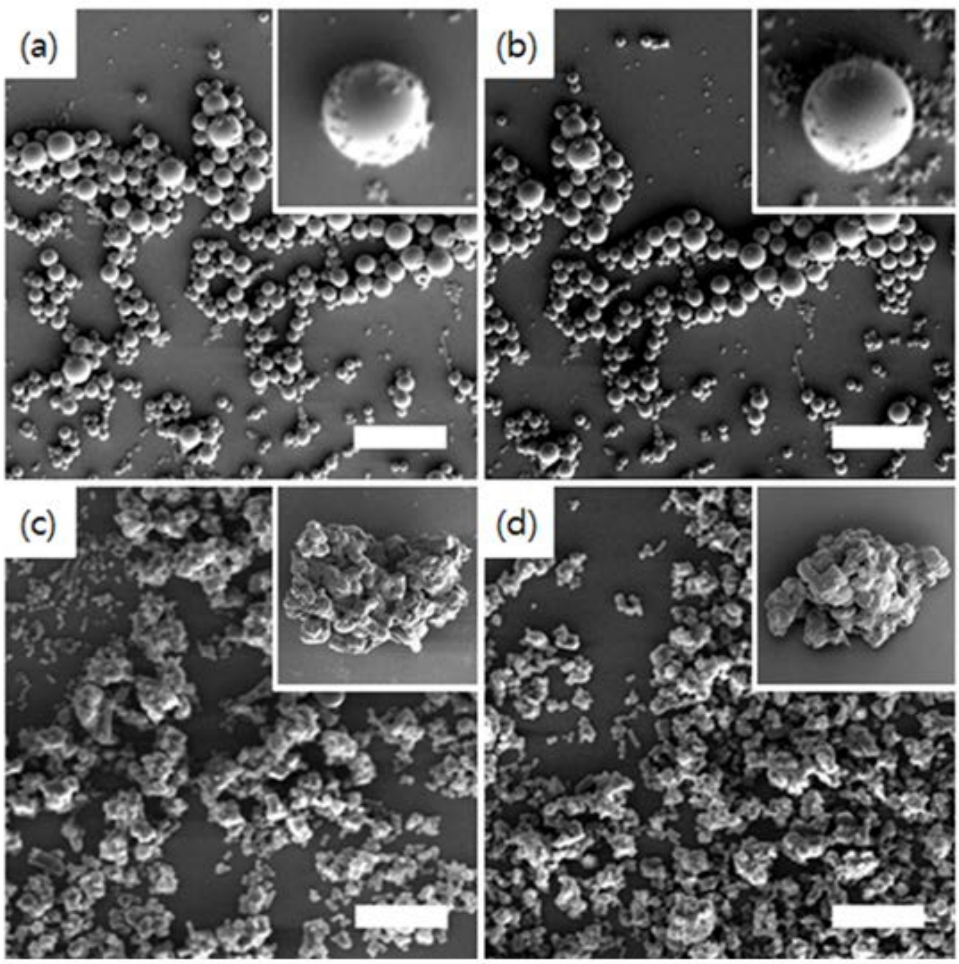

Figure 3.3. Representative scanning electron micrographs of microparticles containing Nile Red. (a) PLGA MS, (b) PLGA/PEG MS, (c) PLGA NM and (d) PLGA/PEG NM. The insets show the microparticle of each kind with a higher magnification. Scale bars = 20 μm.

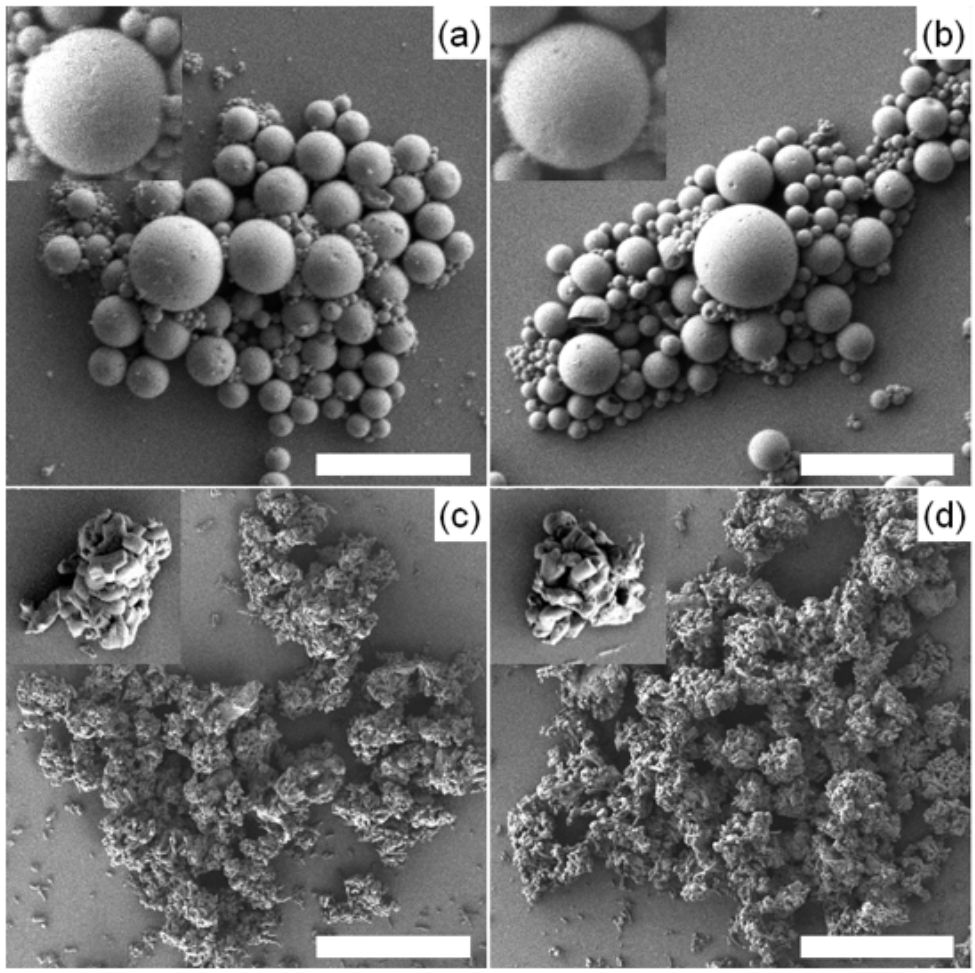

Figure 3.4. Representative scanning electron micrographs of Brimonidine-loaded microparticles, (a) PLGA MS, (b) PLGA/PEG MS, (c) PLGA NM and (d) PLGA/PEG NM. The insets display the microparticle of each kind with a higher magnification. Scale bars = 10 μm.

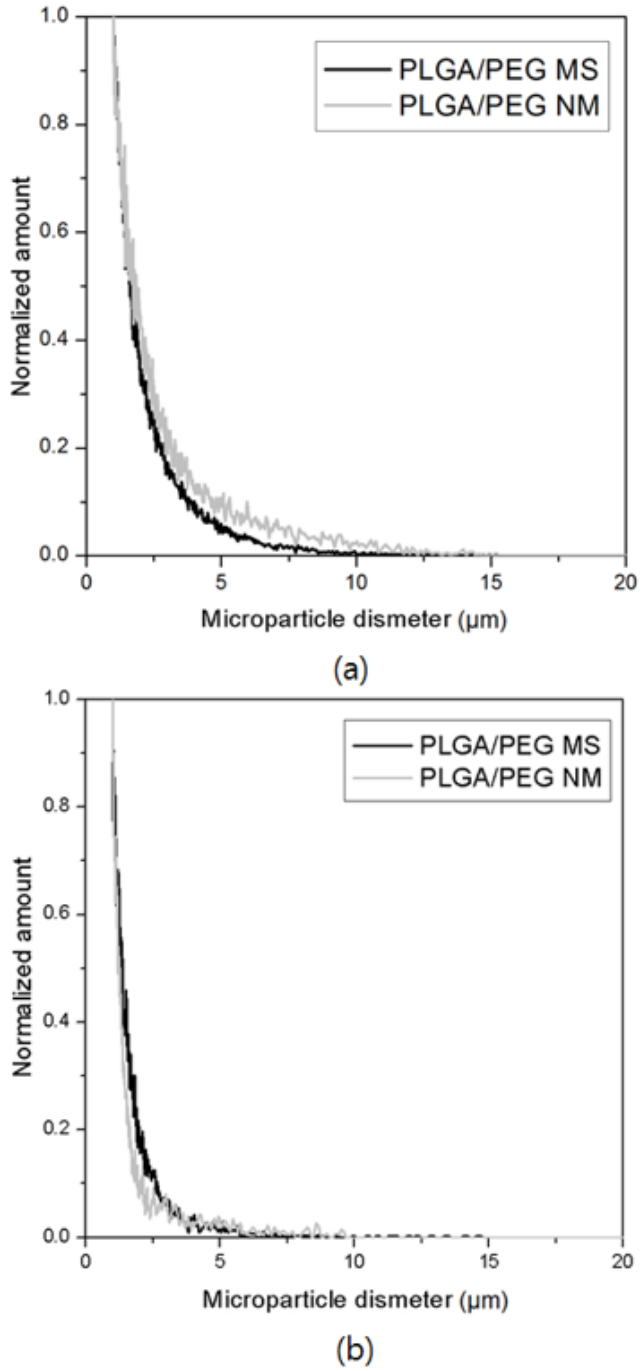

Figure 3.5. Size distribution profiles of PLGA/PEG MS (black) and PLGA/PEG NM (gray), containing (a) Nile Red and (b) BRT.

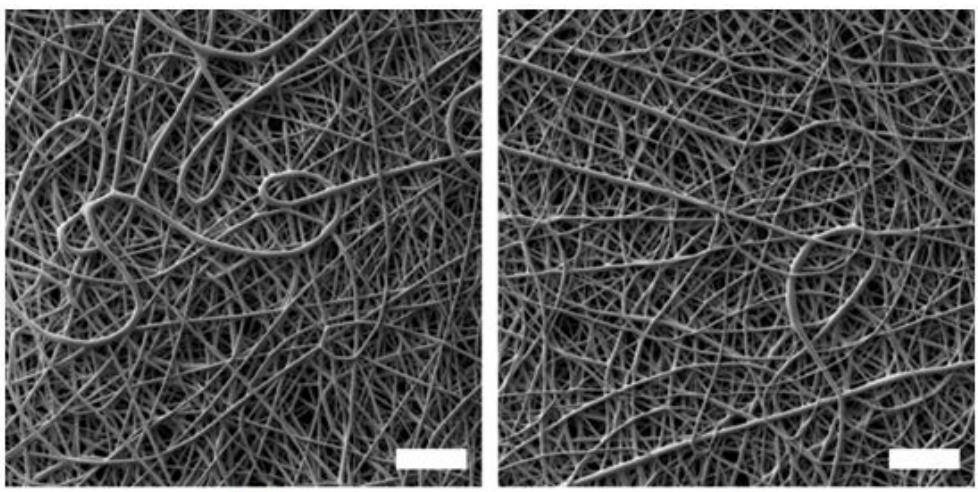

Figure 3.6. Representative scanning electron micrographs of the nanofibrous sheets employed for the fabrication of the nanostructured microparticles. The sheets were composed of (a) PLGA and (b) a blend of PLGA and PEG. Scale bars = 20 μm.

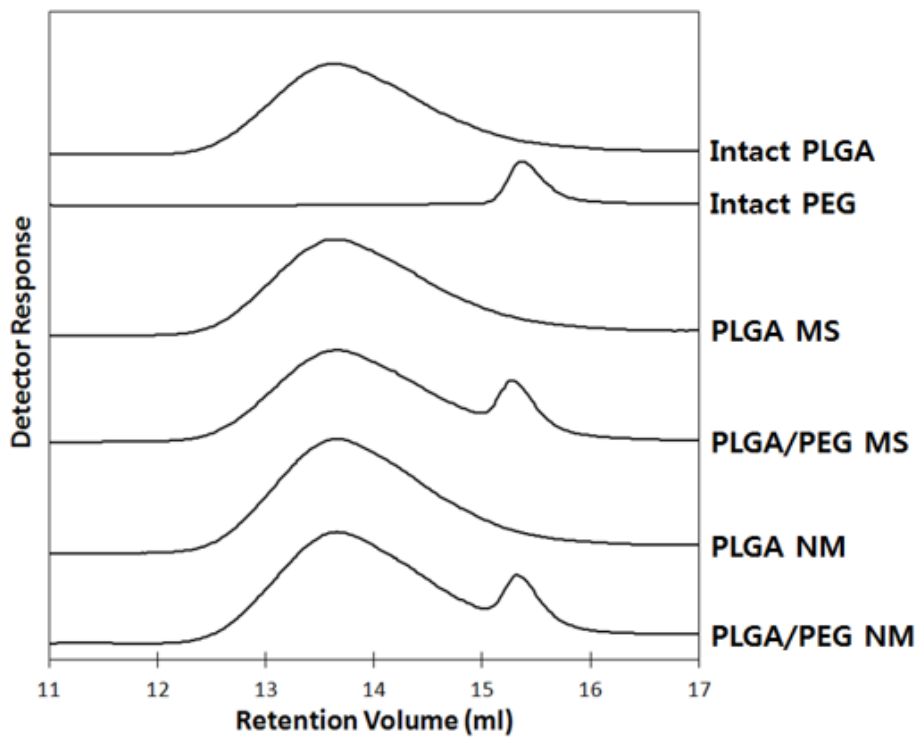

Figure 3.7. GPC spectra of PLGA MS, PLGA/PEG MS, PLGA NM and PLGA/PEG NM.

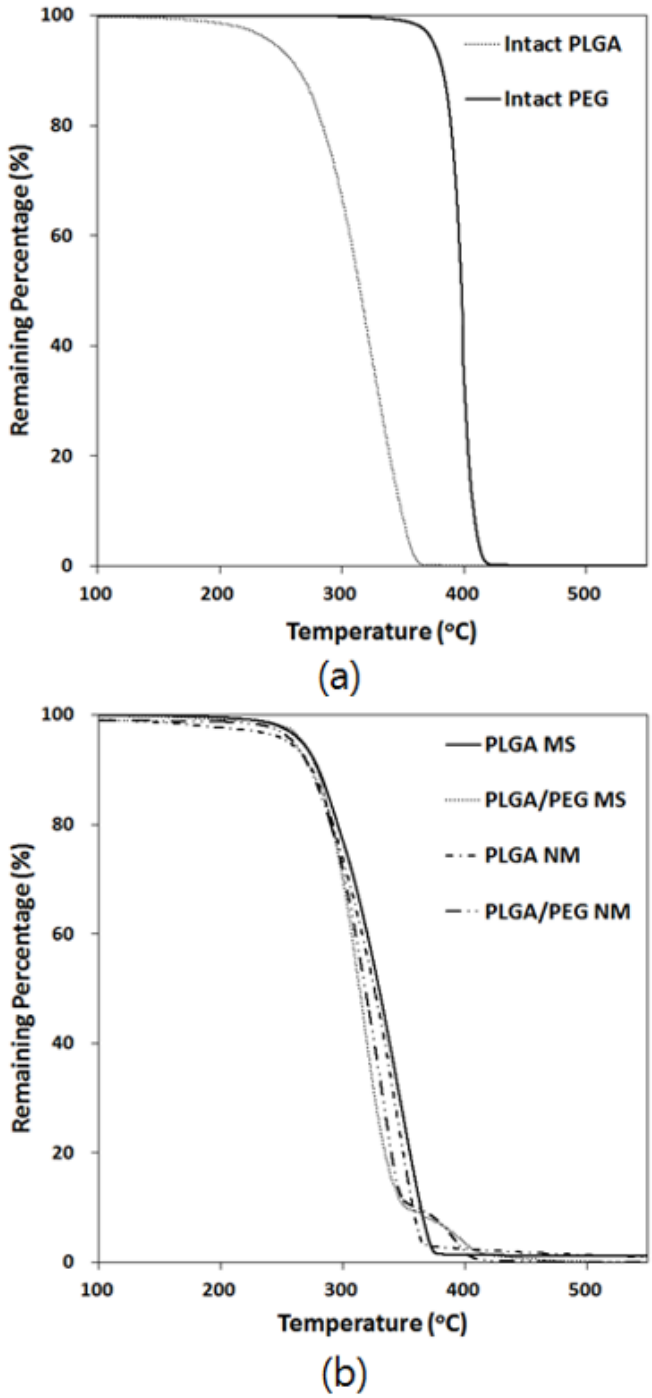

Figure 3.8. TGA spectra of (a) intact PLGA and PEG and (b) the microparticles.

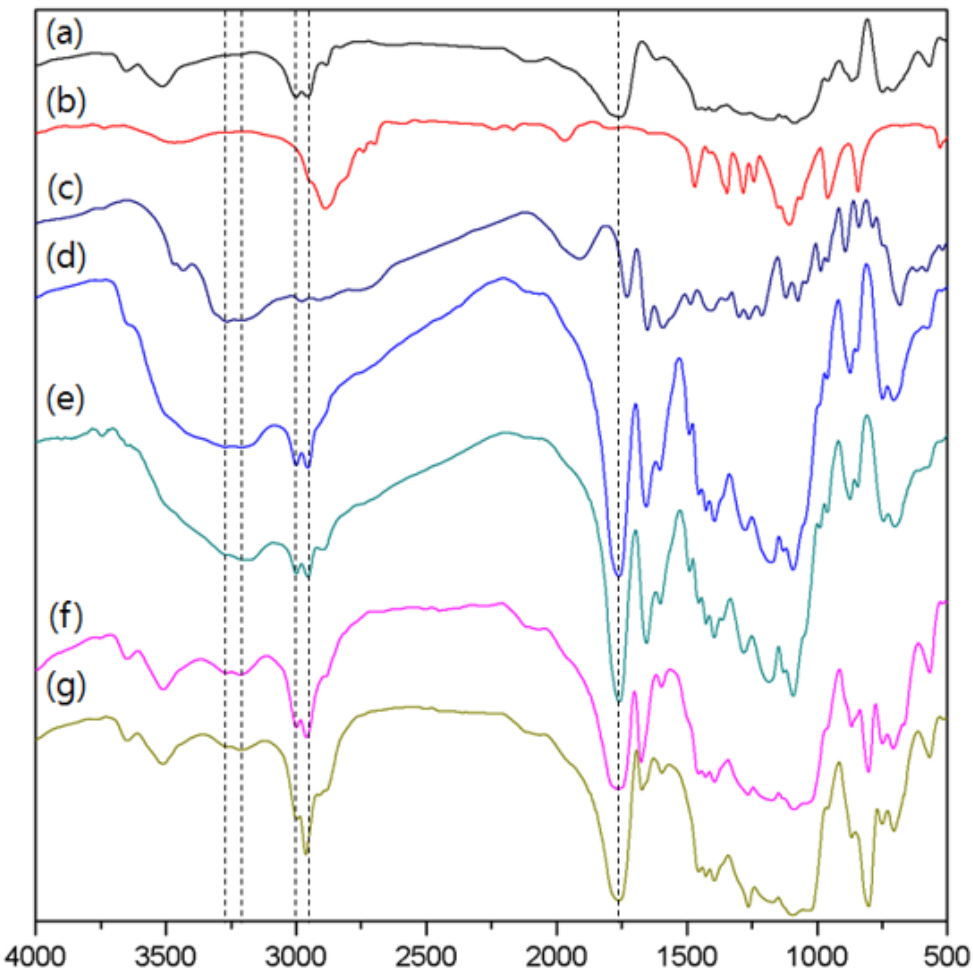

Figure 3.9. FTIR spectra of (a) PLGA, (b) PEG, (c) BRT, (d) PLGA MS, (e) PLGA/PEG MS, (f) PLGA NM and (g) PLGA/PEG NM.

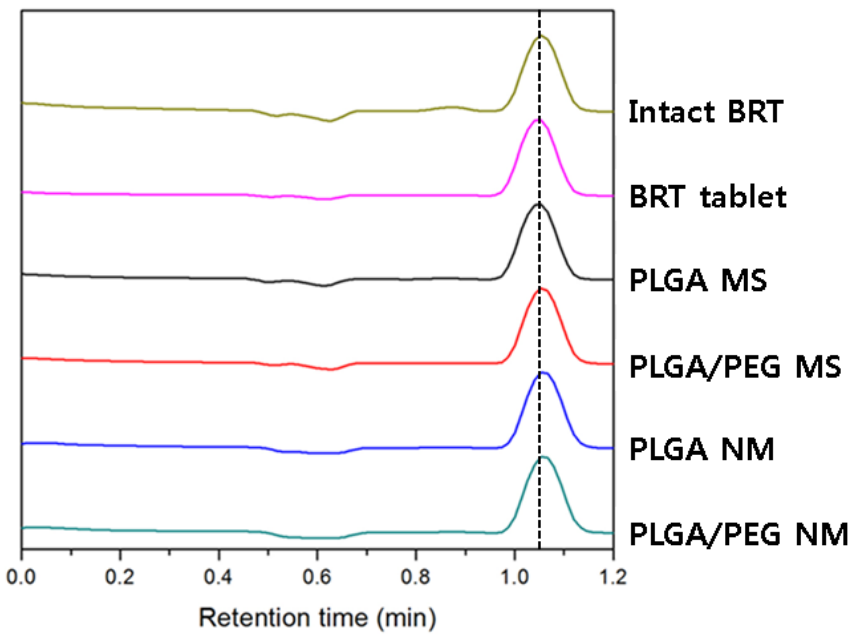

Figure 3.10. HPLC retention profiles of Brimonidine from intact BRT, BRT tablet, PLGA MS tablet, PLGA/PEG MS tablet, PLGA NM tablet and PLGA/PEG NM tablet.

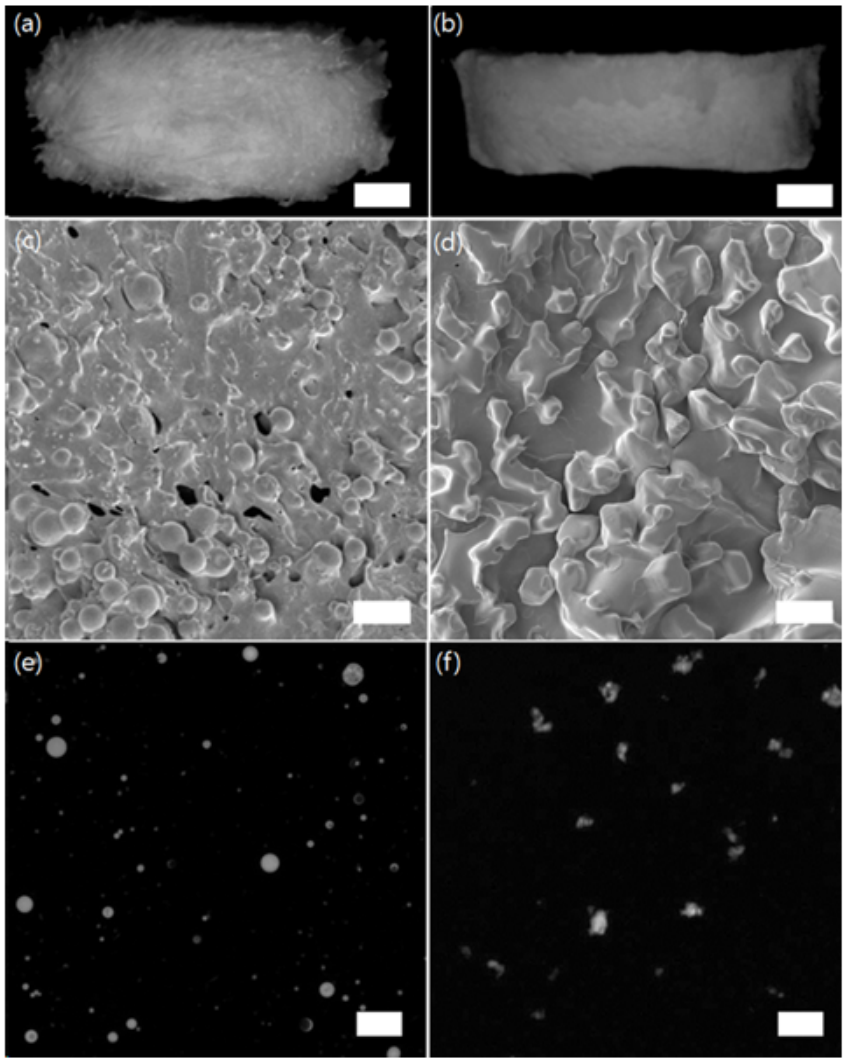

Figure 3.11. Fluorescence micrographs of a dry tablet embedded with Nile Red loaded PLGA/PEG NM from (a) the top view and (b) the side view. SEM images of the surfaces of the tablets containing (c) PLGA/PEG MS and (d) PLGA/PEG NM. Fluorescence micrographs of (e) PLGA/PEG MS and (f) PLGA/PEG NM suspended in pH 7.4 PBS after complete dissolution of the tablet medium. Scale bars = (a–b) 1 mm and (c–f) 20 μm.

3.3.2 *In vitro* Drug Release Profiles

We examined the *in vitro* drug-release profiles of BRT from the BRT tablet, PLGA MS tablet, PLGA/PEG MS tablet, PLGA NM tablet, and PLGA/PEG NM tablet in pH 7.4 PBS media, as shown in Figure 3.12. As expected, almost 100% of BRT was immediately released from the BRT tablet during the first 10 min, since BRT was present in the PVA matrix itself without microparticles and the PVA matrix could be instantly dissolved on contact with aqueous media due to the high porosity and high aqueous solubility of PVA. Regardless of the presence of PEG, the PLGA NM tablet and PLGA/PEG NM tablet exhibited a larger initial burst release of 54.7% and 49.6%, respectively, during the first 30 min, which could be ascribed to the larger specific surface area of NMs originating from the nanostructure. On the other hand, the initial burst during the first 30 min in MS tablets was relatively smaller than in NM tablets, releasing 35.1 %and 32.3% for the PLGA MS and PLGA/PEG MS tablet, respectively. However, the total amount of drug release during the 180 min and afterward was similar for both types of microparticles (61-65%; approximately 33 μg BRT) and was completed in 2 days (2880 min).

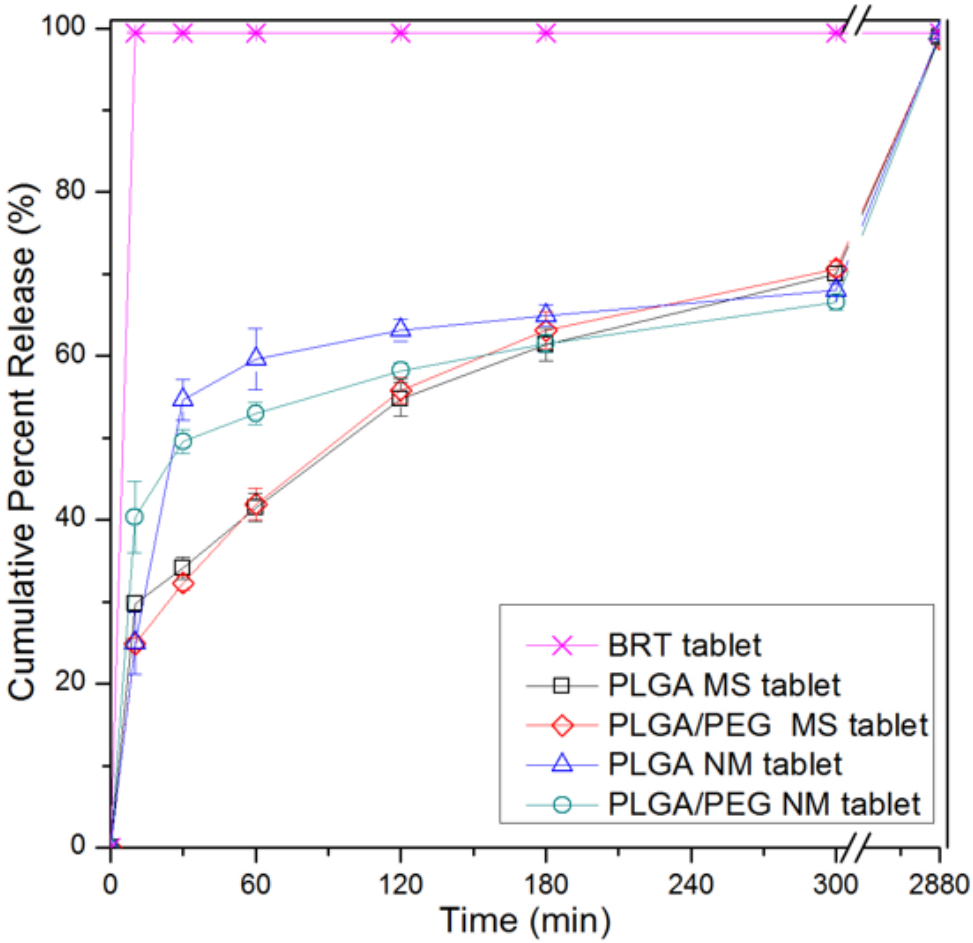

Figure 3.12. *In vitro* release profiles of Brimonidine from tablets embedded without microparticles (BRT tablet) and with PLGA MS, PLGA/PEG MS, PLGA NM and PLGA/PEG NM. Each of tablet contained the same amount of Brimonidine (52.5 μg).

3.3.3 *In vivo* Mucoadhesion Study

We sought to examine the preocular retention property of the microparticles, using the eight different formulations prepared in this work. Thus, each of the formulations was administered to the lower fornix of the rabbit eye *in vivo* and the percentage of microparticles remaining on the eye was measured at scheduled intervals (Figure 3.13). All microparticles in suspension, regardless of their types, exhibited poor preocular retention. Only 7 – 15% of microparticles remained at 10 min and most of the microparticles disappeared from the preocular surface after 30 min, possibly due to expedited tear drainage caused by the addition of fluid[66, 67]. The tablet formulation only could not improve the preocular retention property of the microparticles. In this work, the tablet medium was composed of a water−soluble polymer, PVA and to expedite its dissolution, we prepared it very porous. As a result, the tablet medium dissolved away rapidly within less than 1 min, leaving the microparticles only (Figure 3.11). Therefore, the dissolution rate of the tablet medium should have a minimal effect especially on the microparticles staying on the eye surface for a long time. The PLGA MS tablet exhibited only 14% and less than 10% of remaining microparticles at 10 min and after 30 min, respectively. When combined with mucoadhesiveness, on the other hand, the effect of tablet formulation was observable. For PLGA/PEG MS tablet, the average percentages of remaining microparticles increased from 8% to 27% and from 6%

to 18% at 10 min and 30 min after administration, respectively, as compared with PLGA/PEG MS suspension. A longer time for microparticle interaction with the preocular surface appeared to enhance the mucoadhesion property; however, the improvement was not statistically significant ($p > 0.10$).

The combined effect of nanostructured surface and tablet formulation was also evident. The PLGA NM tablet exhibited a statistically significant increase in preocular retention from 9% to 44% 10 min after administration, as compared with the PLGA NM suspension ($p < 0.001$). When formulated in a tablet, the effect of a rough surface of the NM might play a role to increase their friction on preocular surface, thereby hindering clearance of the microparticles even without mucoadhesion property. The enlarged surface area might also help to increase the adhesion of the microparticles by van der Waals forces [68]. However, this effect was seen to be not apparent, when formulated in suspension, again possibly due to expedited tear drainage caused by additional fluid. The improvement in preocular retention with the PLGA NM tablet was not statistically significant after 30 min.

Among all the formulations, the best preocular retention was observed with a PLGA/PEG NM tablet. The average percentages of remaining microparticles were 73%, 39%, 19% and 13% at 10 min, 30 min, 60 min and 90 min, respectively. Notably, these dramatic increases in retention were statistically significantly different from all other formulations tested in this work ($p < 0.05$). As compared

with the PLGA/PEG NM suspension, the PLGA/PEG NM tablet exhibited 4.8−, 5.5−, 4.5− and 4.8−fold increases in preocular retention at 10 min, 30 min, 60 min and 90 min, respectively. This result implied the apparent effect of tablet dosage form, which avoided rapid tear drainage often observed with suspensions and thus, eventually aided mucoadhesion of the PLGA/PEG NM on the eye surface [69, 70].

To examine the preocular distribution of the microparticles, a whole rabbit eye was fluorescently imaged at schedule intervals after topical administration of each of the eight different microparticle formulations. The anterior surface of the eyeball and lower fornix were exposed for imaging (Figure 3.2). The upper fornix was not imaged since almost no microparticles were seen after administration. Figure 3.14 shows the results, which were consistent with those from quantitative analyses in Figure 3.13. The suspensions did not show much of remaining microparticles on the eye surface (Figure 3.14(a)). Most of the microparticles appeared to be spilled over from the preocular surface and accumulated to the hairy region near the lacrimal duct due to the fluid addition. Although administered in a tablet dosage form, PLGA MS did not seem to adhere well to the preocular surface (Figure 3.14(b)). However, either mucoadhesion or nanostructured surface appeared to improve preocular retention of the microparticles to some extent. The PLGA/PEG MS and PLGA NM, when administered in a tablet form, could be observed until 30

min after administration but most of the microparticles disappeared afterwards.

On the other hand, the PLGA/PEG NM tablet exhibited the highest visibility of the microparticles until 30 min after administration. The microparticles could be seen at the preocular surface for up to 90 min, which disappeared almost completely at 120 min. The microparticles remaining on the preocular surface were found mostly in the lower fornix since the lower fornix was the initial site of administration, where the microparticles were likely to stay.

To achieve the goal of both prolonged preocular retention and potential application for controlled drug delivery, we propose the physical means of microparticle design, i.e., the nanostructured microparticles, in this work. An increased surface area, along with mucoadhesiveness, would allow better interaction of the NM with the mucus layer of the eye. In this work, the PLGA/PEG NM, when formulated in a dry tablet, showed the best preocular retention with the rabbits. Although not being fully translatable to human eyes, the results in this work suggest that the large surface area originated from nanostructure indeed play a significant role on preocular retention of microparticles. The agglomerated nanofibers in each of the NM were not seen to be disassembled in aqueous media and thus, the NM as a whole were envisioned as drug carrier, staying at the preocular surface for a long time and releasing drug into the tear fluid in a sustained manner.

Previously, the microparticles of disc shape also implied the importance of particle morphology on preocular retention [29].

The surface area-to-volume ratios of the microspheres (α) and microdiscs (β) can be calculated by the following equations:

$$\alpha = \frac{4\pi r^2}{\frac{4}{3}\pi r^3} = \frac{3}{r} \qquad \beta = \frac{2\pi r^2 + 2\pi r h}{\pi r^2 h} = 2(\frac{1}{h} + \frac{1}{r})$$

where r and h are a particle radius and disc height, respectively. We assumed a microdisc in shape of a cylinder.

Therefore, the increase in surface area-to-volume ratio for a microdisc can be given by the equation:

$$\frac{\beta}{\alpha} = \frac{2}{3}(1 + \frac{r}{h})$$

In the previous study, the average radius and height of the microdiscs were about 1.6 μm and 1 μm, respectively[29], which, therefore, would give about a 1.7-fold increase in surface area-to-volume ratio, as compared with the spherical microparticles.

On the other hand, the NM prepared in this work exhibited more than a 10-fold increase in specific surface area (Table 3.2), which can also represent the same fold increase in surface area-to-volume ratio. Therefore, when formulated in a rapidly-dissolving dry tablet, more than 70% of the NM could still remain 10 min after administration and more than 10% could still be detected until 90 min (Figure 3.13). Meanwhile, for the previous microdics, the best

retention was about 40% 10 min after administration and almost none remained after 60 min [29].

Therefore, under the same condition employed for *in vivo* preocular retention test, the NM could reside on the eye surface better than the microdiscs. Recently, the inorganic microparticles coated with nanowires exhibited better adherence to the mucus layer or cell membranes[68, 71], which also proved that an enlarged surface area play a significant role for enhanced microparticle reaction with the biological surface in contact. On the other hand, most of the nanostructured microparticles in the previous studies were purposed to increase the loading efficiency of specific biological compounds or control their release by modulating their surface area [72, 73].

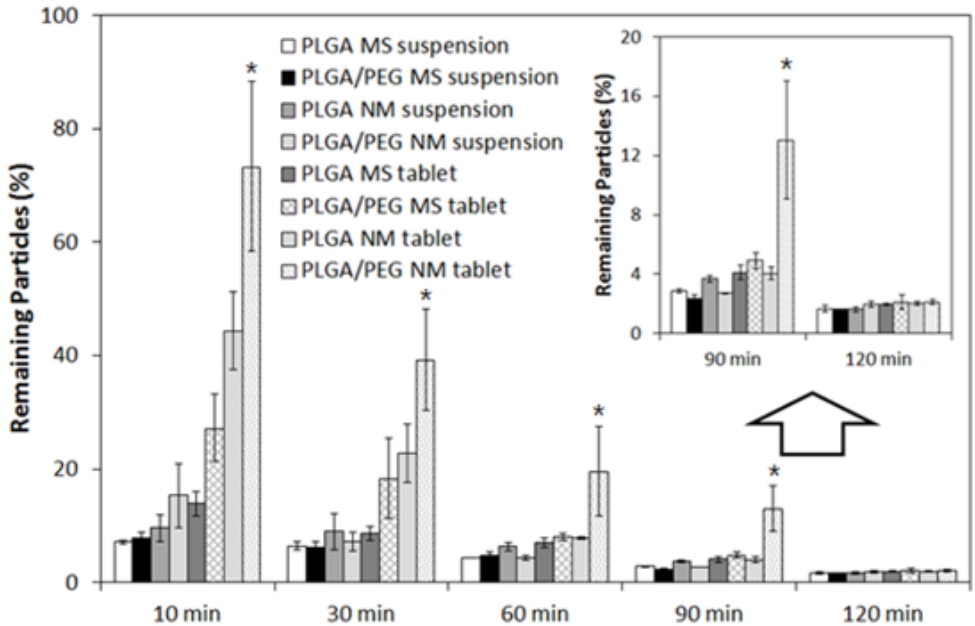

Figure 3.13. *In vivo* preocular retention of microparticles on the rabbit eye. The percentages of microparticles left on rabbit eyes were measured with eight different microparticle formulations at scheduled intervals after administration. *At 10, 30, 60 and 90 min, PLGA/PEG NM tablet was statistically significantly different from all other formulations ($p < 0.05$).

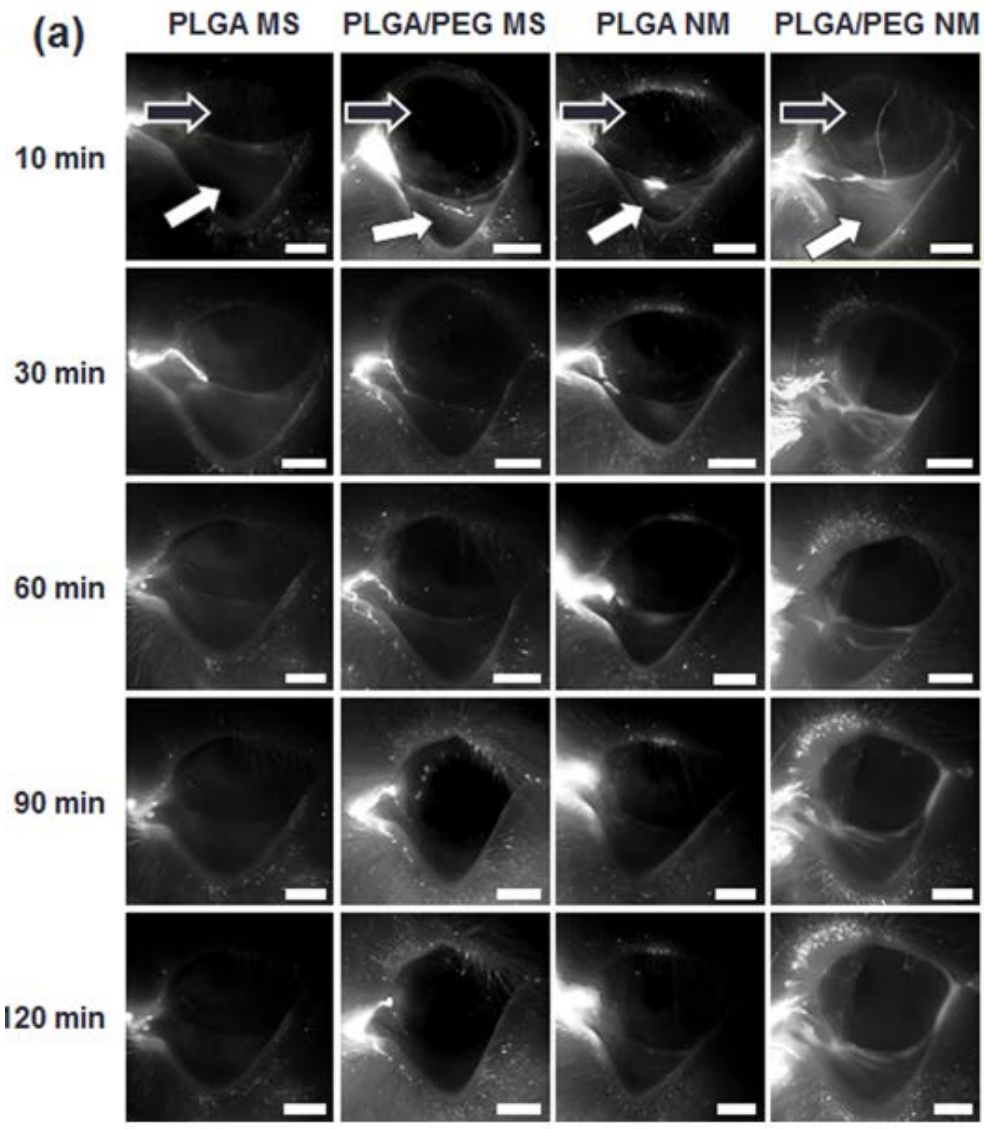
(a)
PLGA MS
PLGA/PEG MS
PLGA NM
PLGA/PEG NM
10 min
30 min
60 min
90 min
120 min

(Continued)

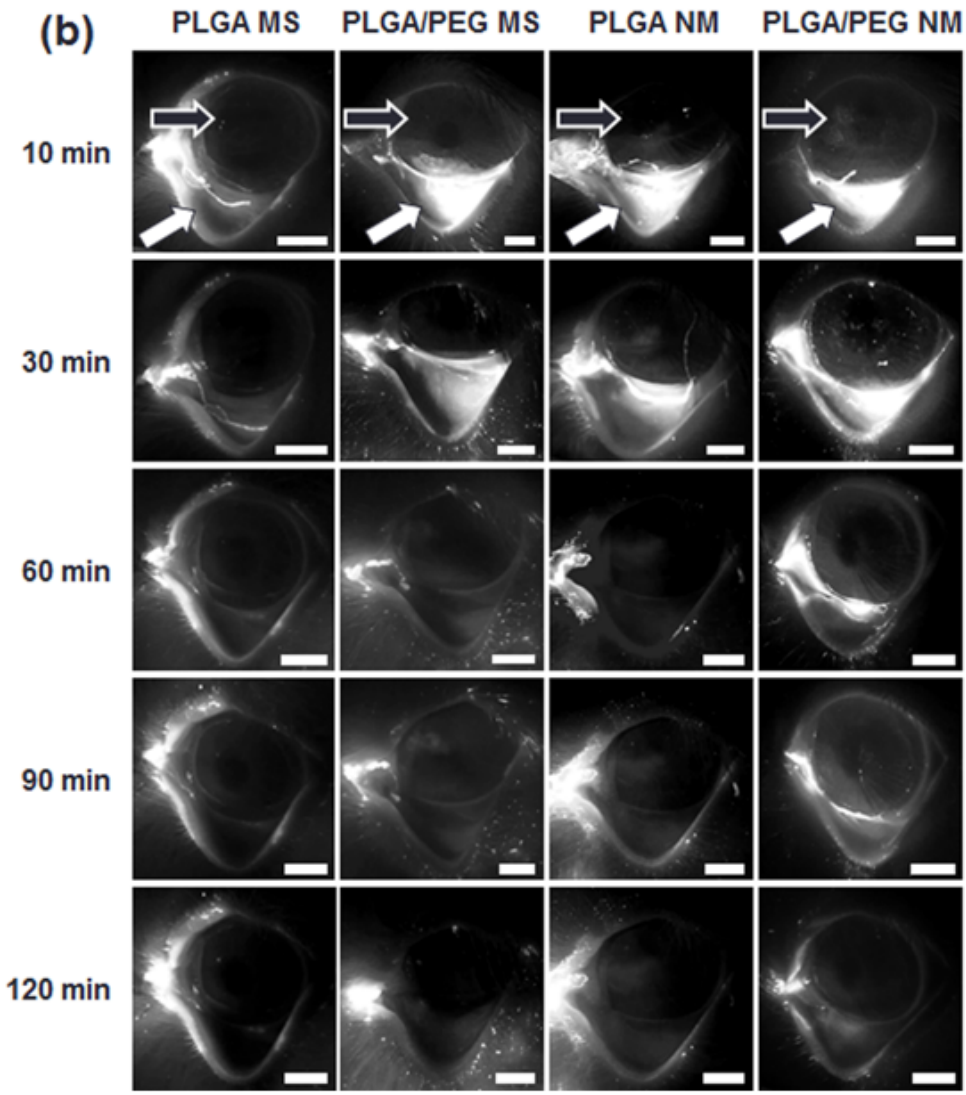

Figure 3.14. Fluorescence images of Nile Red loaded microparticles remaining on the preocular surface of rabbits were obtained at scheduled intervals after administration of each of the four different (a) suspensions and (b) tablets. The black and white arrows indicate the locations of the eyeball and exposed lower fornix of the rabbit eye, respectively. Scale bars = 5 mm.

3.3.4 *In vivo* IOP-lowering Study

To assess the extent and periods of activity of BRT, we measured the IOP of the rabbit eye and evaluated the IOP percentage decrease over time after the installation of each of the formulations containing BRT: Alphagan P (marketed formulation), BRT solution, BRT tablet, PLGA MS tablet, PLGA/PEG MS tablet, PLGA NM tablet, and PLGA/PEG NM tablet. As shown in Figure 3.15, both Alphagan P and the BRT solution exhibited the IOP-lowering effect for 5 h, with a maximum IOP decrease at 2 h post-dose [74]. The IOP decrease in Alphagan P was a little higher than that in the BRT solution due to the presence of a preservative, Purite, in Alphagan P. Purite is known to increase the pH of the formulation (Alphagan P) and the proportion of unionized BRT, resulting in increased absorption of BRT into the eye and an elaborated decrease in IOP [54]. The IOP continued to decrease in the BRT tablet for another 1 h (i.e., for 6 h) due to the increased tear viscosity caused by PVA. The PLGA MS tablet, PLGA/PEG MS tablet, and PLGA NM tablet showed a prolonged IOP-lowering effect for 8–9 h, which was attributed to the preocular retention of microparticles for at least 10 min to release BRT in rabbit tears. The best IOP-lowering effect, which was for up to 12 h, was observed with the PLGA/PEG NM tablet. This could be ascribed to a prolonged residence time of PLGA/PEG NM accompanied by the sustained delivery of BRT at the preocular surface (Figure 3.13) and hence the higher bioavailability of BRT.

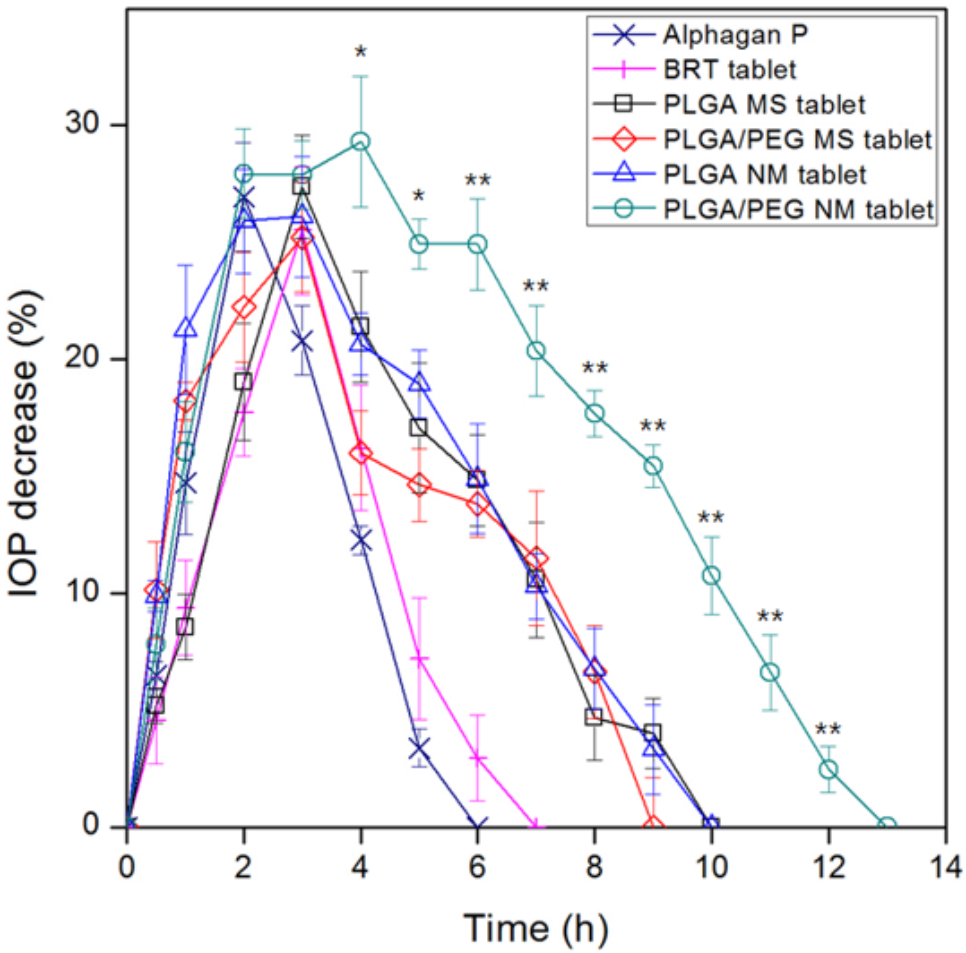

Figure 3.15. Percent decrease in intraocular pressure over time after administration of each of formulations. *PLGA/PEG NM tablet was statistically significantly different from Alphagan P at 4, 5, 6, 7, 8, 9, 10, 11 and 12 h ($p < 0.05$). **PLGA/PEG NM tablet was statistically significantly different from all other formulations at 6, 7, 8, 9, 10, 11 and 12 h ($p < 0.05$).

3.3.5 *In vivo* BRT Concentration in Aqueous Humor (AH)

The drug pharmacokinetics in AH over time after the ocular installation of each of the formulations containing BRT were evaluated with rabbits, as shown in Figure 3.16[54]. For all formulations evaluated in this study, T_{max} appeared identically at 40 min after installation. For Alphagan P and the BRT solution, the concentration of BRT in AH was drastically decreased after T_{max} (40 min) and maintained only until 3 h after installation due to increased tear volume by eye drops and thus the rapid clearance of BRT on the preocular surface. A higher C_{max} was observed in Alphagan P (0.997 μg/ml) than in the BRT solution (0.692 μg/ml) due to the presence of the preservative, Purite. Thus, a higher AUC was obtained in Alphagan P (1.013 μg·h/ml) than in the BRT solution (0.795 μg·h/ml). For the BRT tablet, BRT was observed in AH for another 2 h (i.e., 5 h) with a decrease in C_{max} (0.793 μg/ml); thus, a similar AUC was obtained in the BRT tablet (1.136 μg·h/ml) and Alphagan P (1.013 μg·h/ml). For the PLGA MS tablet, PLGA/PEG MS tablet, and PLGA NM tablet, the BRT concentration was also maintained for 5 h with a significantly increased concentration of BRT at 5 h (0.0385 μg/ml, 0.0292 μg/ml, and 0.0326 μg/ml for the PLGA MS tablet, PLGA/PEG tablet, and PLGA NM tablet, respectively), as compared with the BRT tablet (0.01433 μg/ml). Thus, it enhanced AUC by about 30% (1.300 μg·h/ml, 1.388 μg·h/ml and 1.380 μg·h/ml for

the PLGA MS tablet, PLGA/PEG MS tablet, and PLGA NM tablet, respectively), as compared with Alphagan P (1.013 μg·h/ml). This sustained concentration of BRT in AH and the enhanced AUC from these microparticles could be explained by the sustained and continuous delivery of BRT in rabbit tears from microparticles remaining on the preocular surface. The PLGA/PEG NM tablet showed the best result in terms of the concentration of BRT in AH, where BRT was detected until 7 h after administration and a more than 2-fold increase in AUC (2.078 μg·h/ml), compared with Alphagan P (1.103 μg·h/ml), was observed. This result could be accepted, in that, unlike other types of microparticles, a significant number of PLGA/PEG NMs resided on the preocular surface at and after 60 min, continuously releasing BRT in the rabbit tears. Thus, despite the continuous dilution caused by tear turnover, the BRT concentration in rabbit tears could be maintained, resulting in the higher bioavailability of BRT.

BRT has been used for the treatment of ocular hypertension and glaucoma and extensively studied due to its potential neuroprotective effect [43, 44]. Despite these benefits, Alphagan P, the marketed product of BRT, is often limited in clinical use to some extent due to its drug usage (three times a day) and hence patients' low adherence to the regimen. For better patient adherence and thus treatment, dosing frequency should be reduced to once or twice per day while retaining the same therapeutic effect. In this respect, the PLGA/PEG NM tablet exhibited sustained concentration and BRT

absorption in AH (7 h and 2.078 μg·h/ml, respectively), twice that of Alphagan P (3 h and 1.013 μg·h/ml, respectively) (Figure 3.16 and Table 3.4). The IOP-lowering effect also increased by more than 2-fold in the PLGA/PEG NM tablet (12 h) as compared with Alphagan P (5 h) (Figure 3.16).

Table 3.4. Pharmacokinetic parameters of BRT concentration in aqueous humor after administration of each of the formulations.

Formulation	Cmax (μg/mL)	t_{max} (hr.)	AUC (μg · h/mL)
Alphagan P	0.997	0.667	1.013
BRT solution	0.692	0.667	0.795
BRT tablet	0.793	0.667	1.136
PLGA MS tablet	0.834	0.667	1.300
PLGA/PEG MS tablet	0.910	0.667	1.388
PLGA NM tablet	1.004	0.667	1.380
PLGA/PEG NM tablet	1.201	0.667	2.078

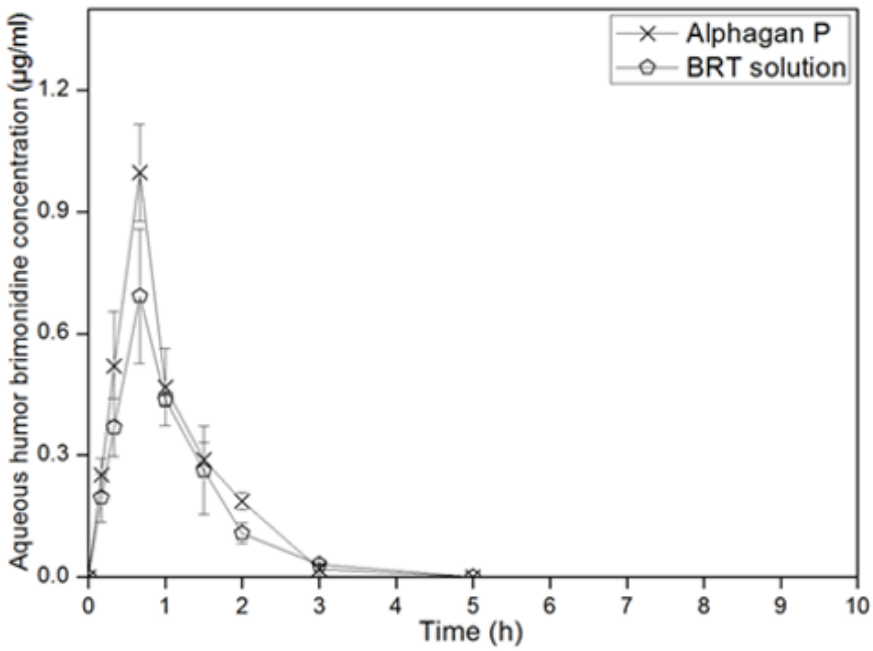

(a)

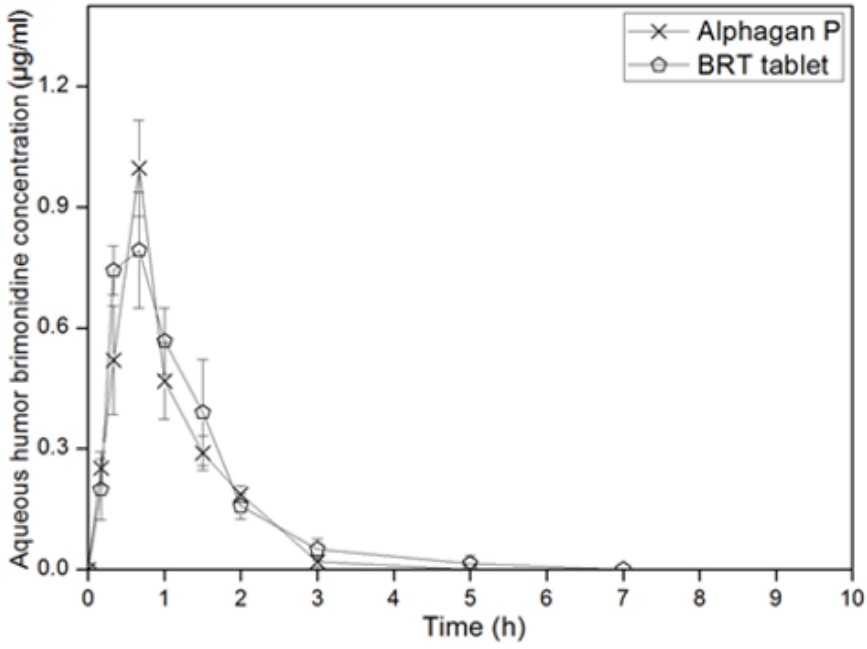

(b)

(Continued)

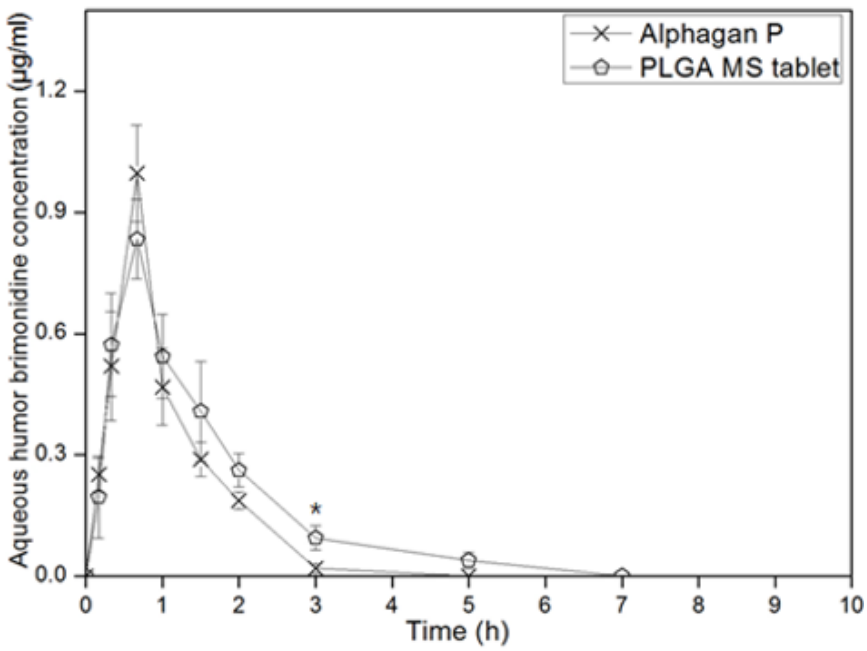

(c)

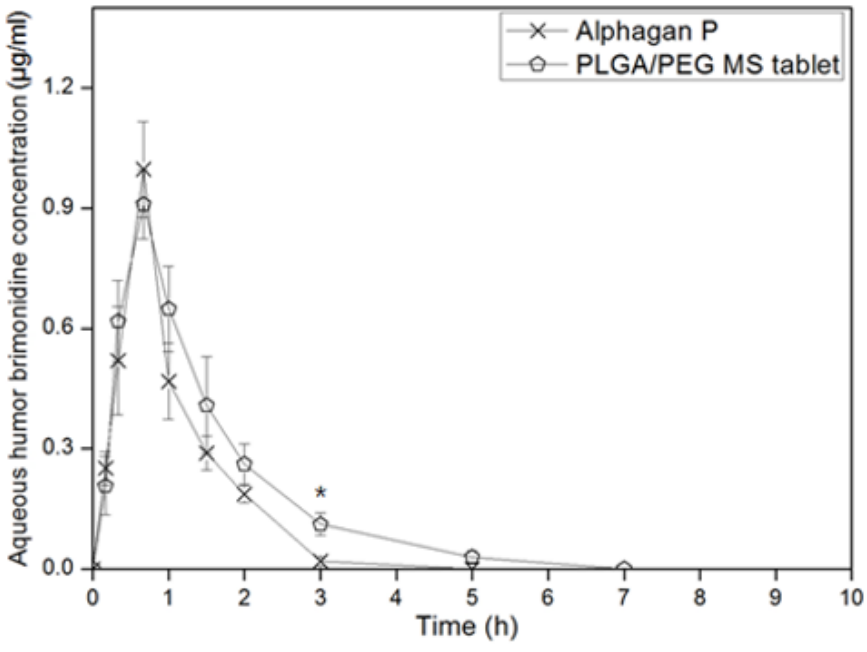

(d)

(Continued)

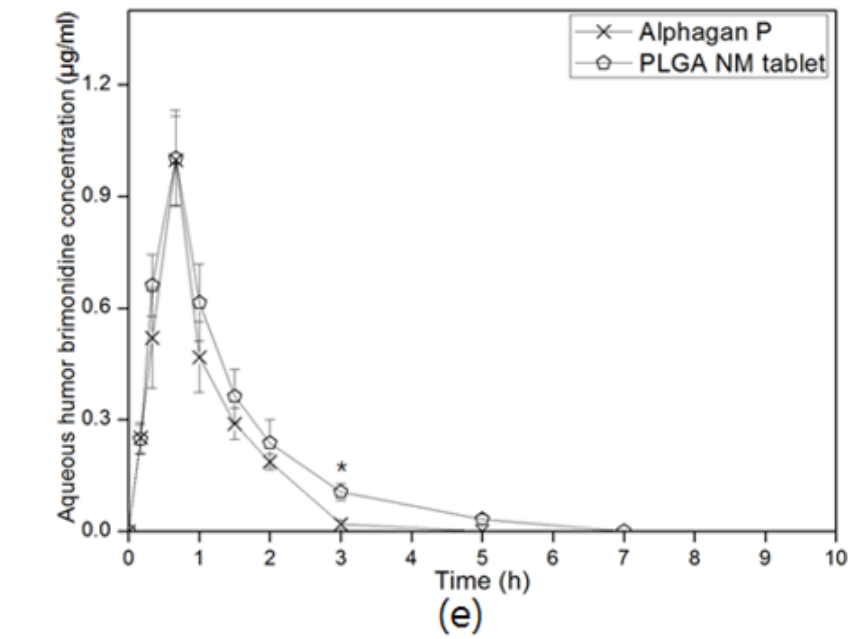

(e)

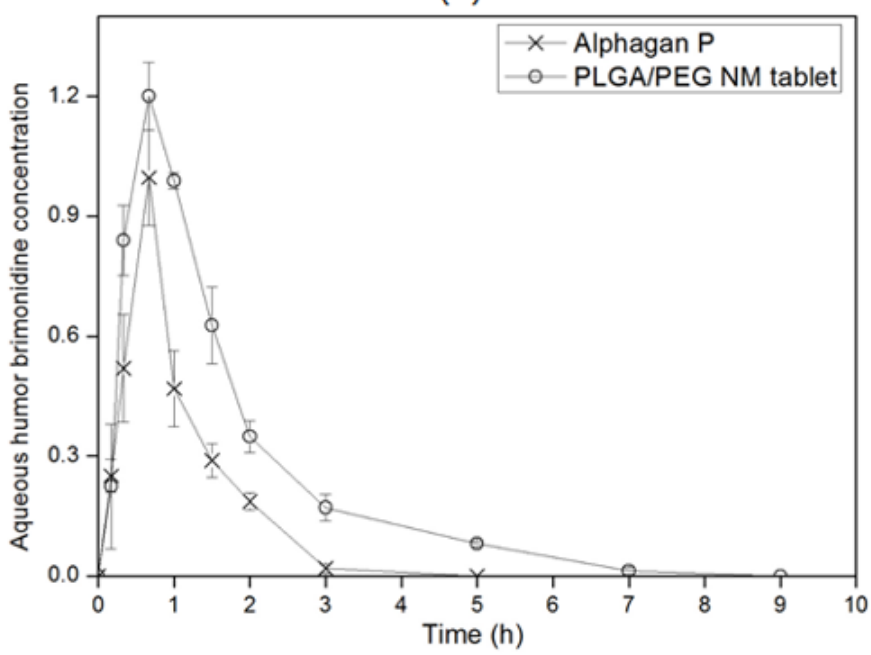

(f)

Figure 3.16. Comparison of BRT concentration in the Aqueous Humor over time with Alphagan P after administration of each of formulations.

3.3.6 Safety Evaluation

We evaluated any changes in the pH levels of rabbit tears after the administration of the PLGA/PEG NM tablet, where an increase or decrease could have an adverse effect. The pH levels of rabbit tears seemed to range between 7 and 8 and remained unchanged after administration, suggesting that no adverse side effect (Figure 3.17) was triggered by the change of microparticles upon installation. In addition, the rabbit eyes were examined by a professional ophthalmologist at scheduled times after administration of the PLGA/PEG NM tablet (Figure 3.18). During the follow-up period, there were no significant complications other than very mild conjunctival injection on the eyes treated with the PLGA/PEG NM tablet. The mild conjunctival injection was also observed in the contralateral normal (sham) eyes, which could be ascribed to dryness when the eye was left open during general anesthesia. The variance in intraocular pressure (IOP) was minimal for one day after administration of the PLGA/PEG NM tablet. The IOP was measured to be 16.8 ± 1.4 mmHg, which could be considered normal for the rabbit eyes [75, 76]. The cytotoxicity test also revealed that the PLGA/PEG NM tablet was not cytotoxic (Figure 3.19) and hence, can be considered a safe formulation.

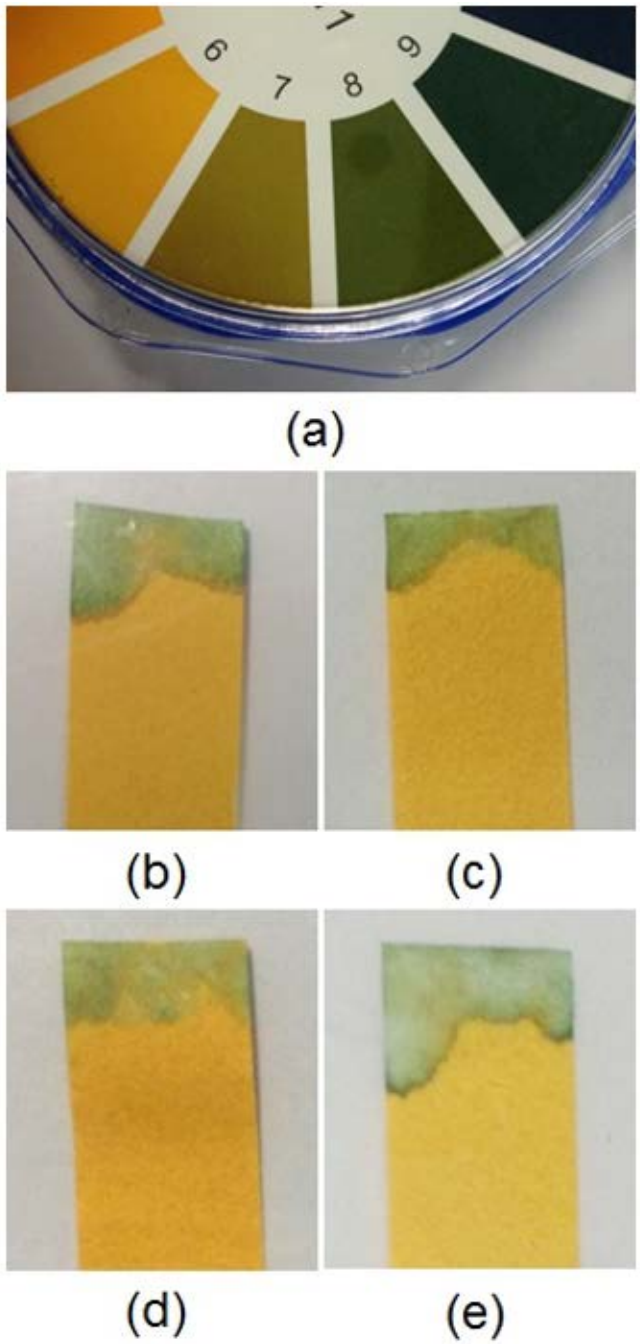

Figure 3.17. Representative images of pH test papers for monitoring of pH in rabbit's tear (a) before, (b) 10min, (c) 30min and (d) 60min after administration of PLGA/PEG NM tablet.

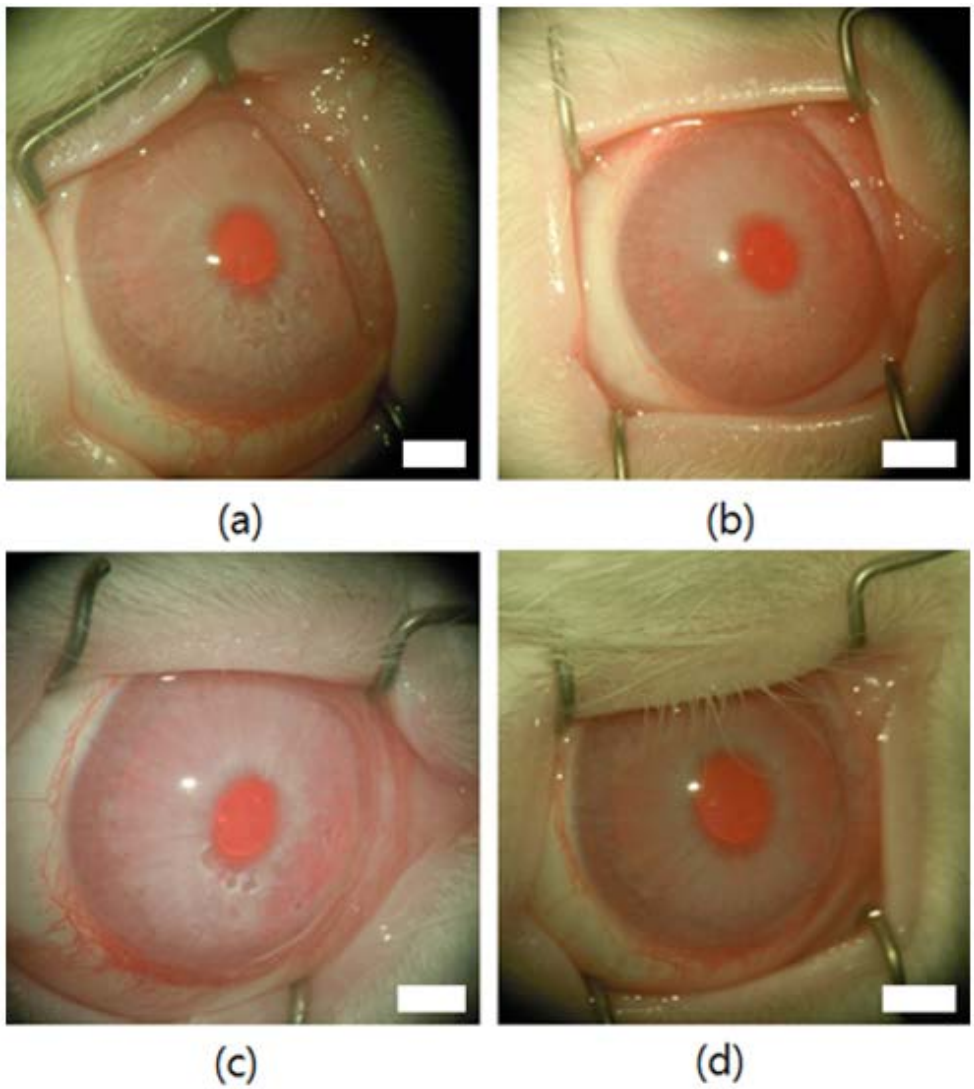

Figure 3.18. Representative images of rabbit eyes for safety evaluation of PLGA/PEG NM tablet. The images were obtained (a) before administration, (b) 1 h, (c) 2 h and (d) 24 h after administration. Scale bars = 5 mm.

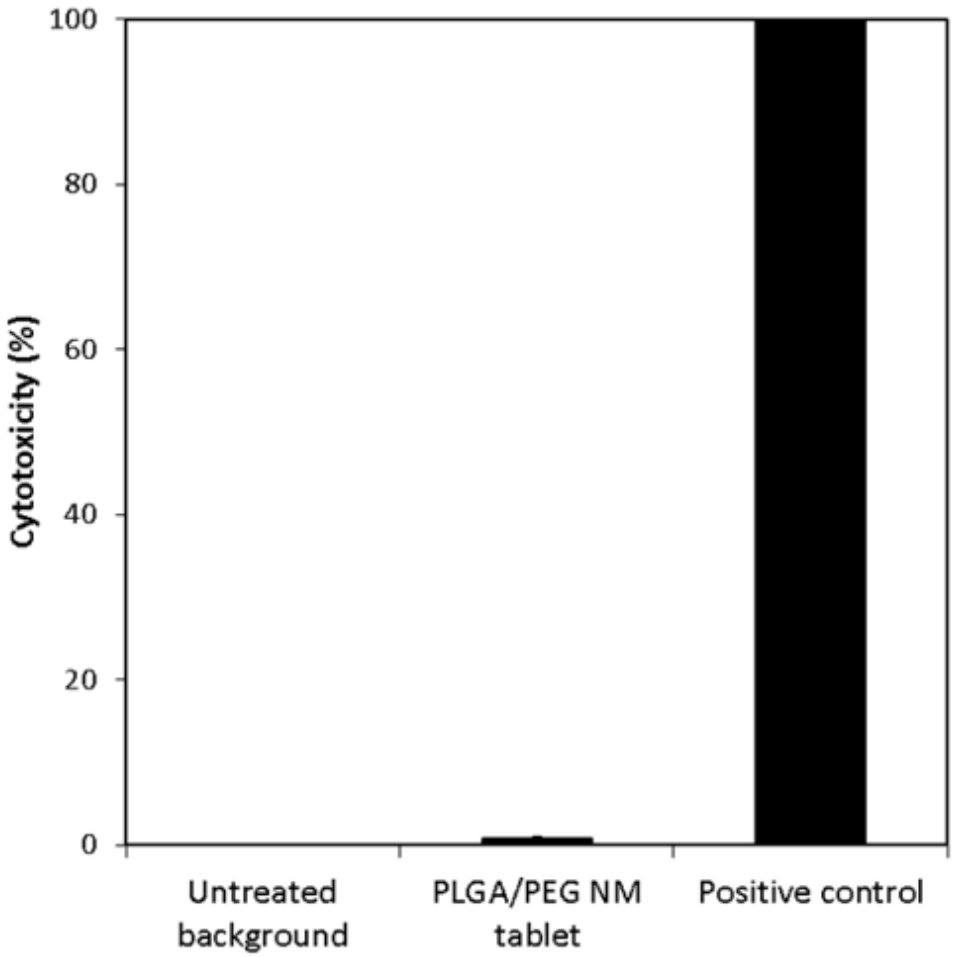

Figure 3.19. Cytotoxicity test results, revealing that the PLGA/PEG NM tablet was not cytotoxic (cytotoxicity % = ~ 0.8%).

3.4 Conclusion

In this work, we suggest the mucoadhesive, nanostructured microparticles for their prolonged preocular retention. The nanostructured microparticles can possess the enlarged specific surface area purposed for better interaction of the microparticles with the preocular mucus surface. In this work, the nanostructured microparticles were prepared simply by milling the nanofibrous sheets to give the entangled nanofibers in each of the microparticles, which exhibited a more than 10-fold increase in specific surface area, as compared with the conventional spherical microparticles. The nanostructured microparticles with an added mucoadhesion promoter can adhere better to the mucus layer of the eye. This interaction can be synergistically enhanced by a rapidly-dissolving dry tablet formulation, which can increase the tear viscosity and also avoid rapid clearance of the microparticles by not giving additional fluid. Thus, the *in vivo* animal experiment revealed that the best preocular retention could be obtained with the PLGA/PEG NM tablet among all formulations and types of microparticles tested due to the synergetic effect of the high surface area and mucoadhesion. While residing on the preocular surface, the microparticles could release the encapsulated drug, BRT, to the surface of the eye in a sustained manner, allowing more of the drug to be absorbed. Accordingly, the PLGA/PEG NM tablet exhibited the most drug absorption as well as the best IOP-lowering effect (12 h) among all formulations and types

of microparticles, including Alphagan P (marketed product of BRT; 5 h), tested in this work. Therefore, we conclude that the nanostructured microparticles containing mucoadhesive polymer in a rapidly-dissolving dry tablet is a novel system for topical drug delivery to the eye.

Chapter 4

A Nanofibrous Sheet-based System for Linear Delivery of Nifedipine

4.1 Introduction

Oral drug delivery systems have been widely accepted due to ease of administration, avoiding a chance of pain or infection possibly involved with needle-based injection [77, 78]. Among diverse types of commercialized drug-delivery products, more than a half of them are designed for an oral administration route [79]. Most oral drug delivery systems were developed to sustain or delay drug release over time, hence enhanced drug bioavailability as well as reduced side effects. Numerous types of drug delivery systems, employing

compressed tablets [80–82], floating dosage forms [83, 84] or microparticles [85, 86], have been investigated, where the drug is slowly diffused via the encasing matrix of biocompatible polymer. In this way, dosing frequency can be reduced, enhancing patients' compliance and acceptance of drug therapy [87].

However, those systems are limited in highly controlled drug delivery since the release pattern is governed mainly by Fickian diffusion. Thus, the drug is released faster at the early stage than the later stage in most cases. In addition, the acquired release patterns might be susceptible to change due to variations in pH, gut motility and food present through the GI tract [88]. For these reasons, controlled delivery of drugs, such as anti–inflammatory, anti–angina or anti–hypertension drugs, would be difficult, where a delivery profile with a constant release rate, i.e., a linear release pattern, is mostly desirable[89]. To resolve this problem, numerous approaches were made, employing more sophisticated delivery systems, such as gastro–retentive matrix[90] and three–dimensionally printed tablets[91, 92], which, however, may still limit their scope in applications. For example, the gastro–retentive matrix would be effective only for the drugs preferentially absorbed in the proximal part of the gastrointestinal (GI) tract. The three–dimensionally shaped tablets would require a slow and complicated fabrication process, which might be considered infeasible in perspectives of large–scale production.

One of the successful strategies for linear drug release is an

osmotic-controlled release oral delivery system (OROS) [89, 93]. Unlike passive diffusion, the osmotic pressure of water actively pushes the drug through an orifice in nano- or micro-scale formed in the capsule. Therefore, as long as a bodily fluid (i.e., water) is present, the OROS can deliver the drug with a constant release rate with high reproducibility regardless the change in condition through the GI tract. However, the OROS still posed some problems with gastric irritation and ulceration caused by unidirectional drug delivery through a narrow orifice, and GI occlusion and fecal discomfort due to a non-degradable hard shell of the OROS [93, 94]. In addition, manufacturing the OROS is somewhat intricate since a delivery orifice has to be prepared by laser-drilling for each of the individual tablets [93, 95].

To address these obstacles, we suggest a nanofibrous sheet based system for linear delivery of oral drug in this work. Nifedipine, a hypertension drug, was employed as a model drug since its approved medication prefers a linear release profile after an oral administration [96]. For controlled release of nifedipine, we fabricated the nanofibrous sheets, possessing micro-scaled pores, by the electrospinning method, which covered and sealed a compressed tablet of nifedipine or its mixture with a solubility enhancer, polyvinylpyrrolidone (PVP) [97]. In this way, the nanofibrous sheets served as a rate-limiting barrier, where various drug release profiles could be obtained according to the thickness of nanofibrous sheets. For example, without the sheets or with the thin

sheets, the drug release would be apparent at the early stage but minimal at the later stage. On contrary, with the thick sheets, the drug release would be greatly suppressed at the early stage but become apparent after a certain lag time. Thus, by combining those two differently-capped drug tablets, we were to realize linear drug release.

The nanofibrous sheets were made of poly (lactic-co-glycolic acid) (PLGA), which is a biocompatible polymer with a long biodegradation period (> 3 weeks) and only susceptible to rapid degradation at a basic condition [9]. Therefore, the nanofibrous sheet could retain its structural integrity (i.e., micro-porosity) while passing the GI tract for almost a day and thus, pH independent drug release, only moderated by the porosity of the nanofibrous sheets, would be possible. After complete drug release, only the sheets softened by water absorption would remain and be excreted, which is expected to be more acceptable than a hard shell of the OROS. In this study, a compressed drug tablet was capped with nanofibrous sheets via a simple physical assembly process, which would be desirable for large-scale production. To assess controlled delivery property of the capped drug tablets, the *in vitro* drug release test was conducted under the simulated GI condition.

4.2 Materials and Methods

4.2.1 Materials

Poly (lactic-co-glycolic acid) (PLGA; 50:50; i.v. = 0.36 dl/g) was obtained from Lakeshore Biomaterials (AL, USA). Nifedipine and polyvinylpyrrolidone (PVP) were purchased from Sigma (MO, USA) and Fluka (MO, USA), respectively. Dichloromethane (DCM) was obtained from JT Baker (NJ, USA). Tetrahydrofurane (THF) and dimethylformamide (DMF) were purchased from Daejung (Korea). Tween 20 was supplied from Amresco (OH, USA).

4.2.2 Preparation of Nanofibrous Sheets

PLGA was dissolved in the solvent mixed with DCM, DMF and THF (3:1:1, v/v/v) to prepare a 30% w/v PLGA solution[98], which was then electrospun under the following conditions (Nano NC, Korea): applied voltage; 20 kV, collector distance; 10 cm, flow rate; 0.6 ml/h. The sheets with four different thicknesses were prepared by collecting the electrospun nanofibers for 60, 120, 140 and 180 min, respectively.

4.2.3 Preparation of Drug Tablets

To prepare a drug tablet, a fine powder of pure nifedipine or a blend of nifedipine and PVP (nifedipine: PVP = 1:5, w/w) was first prepared by milling at 28000 rpm (IKA A11 basic, Brazil). The resulting powder containing 16.5 mg nifedipine was placed into a bore formed in a 7.35 mm-thick Teflon plate, which was then pressed under 321 kg/cm^2 for 60 s to give a noncapped drug tablet. The bore diameters used were 6 mm and 8 mm for the noncapped nifedipine tablet (NCT) and the noncapped nifedipine-PVP tablet (NCPT), respectively (Figure 4.1(a)).To prepare a drug tablet capped with nanofibrous sheets, the sheet was first placed on top of the flat Teflon plate (Figure 4.1(b)), on top of which a ring-shaped aligning stamp was placed. The NCPT was then placed at the center of the stamp ring (Figure 4.1(c)) and the aligning stamp was removed. After that, the NCPT was covered by another nanofibrous sheet of the same kind (Figure 4.1(d)) and slightly pressed with the aligning stamp (Figure 4.1(e)). In this way, the nanofibrous sheet on the very top was folded at a boundary of the NCPT, expressing the location of the NCPT during the rest of fabrication process. The tablet sandwiched with nanofibrous sheets was then pressed with a ring-shaped bonding stamp, pre-heated at 135℃, for 60 s (Figure 4.1 (f)). To avoid heating of the NCPT itself, a heat insulating stamp was also placed with a continuous supply of cooling air at the center of the bonding stamp. In this way, only the sheet in contact with the bonding stamp

melted and attached while the tablet aligned to the center of the stamp was not affected by high temperature (Figure 4.1(g)). Thus, we prepared four distinctly capped tablets: the NCPTs capped with 25 μm-thick sheets (25CPT), 50 μm-thick sheets (50CPT), 62 μm-thick sheets (62CPT) and 75 μm-thick sheets (75CPT).

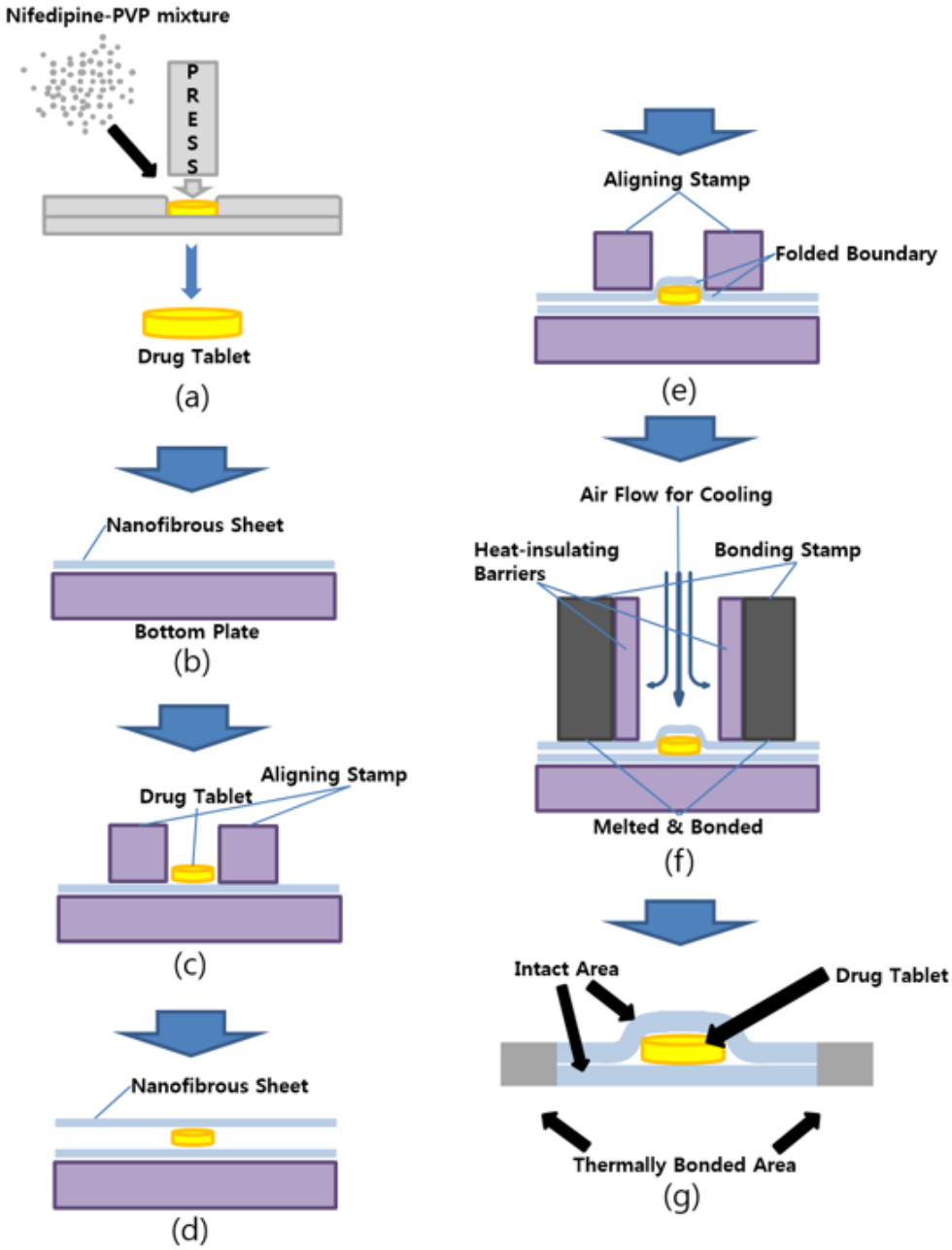

Figure 4.1. Schematic procedure for preparation of the capped drug tablets.

4.2.4 Characterization

A nanofibrous sheet was cut into a 5 mm by 5 mm piece, which was placed on a SEM sample mount and sputter coated with platinum for 10 min (208HR, Cressington Scientific, England). The sample was then imaged by SEM (7401F, Jeol, Japan).

Nanofibrous sheets (5 X 5 mm; 50 μm-thickness) were each immersed in the aqueous media buffered at pHs 1.2 and 6.8, respectively. After incubation for 1, 2 and 4 h at 37℃, the sheet was taken out, washed thoroughly with DI water and freeze-dried for more than two days to eliminate the entrapped water while retaining the morphological structure of the sheet [99]. The sheet was then imaged by SEM as described above.

To assess the pore size distribution through the nanofibrous sheets prepared in this work, the sheets of different thicknesses (25 μm, 50 μm, 62 μm and 75 μm) were each cut into a circular piece of 7.73 mm radius and loaded in a capillary flow porometer (CFP-1500AEL, PMI, NY, USA), where the flow resistance of each sheet was measured under two different conditions: 1) measuring the resistance of a sheet with hollow pores while blowing nitrogen gas, 2) measuring the resistance of a sheet pre-soaked with Galwick fluid (surface tension = 15.9 dynes/cm) while blowing nitrogen gas [100].

4.2.5 *In vitro* Drug Release Test

In vitro drug release experiment was carried out in the release media at 37℃ while continuously stirred at 125 rpm in dark room. Two distinct release media buffered at pHs 1.2 and 6.8 were employed to mimic the fluids present through the GI tract, each containing 1% Tween 20 to increase the solubility of nifedipine and thus, to keep the sink condition during the whole release experiment. For each of the tablets, the experiment was performed for 4 h at pH 1.2 and 24 h at pH 6.8. To assess the effect of pH on drug release, we compared the release profiles at both pHs obtained for up to 4 h, more than a doubled period of the gastric residence time for assurance[101].

We also examined drug release from a combination of two distinctly capped tablets, where the pH of the release media was changed to better simulate the conditions through the GI tract. Thus, the two tablets were immersed together in the release media at pH 1.2 for the first 2 h, which in turn, were moved to the media at pH 6.8 for the rest 22 h.

For all experiments, the aliquot of the release media was sampled at scheduled intervals and assayed spectrophotometrically. Each of the samples was measured in triplicate for statistics.

4.3 Results

4.3.1 Characterization of Nanofibrous Sheets

We have successfully fabricated the nanofibrous sheets of PLGA with the electrospinning method, as shown in Figure 4.2. The sheet was composed of multiple layers of electrospun nanofibers, possessing the pores in micro-size, which would serve as a diffusion path of the drug. The nanofibrous sheets of four different thicknesses (i.e., 25, 50, 62 and 75 μm-thicknesses) were prepared by varying the collection time of nanofibers. The morphologies of all nanofibrous sheets were not different since the nanofibers were collected under the same electrospinning condition employed in this work (data not shown).

However, according to the measurement with the capillary flow porometer (CFP-1500AEL, PMI, NY, USA), the change of pore size distribution was apparent as the sheet thickness varies. As shown in Figure 4.3, the pore size distribution shifted to a smaller size as the sheet thickness increased. The average pore sizes were 1.87 μm, 1.12 μm, 0.96 μm and 0.51 μm for the sheet thicknesses of 25 μm, 50 μm, 62 μm and 75 μm, respectively. This result is expected since thin nanofibrous sheets have rather larger sized voids while small sized voids should appear between distant meshes as the nanofibrous sheets get thicker [102]. The capillary flow porometer actually measures the flow resistance (i.e.,

the relations between the flow across the sheet and the pressure applied to the sheet), which is then calibrated to the pore sizes [100]. Thus, the decrease in pore size displayed by the capillary flow porometer represents the increased difficulty in flow through the nanofibrous sheet, thereby less perviousness as the sheet thickness increases.

In this study, we employed the nanofibrous sheets as a diffusion barrier of the drug, nifedipine for oral delivery, which should be equally effective even while the sheets experience the dynamic environments through the GI tract. For this reason, we purposed only the pores of the sheets to work as a drug–diffusion conduit and thus, such structural integrity should be retained regardless the change in pH. Therefore, we examined the morphology of the nanofibrous sheets after immersion in the aqueous media at two distinct pHs 1.2 and 6.8, mimicking the fluids at the gastric and intestinal cavities, respectively. As shown in Figure 4.4, a significant change in pore size of the sheets was observed in 1 h due to rapid swelling of the nanofibers due to water absorption. However, after swelling, the morphology of the sheets did not seem to change further and did not exhibit noticeable difference between pHs = 1.2 and 6.8. The sheets did not appear to be degraded for up to 4 h at all pHs since PLGA, comprising the nanofibrous sheet, is known to be degraded for a much longer period of time (> 3 weeks) [103].

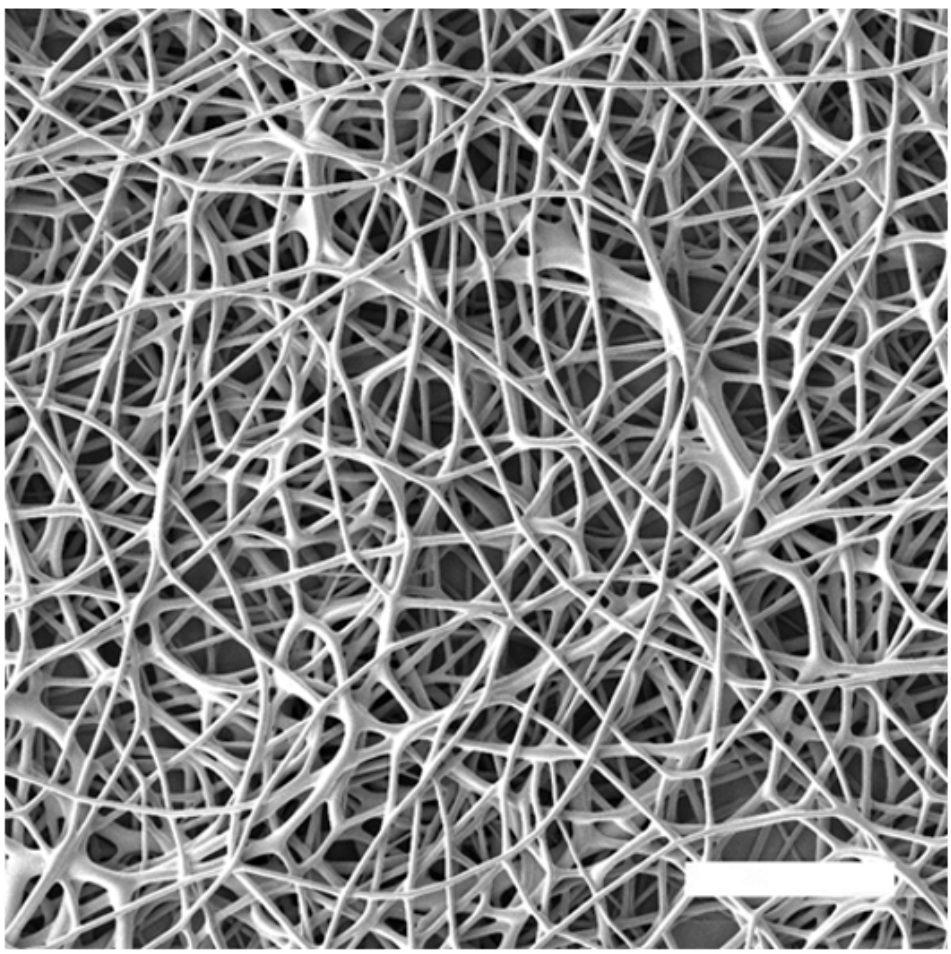

Figure 4.2. Representative scanning electron micrograph of the nanofibrous sheet. Scale bar = 30 μm.

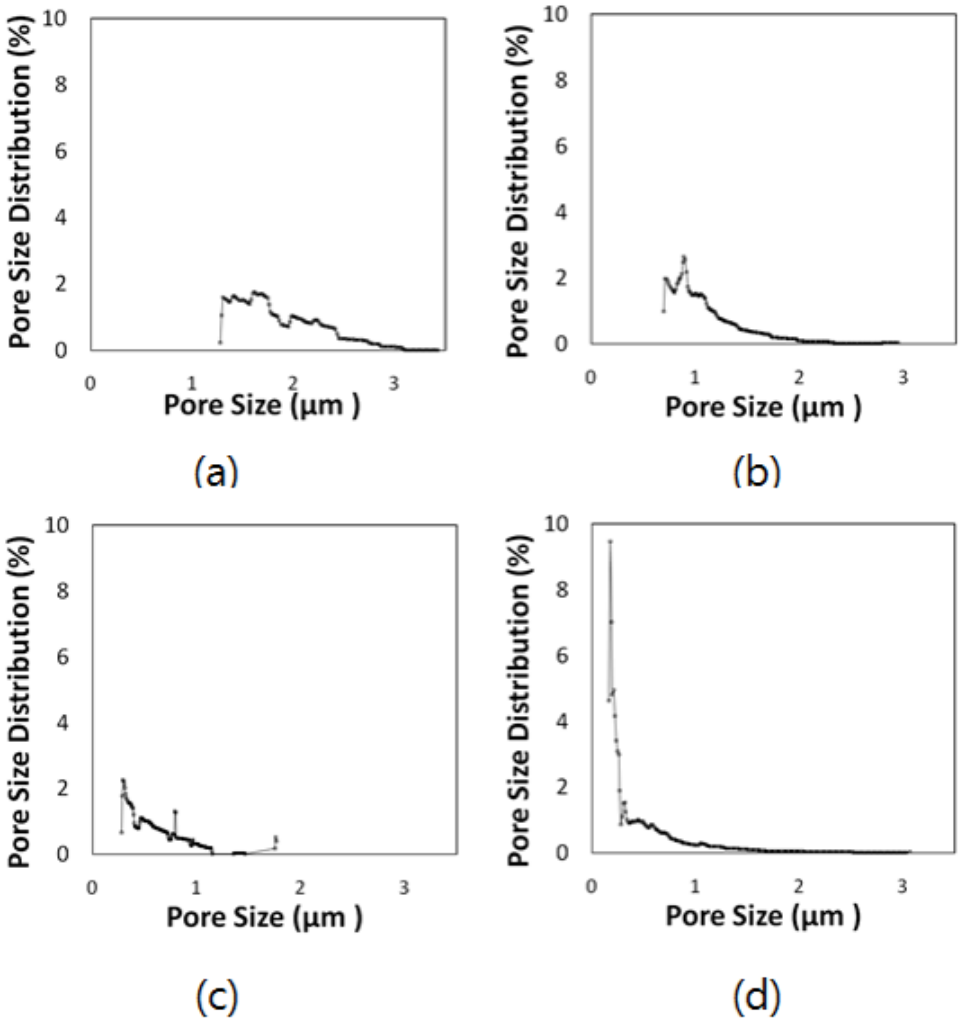

Figure 4.3. Pore size distributions of the nanofibrous sheets measured by a capillary flow porometer. The thicknesses of the sheets were (a) 25 μm, (b) 50 μm, (c) 62 μm and (d) 75 μm.

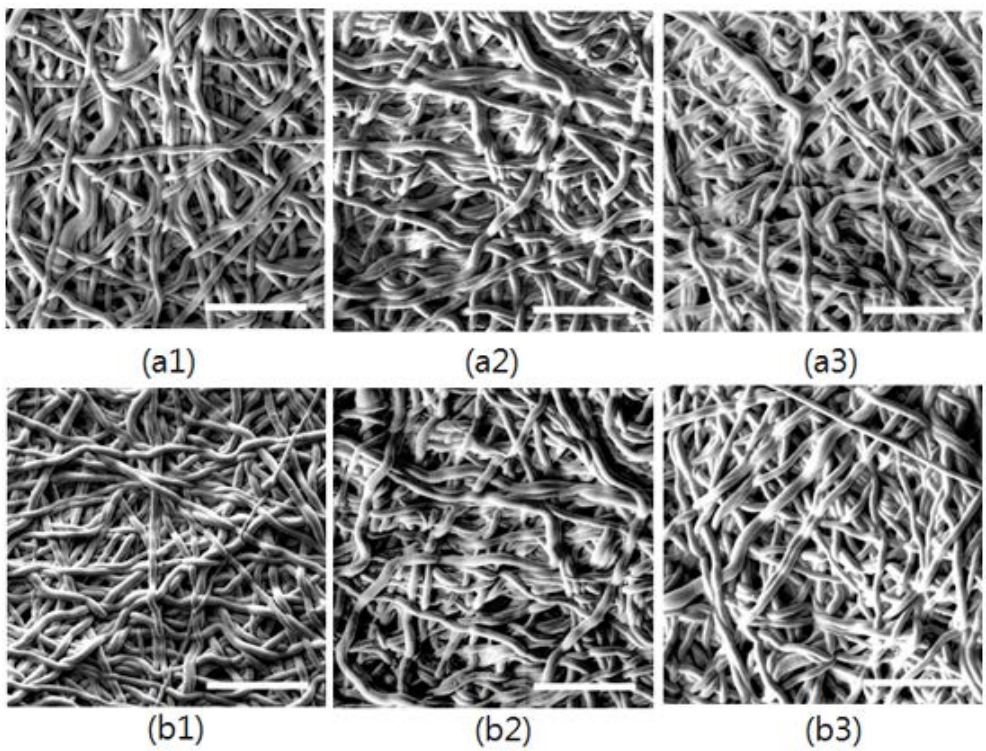

Figure 4.4. Scanning electron micrographs of the nanofibrous sheets after immersion in the aqueous media. The time for immersion and the pH of the media were (a1) 1 h, pH 1.2; (a2) 2 h, pH 1.2; (a3) 4 h, pH 1.2; (b1) 1 h, pH 6.8; (b2) 2 h, pH 6.8; and (b3) 4 h, pH 6.8. Scale bars = 20 μm.

4.3.2 Characterization of Drug Tablets

Figure 4.5 shows the noncapped and capped drug tablets prepared in this work. The NCT was 6 mm in diameter and 1 mm in height (data not shown). For the NCPT, both the diameter and the height increased to 8 mm and 1.85 mm, respectively, due to an increased mass of the tablet by incorporation of PVP (nifedipine:PVP = 1:5, w/w) (Figure 4.5(a)). The NCPTs were then capped with the nanofibrous sheets of four different thicknesses (i.e., 25 μm, 50 μm, 62 μm and 75 μm) to give 25CPT, 50CPT, 62CPT and 75CPT. All tablets prepared in this work were loaded with 16.5 mg nifedipine. Figure 4.5(b) shows the 25CPT, 22 mm in diameter and 2.1 mm in height, which encased the NCPT with the nanofibrous sheets of 25 μm-thickness.

We also examined the morphology of the nanofibrous sheets at the different locations of the capped tablet. The center portion of the capped tablet exhibited an intact porous structure (Figure 4.5(c)), indicating that the center of a ring-shaped bonding stamp was properly insulated during the thermal stamping process (Figure 4.1(f)). The nanofibrous sheets in contact with the bonding stamp appeared to be melt and firmly attached, showing a smooth surface without a fibrous structure (Figure 4.5(d)). The boundary between the intact and melted portions was also evident, as shown in Figure 4.5(e). In this way, the NCPT could be completely sealed within the nanofibrous sheets, where the drug diffusion would be determined

mainly by the intact center portion of the capped tablet (i.e., the intact nanofibrous sheets with micro-porosity).

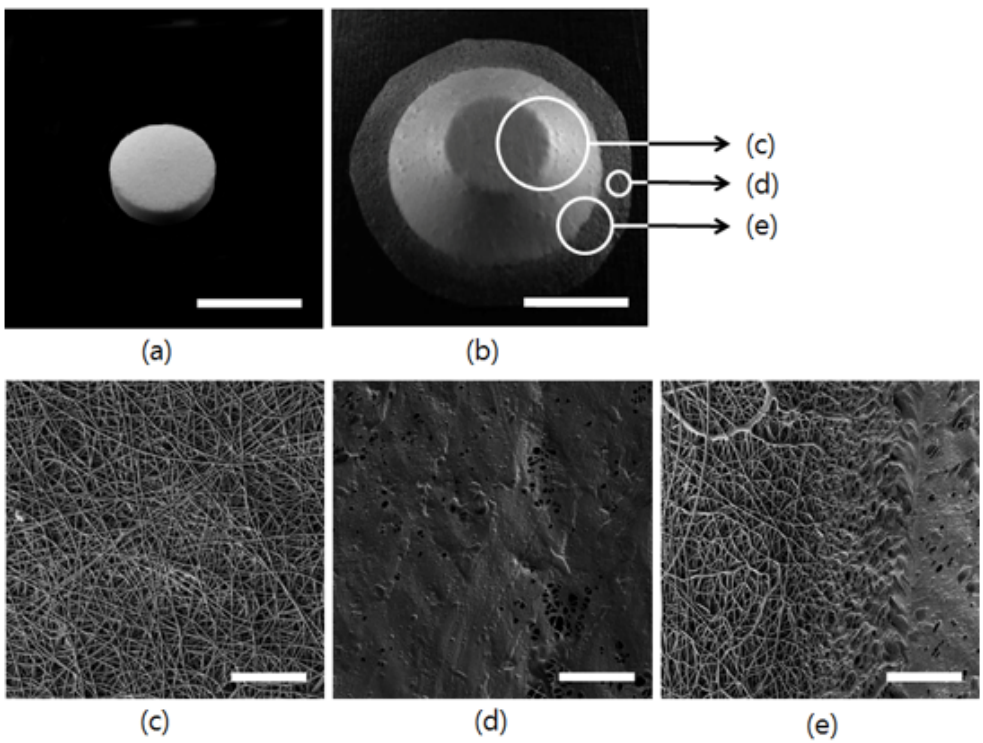

Figure 4.5. Representative optical images of (a) NCPT and (b) 25CPT. Morphologies of (c) intact portion, (d) melt portion and (e) boundary between intact and melt portions were observed using a scanning electron microscope. Scale bars = (a–b) 8 mm and (c–e) 100 μm.

4.3.3 *In vitro* Drug Release Profiles

The *in vitro* drug release experiments were conducted with the release media buffered at pHs 1.2 and 6.8 to simulate the fluids present through the GI tract. First, we tested the *in vitro* drug release profiles of the noncapped tablets. In this work, we purposed to deliver 100% nifedipine during 24 h, a known residence time of the orally administered formulation in the GI tract [88, 104]. However, this could not be achieved with the tablet composed of nifedipine only (i.e., the NCT) since the drug is known to be poorly soluble in the aqueous media (5–6 μg/ml at pH 2.2 – 10.0) [105]. Thus, we also prepared the noncapped tablet with a solubility enhancer, PVP (i.e., the NCPT) [97] to enhance drug dissolution and compared its release profile with that without PVP (i.e., the NCT). Figure 4.6 shows the release profiles of the NCT and the NCPT at pH 6.8. As expected, the drug release was not efficient with the NCT, where less than 40% drug was released during 24 h. However, with incorporation of PVP (nifedipine: PVP = 1:5, w/w), the drug release rate increased dramatically, exhibiting almost 100 % drug release during 24 h.

Although the dissolution of nifedipine was greatly enhanced, the release profile was not yet controlled since more than 40% drug was rapidly released during the first 30 min (Figure 4.6). In this study, therefore, the NCPT was capped with the nanofibrous sheets of various thicknesses to suppress such an initial burst and even to achieve a lag phase of drug release. The drug release profiles of the

NCPT and all capped tablets were examined at both pHs 1.2 and 6.8, as shown in Figure 4.7. Regardless the pH, the drug release was more retarded as the sheet thickness increased. The total percent release during the first 4 h decreased gradually from 65 – 69% to 4 – 7% as the sheet thickness increased from 0 μm to 75 μm.

We also compared the release patterns of the tablets at pHs 1.2 and 6.8. As shown in Figures 4.7 and 4.8, for each type of the tablets, similar release patterns were observed at both pHs for up to 4 h, which is more than a doubled period of the known gastric residence time [101]. It appeared that the drug release was mediated mostly by the physical structure of the sheets (i.e., porosity), which did not seem to be affected by the pH, as depicted in Figure 4.4.

We continued the drug release experiment with the NCPT and all capped tablets at pH 6.8 until 24 h. The drug release was still more retarded as the thickness of the sheets increased, as shown in Figure 4.9. Notably, with the sheets thicker than 50 μm, i.e., for 50CPT, 62CPT and 75CPT, a lag phase of drug release became evident. The lag times, where the drug release was much suppressed (< 20%), were 2, 8 and 10 h for 50CPT, 62CPT and 75CPT, respectively, which clearly increased with the sheet thickness. Notably, for all capped tablets, after a certain lag time, drug release recovered the release rate almost similar to that of the NCPT (i.e., more than 80% release during 16 h). The nanofibrous sheets appeared to work just as barrier for intrusion of aqueous bodily fluid. Thus, once the liquid connection between the outer media and the

drug core was established, drug release did not seem to be significantly mediated by highly porous nanofibrous sheets. For all tablets, almost 100% drug was released in 24 h.

In this work, we were to achieve a linear drug release profile by employing a combination of two distinctly capped tablets. As shown in Figure 4.9, the noncapped tablet or the tablet capped with thin sheets exhibited fast drug release at the early stage, which, however, slowed down afterwards. On contrary, the tablets capped with thick sheets showed facilitated drug release at the late stage but the drug release was greatly suppressed at the early stage. Therefore, with a proper combination of two different types of the tablets, the drug release at the early and late stages would be each compensated and hence, linear drug release would be possible.

We first predicted drug release from a combination of two distinctly capped tablets by simply calculating the average (arithmetic mean) of the two capped tablets at each time point, using the following equations, based on the *in vitro* drug release profiles already obtained for each of the individual tablets (Figure 4.9):

$$\mathrm{PDR(t)} = \frac{\mathrm{ODR1\ (t) + ODR2\ (t)}}{2}$$

where t is the time point (0.5–24 h); PDR(t) is the predicted drug release at time point (t); and ODR1(t) and ODR2(t) are the experimentally observed drug releases of two differently capped

tablets at time point (t).

All possible combinations of the two tablets were generated to assess the linear least square fits to their *in vitro* drug release data, where a resultant value closer to 1.000 showed better linearity of the drug release.

A total of 10 different combinations were tested: NCPT and 25CPT; NCPT and 50CPT; NCPT and 62CPT; NCPT and 75CPT; 25CPT and 50CPT; 25CPT and 62CPT; 25CPT and 75CPT; 50CPT and 62CPT; 50CPT and 75CPT; and 62CPT and 75CPT. Among those combinations, the tablets of 50CPT and 75CPT were expected to show a good correlation with linear release ($R^2 > 0.983$), as shown in Table 4.1 and Figure 4.10. To confirm this, we actually employed the two tablets of 50CPT and 75CPT and performed the *in vitro* drug release experiment. At this time, the two tablets were immersed together in the release media at pH 1.2 for 2 h and at pH 6.8 for the rest 22 h to better mimic the condition through the GI tract. Since each tablet prepared in this work was loaded with 16.5 mg nifedipine, the dose amount of two tablets became about 33 mg, which is similar to that of the marketed medication, Adalat® OROS 30 (Bayer HealthCare AG, Germany) [106]. As shown in Figure 4.11, the drug release from a combination of 50CPT and 75CPT was reproducible (i.e., similar to the predicted *in vitro* drug release profile), also exhibiting a fairly good correlation with a linear release pattern ($R^2 > 0.986$). In addition, we calculated a similarity factor, using the following equation [107], where two drug release profiles are

regarded as the same when the similarity factor is 100 and similar when the similarity factor is equal to or larger than 50. The similarity factor was 90.43 between expected drug release and actual drug release from a combination of 50CPT and 75CPT, suggesting their similar drug release patterns.

$$f_2 = 50 \bullet \log \{[1 + (1/n)\sum_{t=1}^{n}(R_t - T_t)^2]^{-0.5} \bullet 100\},$$

where n is the number of time points, and R_t and T_t are the cumulative amount of drug release from the expected and the actual combinations at the time point (t), respectively.

Table 4.1. Linear least square fits to the *in vitro* drug release data obtained with all possible combinations of two distinctly capped tablets.

Combination of two tablets	R^2
NCPT & 25CPT	0.2027
NCPT & 50CPT	0.4382
NCPT & 62CPT	0.7166
NCPT & 75CPT	0.8278
25CPT & 50CPT	0.7078
25CPT & 62CPT	0.8901
25CPT & 75CPT	0.9626
50CPT & 62CPT	0.9318
50CPT & 75CPT[a]	0.9833
62CPT & 75CPT	0.9513

[a]A fairly good correlation with linear release was expected with a combination of 50CPT and 75CPT.

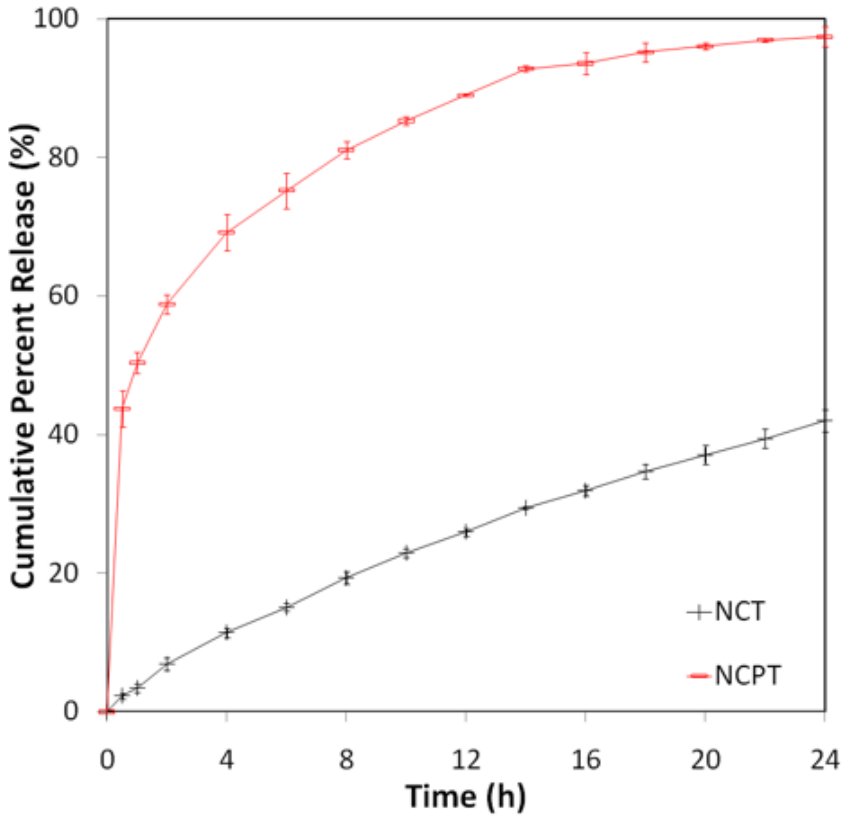

Figure 4.6. *In vitro* release profiles of nifedipine from NCT and NCPT at pH 6.8.

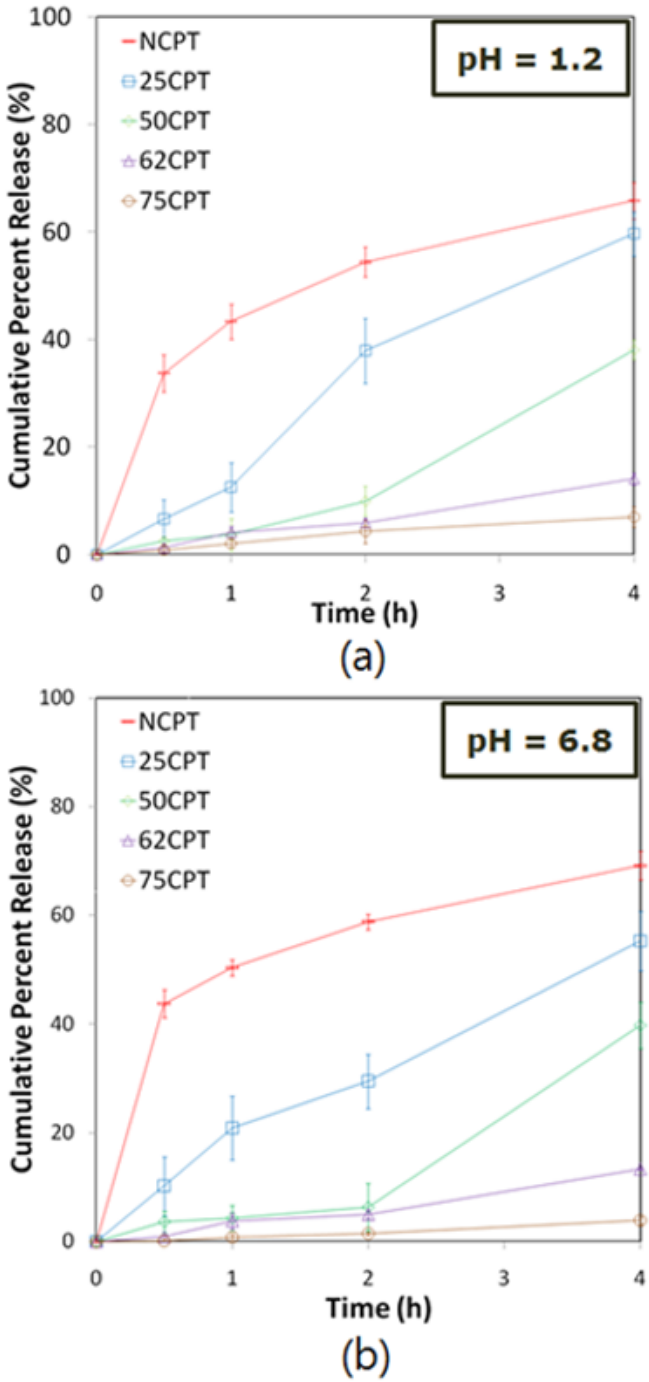

Figure 4.7. *In vitro* release profiles of nifedipine from NCPT, 25CPT, 50CPT, 62CPT and 75CPT for 4 h (a) at pH 1.2 and (b) at pH 6.8.

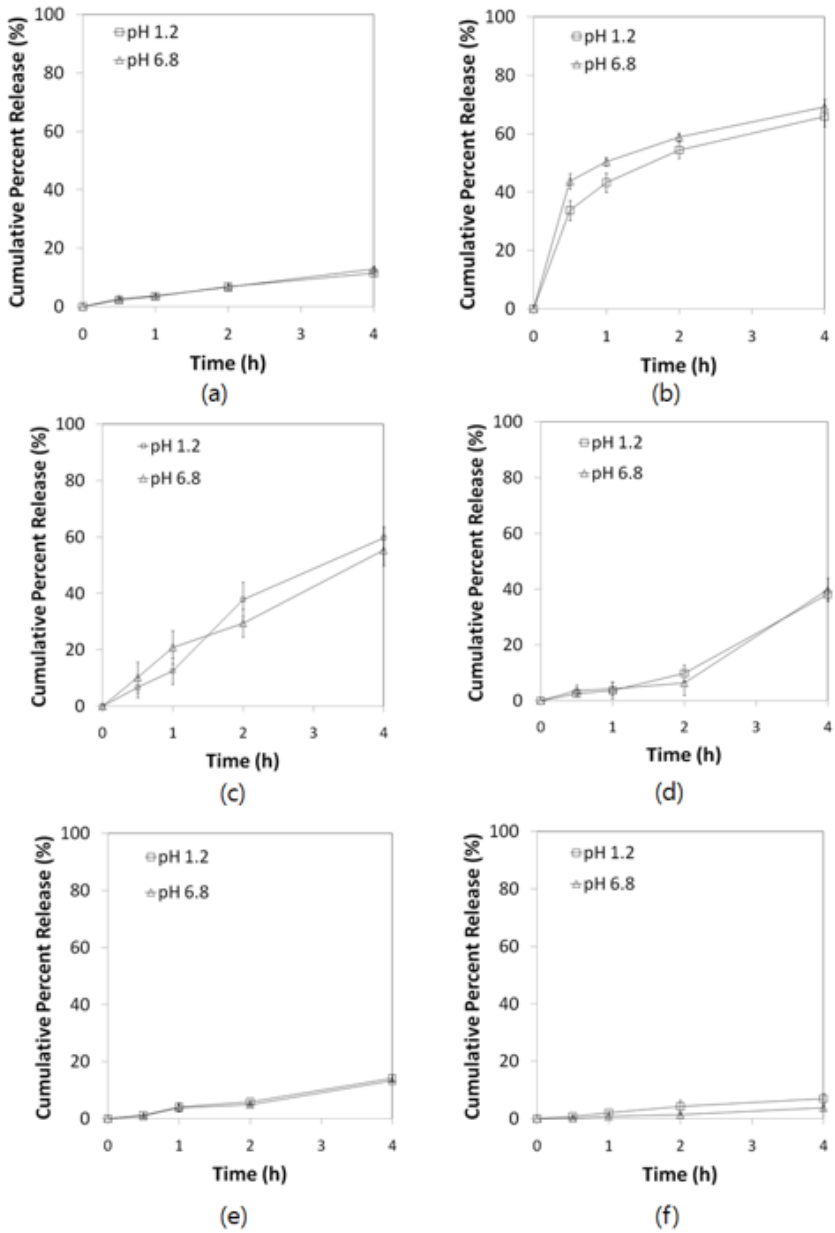

Figure 4.8. *In vitro* release profiles of nifedipine from (a) NCPT, (b) 25CPT, (c) 50CPT, (d) 62CPT and (e) 75CPT at pHs 1.2 and 6.8 for 4 h. The same graphs from Figure 4.7 were re-plotted to assess the effect of pH on drug release.

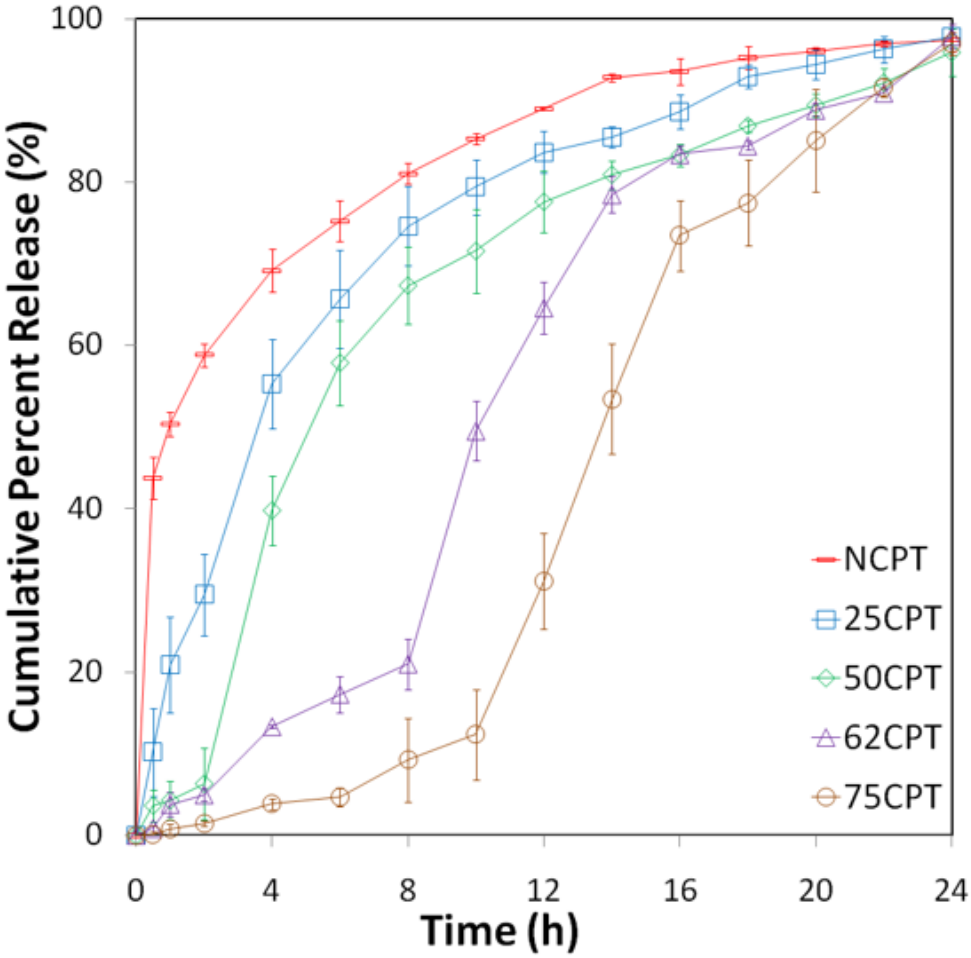

Figure 4.9. *In vitro* release profiles of nifedipine from NCPT, 25CPT, 50CPT, 62CPT and 75CPT for 24 h at pH 6.8.

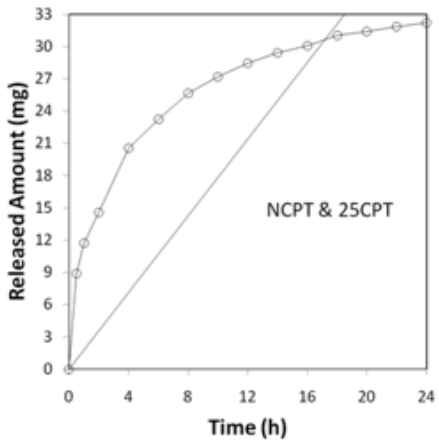

(a)

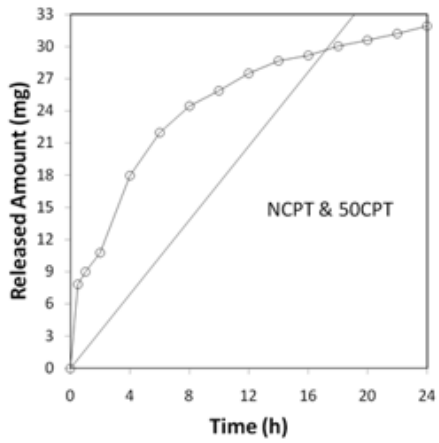

(b)

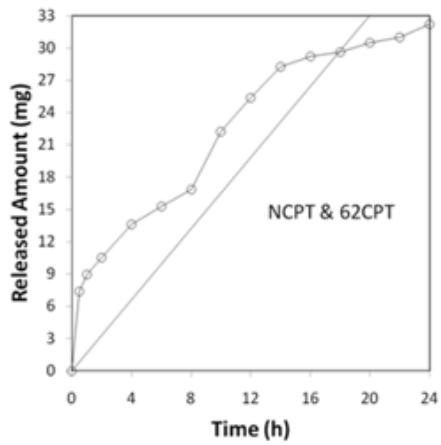

(c)

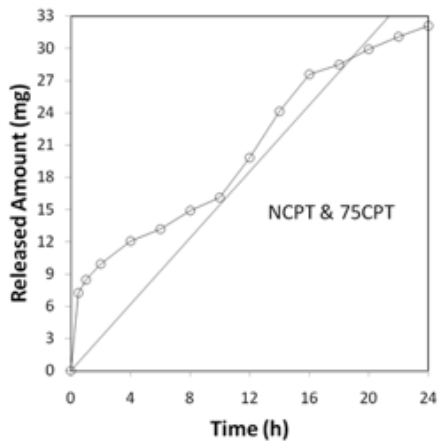

(d)

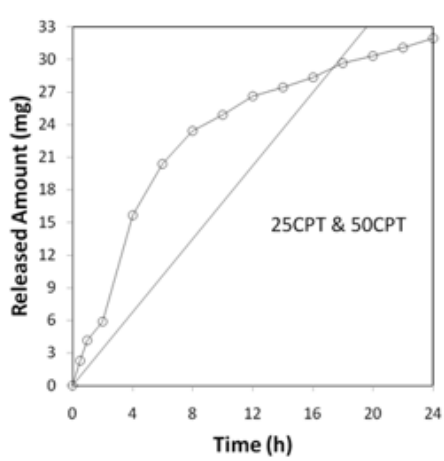

(e)

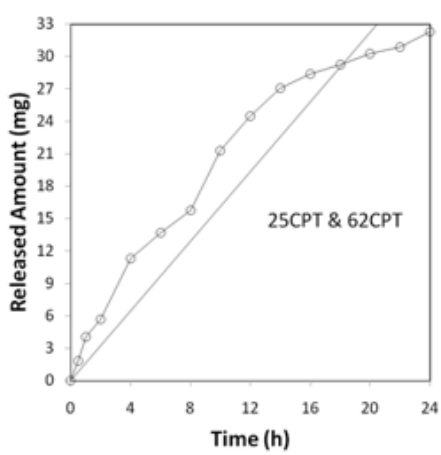

(f)

(Continued)

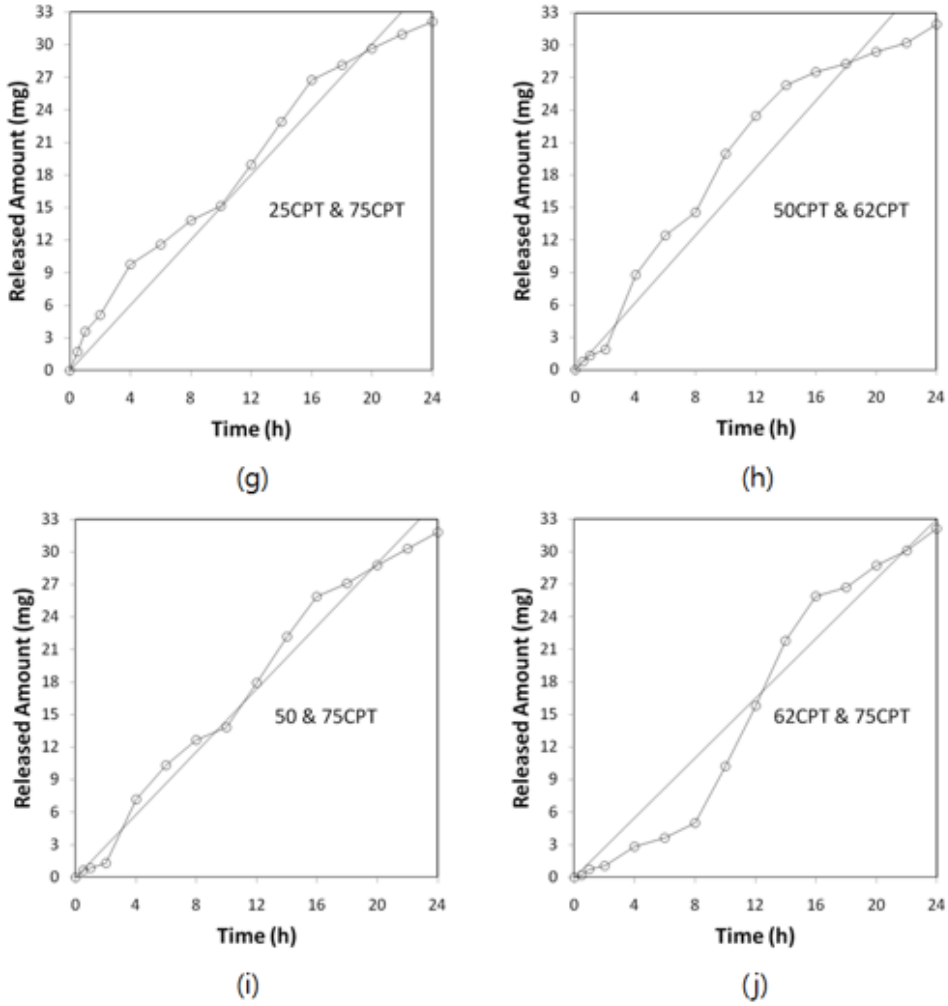

Figure 4.10. Predicted drug–release profiles of a combination of two distinctly capped tablets prepared in this work. A total of 10 different combinations were tested: (a) NCPT and 25CPT; (b) NCPT and 50CPT; (c) NCPT and 62CPT; (d) NCPT and 75CPT; (e) 25CPT and 50CPT; (f) 25CPT and 62CPT; (g) 25CPT and 75CPT; (h) 50CPT and 62CPT; (i) 50CPT and 75CPT; and (j) 62CPT and 75CPT. A dashed line shows a linear trend line fit to the predicted release profile of the two tablets.

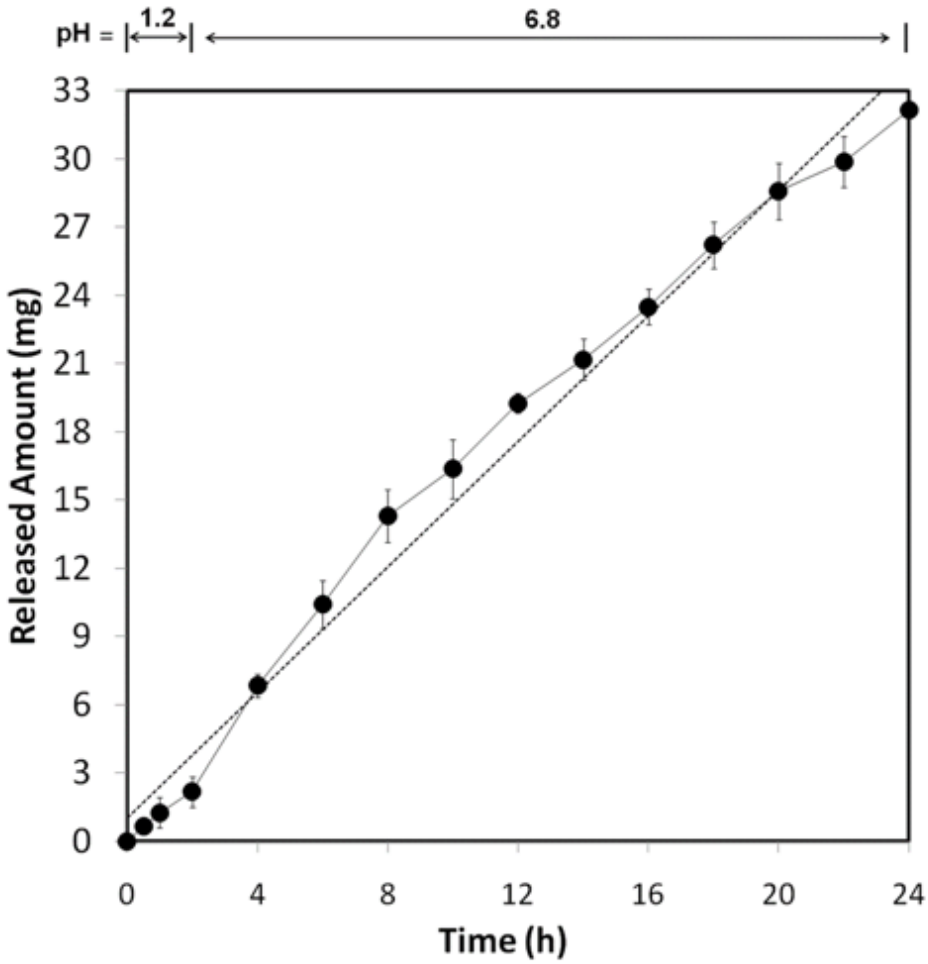

Figure 4.11. *In vitro* release profiles of nifedipine from a combination of two distinctly capped tablets, 50CPT and 75CPT. The pH of the release media was 1.2 for 2 h and 6.8 for the rest 22 h. A dashed line shows a linear trend line fit to the release profile of the two tablets.

4.4 Discussion

Oral drug delivery systems have been widely studied to improve drug bioavailability and reduce adverse side effects [77, 78]. Among them, linear drug delivery is of great interest since with a constant release rate, a drug concentration can be maintained in a highly controlled manner even with reduced dosing schedules. For that reason, many of linear delivery systems for oral drugs have been investigated [79], the release profiles of which, however, might be hard to control with high reproducibility due to variations in pH and gut motility present through the GI tract [88].

In this sense, the OROS is quite successful in achieving reproducible linear drug release [89, 93]. The osmotic pressure of water actively pushes the drug out of the tiny delivery orifice, hence linear drug release independent of the conditions in the GI tract. In spite of such advantages, the OROS is still limited in perspectives of patients' compliance. A hard capsule of the OROS may cause GI occlusion and fecal discomfort [93, 94]. The drug may be released specifically towards the gastric wall via a tiny orifice on the OROS capsule, possibly resulting in gastric irritation or ulceration. In addition, a delivery orifice has to be laser-drilled for each of the OROS capsules, hence intricate fabrication process [93, 95].

Therefore, as a part of effort to develop a new form of oral drug delivery system to address those problems, we suggest a nanofibrous sheet-based system, considering these design

parameters: (i) linear drug release with pH independency, (ii) drug release in all directions, (iii) soft carrier and (iv) simple fabrication method. To achieve linear drug release, we employed a combination of two distinctly capped tablets, (i.e., 50CPT and 75CPT), each exhibiting a different lag time of drug release (Figure 4.9). The tablet capped with a thin sheet (i.e., 50CPT) released most of the drug at the early stage while a thick sheet (i.e., 75CPT) allowed drug to be released mostly at the late stage after a long lag time. Therefore, when combined as a single system, those two tablets, each compensating drug release at the early and late stages, showed almost linear drug release during 24 h (Figure 4.11).

The tablets, 50CPT and 75CPT, exhibited the drug release profile independent of the pH. As shown in Figure 4.7, the drug release pattern was not very different at both pHs 1.2 and 6.8 when tested during 4 h, almost a doubled period of the reported gastric residence time [101]. This could be ascribed to similar morphology of the nanofibrous sheets observed at both pHs 1.2 and 6.8 (Figure 4.4), indicating that the pores on nanofibrous sheet, a major pathway of drug diffusion, could be well retained regardless the pH conditions. Again, PLGA, comprising the nanofibrous sheet, would not degrade while residing for about 24 h in the GI tract [103].

For the capped tablets suggested in this work, the drug would be released in every direction through the intact portion of the nanofibrous sheet (Figure 4.5(c)). When the drug release was complete, the drug tablet dissolved and disappeared, where only the

nanofibrous sheet remained. The sheet, although not degraded, was swollen when submerged in the aqueous media (Figure 4.4) and thus, only a soft and empty capsule would be left for excretion.

In this study, we prepared the drug tablets and the nanofibrous sheets separately and simply assembled them to give the capped tablets. This fabrication method has several advantages in regard to large scale production. A mixed powder of nifedipine and PVP was compressed to give the drug tablet, the process of which has been already widely adapted in pharmaceutical industry [108]. We capped the resulting tablets with the nanofibrous sheets by using an aligning stamp and a bonding stamp in sequence. The aligning stamp could position the drug tablet in a fixed location, where the bonding stamp could be applied just to heat the area around the drug tablet. The drug would not go through thermal degradation due to the use of the insulating stamp and cooling air. If nanofibrous sheets of large area and the stamps containing multiple rings were envisioned, multiple drug tablets could be capped and sealed at once with the method described in this work. Many researchers have already reported that the nanofibrous sheets of large area could be well fabricated with the electrospinning method [109].

Our tablet system may need to be improved further for the following reasons: the capped tablets are still not very small (Figure 4.5(b)) and two tablets are needed to achieve linear drug release (Figure 4.11). To be more acceptable, therefore, the size of the capped tablets may need to be small enough to be packed in a single

capsule, possibly composed of water-soluble material. In this way, the capsule itself would easily dissolve in the bodily fluid after swallowing, releasing two distinctly capped tablets at once in the gastric cavity. The study is in progress to reduce the size of the capped drug tablets by using the aligning and bonding stamps in small size or different shape, where, however, the drug release profile is expected to not change much since the same type of nanofibrous sheets can be employed as a diffusion barrier.

4.5 Conclusion

Linear delivery of oral drug is difficult due to the inconsistent environment present through the GI tract. The OROS, indeed, is one of the successful products for linear delivery of oral drug, which, however, may still have a room for improvement due to a non-degradable hard capsule and complicated fabrication process involved with laser-drilling delivery orifice. To address these, we developed a nanofibrous sheet-based system as replacement technology for linear delivery of oral drug in this work. A blend of a model drug, nifedipine and a solubility enhancer, PVP was compressed to give a drug tablet, which in turn, was capped and sealed with nanofibrous sheets made of a biocompatible polymer, PLGA. The capped drug tablets can be prepared by a simple multi-step process of stamping, hence ease of fabrication. In addition, this delivery system can be more acceptable since only the soft nanofibrous sheets remain after completing drug release.

The capped drug tablets can release the drug in a sustained manner, even showing various lag times of drug release, depending on the thickness of nanofibrous sheets. Therefore, we suggest a combination of two tablets, each showing a distinct profile of drug release, to achieve linear drug release. In this work, the two tablets capped with nanofibrous sheets of 50 μm- and 75 μm-thickness, respectively, when combined as a single system, exhibited almost linear release of nifedipine during 24 h. The drug release profiles

were reproducible regardless the pH, which could be ascribed to the non-different morphological structure of nanofibrous sheets at both pHs 1.2 and 6.8. Overall, we conclude that a proper combination of two tablets, each capped with nanofibrous sheet of different thickness, is a novel method of linear delivery of oral drug.

Chapter 5

Polymeric Nanofiber-coated Esophageal Stent for Sustained Delivery of an Anticancer Drug

5.1 Introduction

Esophageal cancer ranks as the sixth most common malignancy in the world with a 5-year survival rate of less than 10%[110], and is responsible for 15,000 cancer deaths in the United States and for 300,000 deaths in the world in 2009[111]. Although surgical removal of esophageal tumor could be a way of treatment, which, however, is acceptable to only 50% of the patients due to late tumor detection and early extramural spread of unresectable cancers or

radiographically visible metastases at the time of diagnosis of esophageal cancer[112, 113]. Treatment, therefore, focuses mainly on palliation therapy of dysphagia and odynophagia, employing a stent to mechanically open a blocked esophagus, thereby allowing feeding capacity and improving quality of life.

Various types of esophageal stents, made of metal, plastic or bioabsorbable polymer, have been technically evolved [114-117] and many of them are already in clinical use to relieve dysphasia [114, 115]. These stents are designed to possess good mechanical flexibility for ease of insertion and elimination of excessive esophagus dilation [114, 116]. However, for almost all cases, the esophageal stents suffer from re-occlusion due to rapid growth of tumors around the stent to shorten the effective lifespan of the treatment, hence multiple of major surgeries for stent replacement [114, 115].

In this sense, local and sustained delivery of an anti-cancer agent would be advantageous to suppress the tumor growth around the esophageal stent. In such systems, the drug would be released specifically towards the cancerous tissues in the esophagus, possibly achieving effective drug bioavailability around a stent for a prolonged period of time without unnecessarily high systemic drug exposure. However, to our knowledge, the esophageal stents enabled with delivery of an anti-cancer drug have not been widely studied, as compared with the other different types of drug-eluting stents, such as vascular stents [118, 119].

Recently, the esophageal stents were coated with biocompatible polymers, such as ethylene-vinyl acetate (EVA) and silicone, as a delivery medium for an anti-cancer drug[120-122], which could release the drug in a sustained pattern for a prolonged time, achieving high drug bioavailability near the site of action and thus, alleviating restenosis. In spite of those potential advantages, the coating process employed for the above-mentioned stents may still have room for improvement since it was a multi-step procedure, composed of separate fabrication of each of the individual drug-delivery layers and assembly of the resulting layers and a stent. For example, for the stent coated with a drug loaded silicone layer, the layers were prepared separately on a jig of the shape of a stent, which were isolated from a jig, and then assembled and bonded with a stent [120]. The EVA-coated stent also needs assembly of a drug-loaded polymeric layer, which was again prepared separately, and a stent, where a heat and pressure were applied for their bonding [121, 122]. Especially for the assembly procedure, a manual process may be needed to align and bond the layer on a stent properly.

In this sense, the electrospinning method may benefit from easy coating of an esophageal stent with drug-loaded biocompatible polymer. Simple electrospinning of a solution of drug and polymer could prepare the coated layers on top of a stent without any additional procedures. Nanofibers of drug-loaded polymer would be deposited almost in a dry form, which might also decrease the time for solvent removal. For this reason, many different stents other than

an esophageal stent were successfully coated with drug or polymer [123, 124].

In this work, we coated an esophageal stent with the electrospinning method, employing poly (lactic-co-glycolic acid) (PLGA) and 5-fluorouracil (5-FU) as a polymeric coating layer and a model anti-cancer drug, respectively. 5-FU is widely used for treatment of cancers of the aerodigestive and esophageal tracts, which is known to inhibit the nucleotide synthetic enzyme, thymidylate synthase, which is necessary for DNA replication and repair, causing cell cycle arrest and apoptosis [125]. PLGA is known to be highly biocompatible, degrading into lactic and glycolic acids, which are common metabolites found in the body [126].

We coated the esophageal stents with three different layers composed of drug-loaded PLGA nanofibers (DPN) and PLGA nanofibers only (i.e., PLGA nanofibers without the drug) (PN). Thus, the stents were coated with the DPN layer only, or the PN layers were additionally coated over the DPN layer to better control drug release. We varied the collection time of PN layers to 0 min, 60 min and 90 min to give the three differently coated stents (i.e., DPNS1, DPNS2 and DPNS3, respectively) in this work. For DPNS1, only the DPN layer was coated on a stent, where PLGA nanofibers themselves served as a wall material to sustain drug release. For DPNS2 and DPNS3, the PN layers on top of the DPN layer worked as an additional rate-limiting barrier, where the drug release profiles could be varied according to the thickness of PN layer.

5.2 Materials and Methods

5.2.1 Materials

Poly (lactic-co-glycolic acid) (PLGA; 50:50; lot number LX00195-116; i.v. = 0.46 dL · g^{-1}; average MW = 42,000) was obtained from Lakeshore Biomaterials (AL, USA). 5-FU was purchased from Sigma (MO, USA). Dichloromethane (DCM), tetrahydrofuran (THF) and dimethylformamide (DMF) were obtained from JT baker (NJ, USA), Daejung (Korea) and Mallinckrodt (MO, USA), respectively. Phosphate-buffered saline (PBS; pH 6.5) was obtained from Seoul National University Hospital Biomedical Research Institute. Esophageal stents (E02010) were a kind gift from TaeWoong Medical (Korea).

5.2.2 Preparation of Coated Esophageal Stents

The esophageal stents were coated with PLGA nanofibers loaded with an anti-cancer drug, 5-FU by the electrospinning method. First, 600 mg PLGA or a blend of 600 mg PLGA and 18 mg 5-FU was dissolved in a 2 ml solvent mixed with DCM, THF and DMF (3:1:1 = v/v/v) to give a PLGA solution or a 5-FU and PLGA solution (the initial drug loading of 3% w/w)[109], respectively. The resulting solution was electrospun on top of the stents under the following conditions (Nano NC, Korea): applied voltage: 20 kV, collector

distance: 10 cm, flow rate: 0.6 $ml \cdot h^{-1}$, rotation speed of an esophageal stent: 1000 rpm.

The stents were coated to possess three different layer properties, giving DPNS1, DPNS2 and DPNS3. To prepare DPNS1, a PLGA and 5-FU solution was electrospun for 30 min to prepare a DPN layer only. To prepare DPNS2 and DPNS3, a PLGA solution was first electrospun for 60 min and 90 min, respectively, then a PLGA and 5-FU solution for 30 min, and a PLGA solution for another 60 min and 90 min, respectively. In this way, both top and bottom of a DPN layer could be completely covered by additional PN layers for both DPNS2 and DPNS3. The resulting layers were then lyophilized under high vacuum for more than 48 h in order to remove any residual solvent [127].

5.2.3 Characterization

A nanofiber layer was detached from the stents and cut into a 5 mm × 5 mm piece, which was then placed on a SEM sample mount and sputter coated with platinum for 10 min (208HR, Cressington Scientific, England). The sample was then imaged by SEM (7501F, Jeol, Japan).

Crystallinity of PN and DPN was examined by an X-ray diffractometer (D/MAX RINT 2200-Ultima, Rigaku, Japan) equipped with Ni-filtered Cu-Kα radiation (λ = 1.5418 Å). The samples were deposited on a glass substrate and continuously scanned at the

tube voltage and the current of 40 kV and 30 mA, respectively [128]. The 5-FU and intact PLGA were also analyzed for comparison.

A differential scanning calorimetry (DSC, DSC2901, TA instruments, DE, USA) was performed to examine the thermal properties of PN and DPN. A piece of a PN or DPN layer (each 7.5 mg) was placed in a hermetic pan under nitrogen gas flow, where the temperature was raised from 0 °C to 150 °C at a rate of 5 °C · min^{-1}, and then cooled at the same rate. This cycle was repeated five times to confirm the reproducibility.

The coated layers on DPNS1, DPNS2 and DPNS3, each detached from the stents, were cut into a 1 cm × 1 cm piece and then completely dissolved in 1 ml DCM. After that, 14 ml of phosphate buffered saline (pH 6.5) was added to the resulting solution, which was sonicated at 80 W for 5 min (Model 500 Digital Sonic Dismembrator, Fisher Scientific, PA, USA) and centrifuged at 4,800 rpm for 30 min at 20℃ (Allegra 21R, Beckman, CA, USA). The supernatant was taken and analyzed by high performance liquid chromatography (HPLC, Agilent 1100 series, Agilent Technologies, CA, USA) using a Zorbax® C18 column (4.5 mm × 25 mm, 5 μm; Agilent Technologies, CA, USA). The mobile phase was prepared by mixing an aqueous solution of 0.02 M phosphoric acid and methanol (98:2; v/v). The flow rate and injection volume were 0.8 ml · min^{-1} and 10 μl, respectively. The column temperature was maintained at 20℃ and the UV absorbance was measured at 265 nm.

5.2.4 *In vitro* Degradation Study

To examine the *in vitro* degradation profiles, the coated layers of DPNS1, DPNS2 and DPNS3, each detached from the stents, were cut into a 1 cm × 1 cm piece and their initial weights were measured. Each of the samples was then placed in 2 ml of an aqueous medium buffered at pH 6.5 and incubated at 37℃ for 3 weeks. At scheduled intervals, the samples were taken out, washed thoroughly with DI water and freeze-dried for more than two days. The weights of the resulting samples were measured and compared with their initial weights.

5.2.5 *In vitro* Drug Release Test

The coated layers from DPNS1, DPNS2 and DPNS3, each detached from the stents, were cut into a 1 cm × 1 cm piece, which was then immersed in the aqueous media buffered at pH 6.5 at 37℃. The aliquot of the release media was sampled at scheduled intervals and assayed with HPLC as described above. The experiments were performed in triplicate for statistics.

5.3 Results and Discussion

5.3.1 Characterization of Coated Esophageal Stents

In this work, we coated the stents with drug-loaded polymeric layers for their potential application to local and sustained delivery of an anti-cancer drug around the esophagus. For this purpose, we employed PLGA and 5-FU as a wall material and a model anti-cancer drug, respectively, which were electrospun to deposit nanofiber layers on top of a stent. Figure 5.1 shows the optical images of the esophageal stents before and after coating. A bare stent used in this work (E0210, TaeWoong Medical, Korea) was braided with nitinol wire to give mechanical flexibility for ease of insertion. The flanges were formed at both proximal and distal ends to avoid stent migration [129], which were 28 mm in diameter and 15 mm in length. The body part of a stent was 20 mm in diameter and 70 mm in length. Figure 5.1(b) shows a representative image of the stent coated with nanofiber layers of PLGA loaded with 5-FU (i.e., DPNS1), revealing that the stent could be seamlessly coated with the electrospinning method employed in this work. Regardless of the presence of 5-FU, the electrospun layer of PLGA exhibited an apparent nanofibrous structure, as shown in Figure 5.2.

To control drug release, we coated the stents with three different types of nanofiber layers to give DPNS1, DPNS2 and DPNS3,

respectively (Table 5.1). The DPNS1 was prepared by electrospinning a solution of PLGA and 5-FU to coat a stent with a DPN layer (i.e., a layer with PLGA and the drug) only. For DPNS2 and DPNS3, a PLGA solution was first electrospun to coat a stent with a PN layer (i.e., a layer with PLGA only), on top of which a DPN layer was coated and then, a PN layer was coated again over the top of a DPN layer. In this way, an additional diffusion barrier could be formed around a DPN layer for both DPNS2 and DPNS3. The times for coating each of the layers were 0 min PN; 30 min DPN; 0 min PN, 60 min PN; 30 min DPN; 60 min PN, and 90 min PN; 60 min DPN; 90 min PN for DPNS1, DPNS2 and DPNS3, respectively. The average thicknesses of the resulting layers were 0 μm PN; 70 μm DPN; 0 μm PN, 134 μm PN; 54 μm DPN; 98 μm PN, and 192 μm PN; 47 μm DPN; and 122 μm PN for DPNS1, DPNS2 and DPNS3, respectively (Table 5.1).

Notably, although the DPN layers were deposited during the same time period (30 min) for all stents, the thickness of DPN layer decreased as the thickness of the inner PN layer on top of a stent increased. This could be ascribed to the electric insulation formed by the PN layer first deposited on a stent [130], which appeared to reduce the electric field strength as the thickness of the PN layer increased. For the same reason, the outer PN layer deposited on top of the DPN layer was thinner than the inner PN layer initially deposited on top of a stent although both PN layers were collected during the same time period (Table 5.1).

Table 5.1. Layer compositions and thicknesses of nanofiber layers coated on the stents.

Layer type	Layer composition[a]	Thickness (μm)
DPNS1	PN (inner)	0 ± 0.0
	DPN (middle)	70 ± 1.6
	PN (outer)	0 ± 0.0
DPNS2	PN (inner)	134 ± 1.0
	DPN (middle)	54 ± 0.7
	PN (outer)	98 ± 1.0
DPNS3	PN (inner)	192 ± 1.1
	DPN (middle)	47 ± 0.7
	PN (outer)	122 ± 0.6

Values are mean ± SD.

[a] The inner PN layer is located on the very top of the stent and the outer layer is on the very outside of the three layers of PN, DPN and PN. The DPN layer is sandwiched between two distinct PN layers.

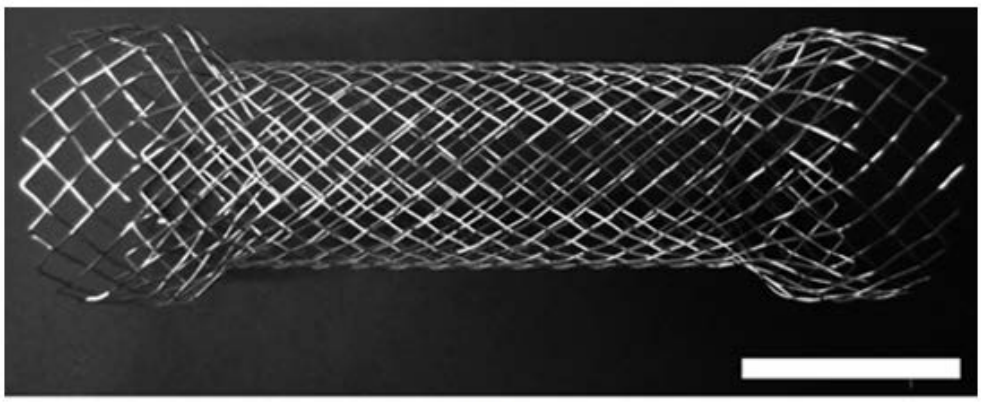

(a)

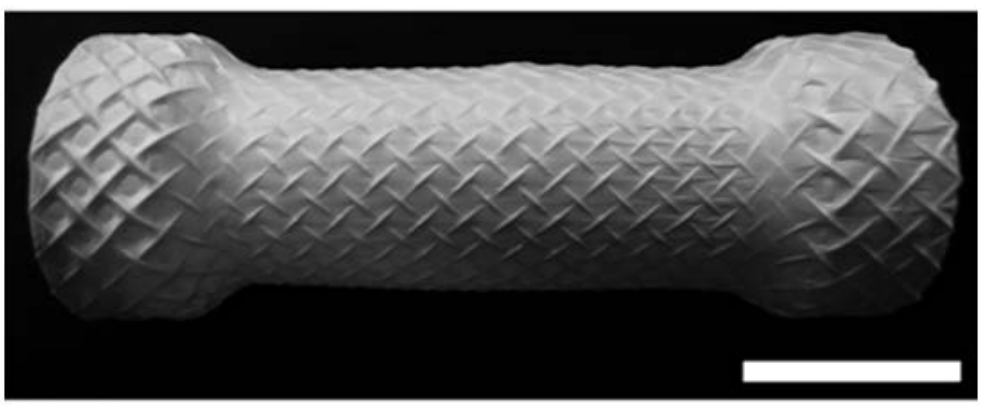

(b)

Figure 5.1. Representative optical images of (a) a bare esophageal stent and (b) an esophageal stent coated with DPN. Scale bars = 20 mm.

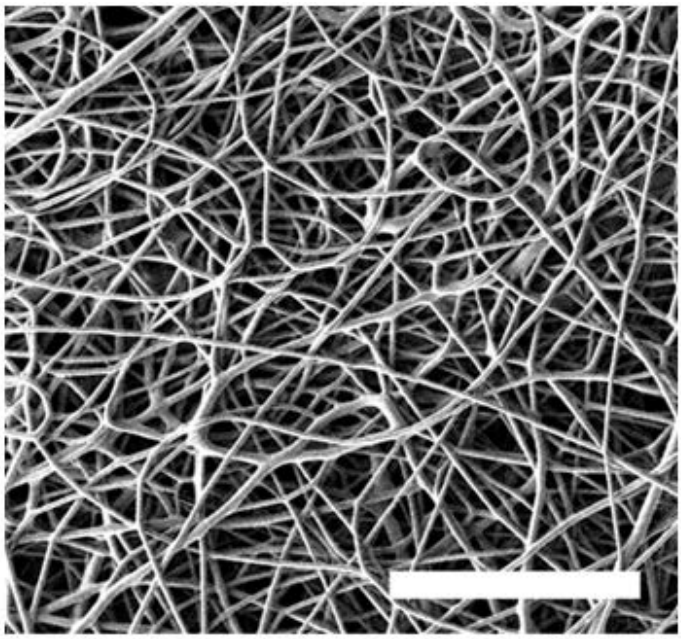

(a)

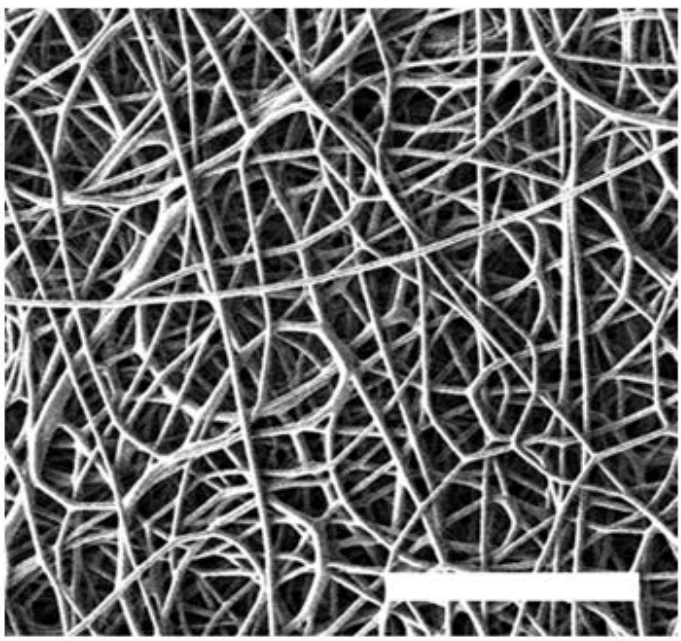

(b)

Figure 5.2. Scanning electron micrographs of (a) PN and (b) DPN. Scale bars = 50 μm.

5.3.2 Characterization of Coating Layers

Figure 5.3 shows the XRD patterns of 5-FU, intact PLGA, PN and DPN. 5-FU exhibited a crystalline peak at $2\theta = 28^{\circ}$, while intact PLGA and PN were amorphous with no crystalline peaks[128, 131]. However, even with the presence of 5-FU, the DPN showed no XRD peaks, suggesting that the 5-FU molecules were homogeneously distributed in the DPN layer without forming an evident crystalline structure.

Figure 5.4 shows the results from DSC analysis of 5-FU, intact PLGA, PN and DPN. T_g of intact PLGA was obtained at 48.1℃, which was lowered to 38.2℃ with the PN. The decrease in T_g could be ascribed to a large surface to volume ratio of the PLGA nanofiber layers embedded with air as a plasticizer, increasing the spacing and free volume in nanofibers, thereby more flexibility of the polymer chains [132]. T_g did not vary much with the DPN as compared with the PN but slightly lowered to 36.8℃, which might be ascribed to the presence of 5-FU.

Table 5.2 shows the loading amounts of 5-FU per cm^2 of each of the coating layers from DPNS1, DPNS2 and DPNS3. The drug loading amounts decreased as the thickness of additional PN layers increased, which was somewhat expected since the thickness of a DPN layer decreased with the presence of a PN layer. As described above, the addition of the PN layer resulted in insulation to cause reduction in electric field strength, thereby a decrease in total amount

of the collected DPN nanofibers. Thus, the average loading amounts of 5-FU were 15.66 μg, 12.42 μg and 10.62 μg per cm^2 for DPNS1, DPNS2 and DPNS3, respectively. Where a DPN layer of the same thickness was assumed to be collected, the drug amounts per cm^2 should not be very different for all coated stents, as shown in Table 5.2. Thus, the drug loading efficiencies were 72.9%, 74.9% and 73.6% for DPNS1, DPNS2 and DPNS3, respectively.

Table 5.2. Drug loading amounts and efficiencies in nanofiber layers coated on the stents.

Layer type	Thicknesses of DPN (μm)	Drug amount (μg per cm^2)	Drug amount[a] (μg per cm^2)	Drug loading efficiency[b] (%)
DPNS1	70 ± 1.6	15.66 ± 0.76	15.66	72.9
DPNS2	54 ± 0.7	12.42 ± 0.29	16.10	74.9
DPNS3	47 ± 0.7	10.62 ± 0.27	15.82	73.6

Values are mean ± SD.

[a] The drug amounts per cm^2 were calculated, assuming the same thickness of the collected DPN layers (70 μm).

[b] The drug loading efficiency was calculated in percentage by dividing the actual loading amount in nanofibers by the initial loading amount.

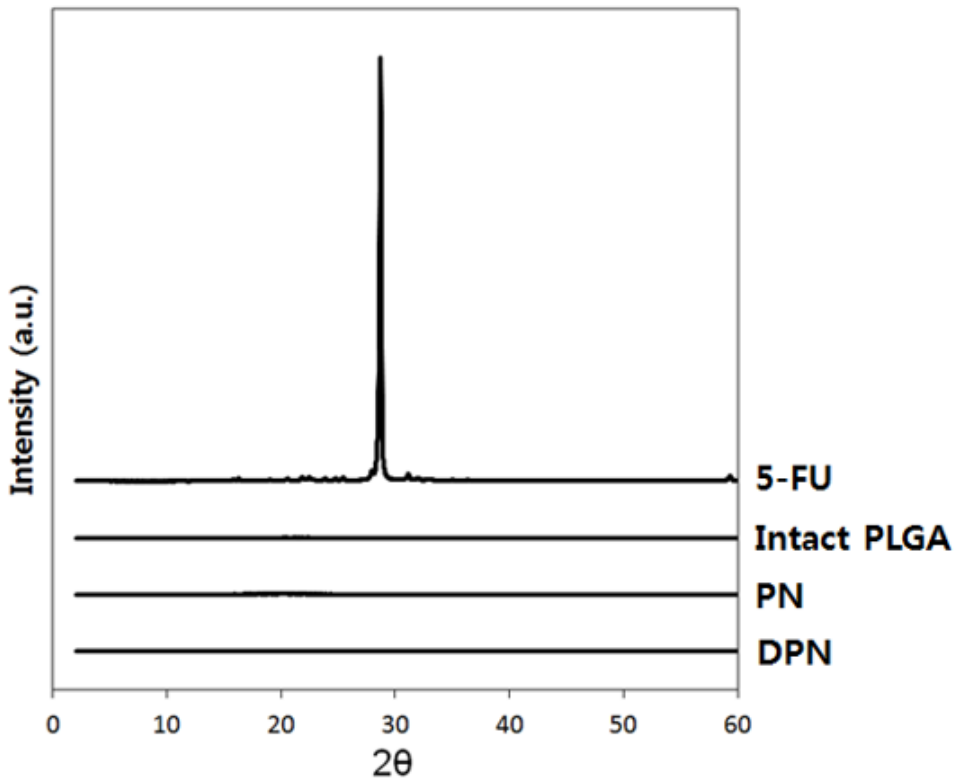

Figure 5.3. X-ray diffraction patterns of 5-FU powder, intact PLGA, PN and DPN.

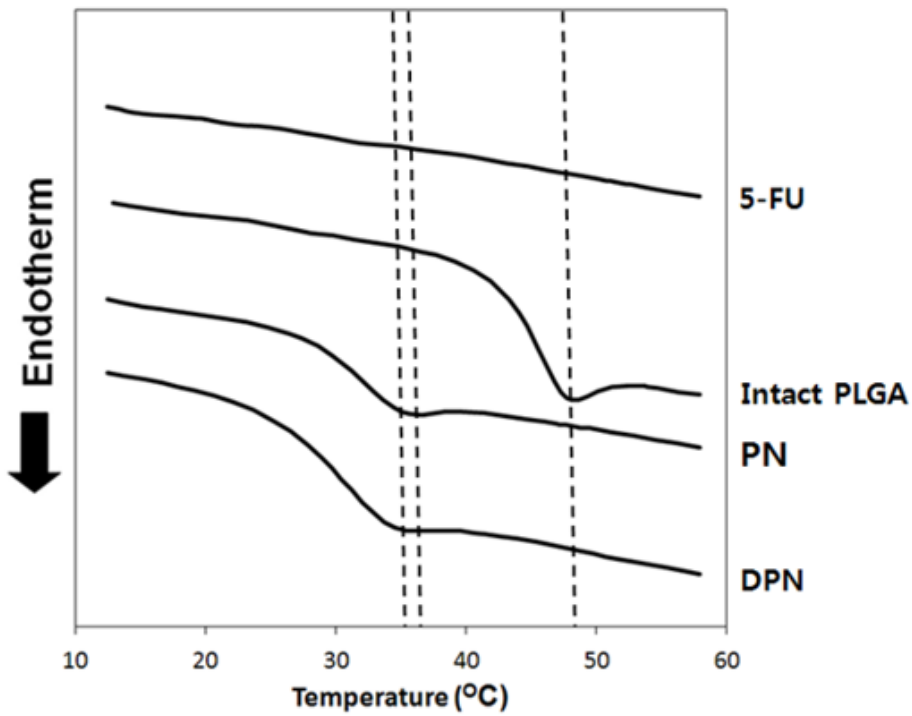

Figure 5.4. Differential scanning calorimetry thermograms of 5-FU powder, intact PLGA, PN and DPN. The dashed lines indicate T_g of intact PLGA, PN and DPN.

5.3.3 *In vitro* Degradation of Coating Layers

We examined *in vitro* degradation behaviors of nanofiber layers from DPNS1, DPNS2 and DPNS3 by measuring the change in remaining amount after immersion in the aqueous media at pH 6.5, mimicking the biological fluid at the esophagus [133]. Figure 5.5 shows the remaining amount percent of the coating layers from each of the stents prepared in this work, all of which exhibited an apparent decrease in their remaining amount. The degradation of DPNS1 layer seemed to be relatively faster, especially for the first 2 days, than that of DPNS2 and DPNS3 layers, which could be attributed to rapid drug release via the DPN layer, leaving the pores on the layer to give a large surface area interacting with the surrounding medium. On the other hand, the additional PN layers seemed to prevent this rapid pore formation for DPNS2 and DPNS3, hence relatively slower degradation. After 21 days of immersion, the remaining amount decreased to 62%, 68% and 68% for DPNS1, DPNS2 and DPNS3, respectively.

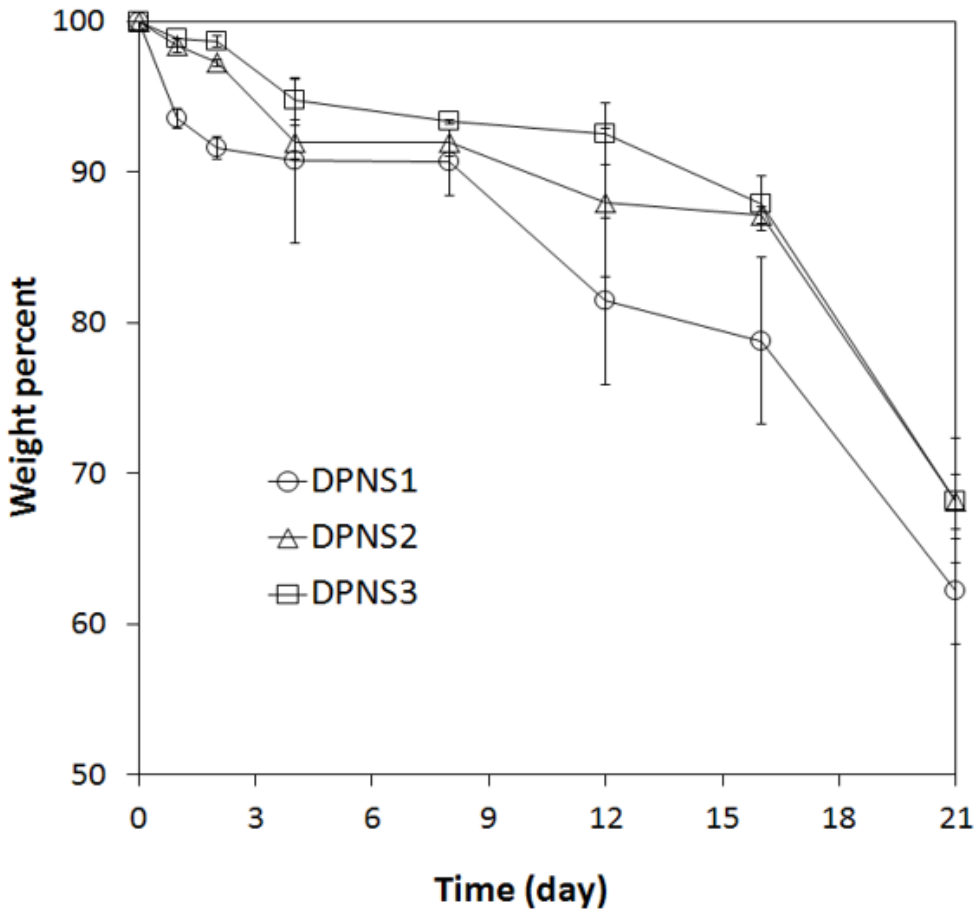

Figure 5.5. Weight percent of the remaining nanofiber layers from DPNS1, DPNS2 and DPNS3 after degradation to their initial weights.

5.3.4 *In vitro* Drug Release Profiles

We examined the *in vitro* release profiles of 5-FU with the coating layers, each detached from DPNS1, DPNS2 and DPNS3, respectively. As shown in Figure 5.6, almost 70% of the drug was released from the DPNS1 layers during the first day, which was completed in 6 days. This rapid release could be due to a hydrophilic nature of 5-FU, which is known to be highly soluble in the aqueous media (~12.5 $mg \cdot ml^{-1}$) [134], and thus, a release pattern appears to be not determined by polymer degradation but be controlled mostly via drug diffusion. To prolong drug release, therefore, we added the PN layers as an additional diffusion barrier. As a result, the layers from DPNS2 and DPNS3 continued drug release on 6 day, still containing about 11.3% and 21.7% of the drug remaining in the layers, respectively and thus, drug release was also more sustained as the thickness of the PN layer increased. A period of drug release was extended to 15 days and 21 days for DPNS2 and DPNS3, respectively.

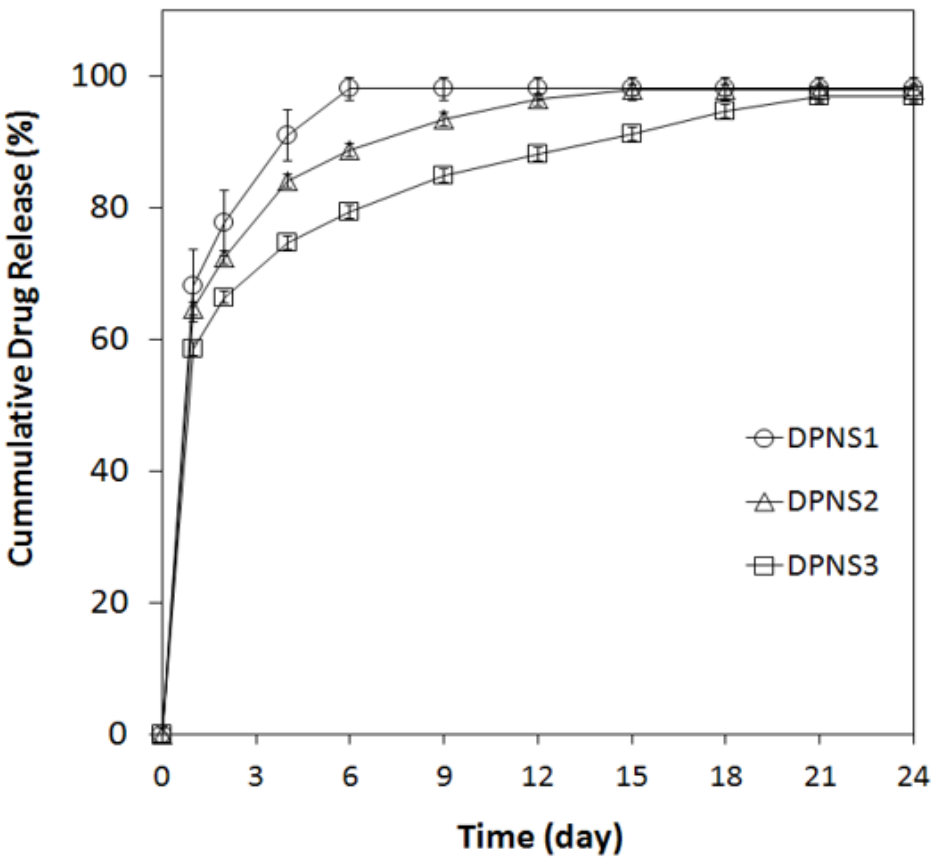

Figure 5.6. *In vitro* release profiles of 5-FU from DPNS1, DPNS2 and DPNS3.

5.4 Discussion

An esophageal stent is accepted in clinical use to mechanically open an esophagus clogged by cancerous tissues, allowing feeding capacity as well as improving a life quality of the patients [114, 115]. Various types of esophageal stents have been developed for this purpose [114-117], many of which, however, still pose problems of re-occlusion due to rapid growth of tumors around the stent. This reduces the effective lifespan of the stent, needing multiple times of major surgeries for stent replacement [114, 115].

To resolve this, the esophageal stents enabled with local delivery of an anti-cancer drug have been developed by coating the surface of the stents with biocompatible polymers, such as ethylene-vinyl acetate (EVA) and silicone [120-122]. This coated layers of polymer were loaded with an anti-cancer drug, where a drug could be released in a sustained manner over a prolonged period of time, achieving high drug bioavailability around the stent and thus, alleviating restenosis.

Inspired by those previous results, we coated a stent with the electrospinning method to prepare a nanofiber layer of a biocompatible polymer, PLGA, on top of a stent[126], where an anti-cancer drug, 5-FU, was loaded to be released in a sustained manner (Figure 5.1). In the coating layers, the drug was seen to be homogeneously distributed in a molecular level (Figure 5.3), suggesting that local toxicity of an anti-cancer drug, 5-FU, possibly

caused by crystallized drug particulates in the layer, be highly improbable. After complete drug release, the PLGA nanofiber layers should be biodegraded into lactic acids and glycolic acids, which are common metabolites found in the body, to disappear eventually (Figure 5.5).

However, the stents coated with this single layer composed of the polymer and drug (i.e., the DPN only) was limited in a relatively short period of drug release only for 6 days (DPNS1). To further control drug release, therefore, we coated the stents with the multi-layered nanofibers composed of drug-loaded polymer (i.e., DPN) and polymer only (i.e., PN). In this work, we added the PN layers surrounding the DPN layer as an additional diffusion barrier. Thus, the DPN layer was sandwiched with two distinct PN layers. As a result, drug release could be more prolonged for up to 21 days (DPNS3) as the thickness of PN layer increased (Figure 5.6). Considering about 100 days of a median survival period of patients with esophageal cancer after stent placement [135], we envision that the period of drug release can be optimized by simply varying the thickness of the PN layers as a more resistive diffusion barrier.

The electrospinning method employed for coating the esophageal stents in this work could benefit from a simple fabrication procedure. Previously, to coat the stents with drug-delivery layers, each of the coating layers was separately prepared, which was then assembled manually with a stent, employing a solvent or heat for their attachment [120-122]. With the electrospinning method, the

nanofibers of drug-loaded polymer were directly deposited on top of a stent to form a layer enabled with drug delivery. Therefore, the coated stents would not need any additional procedures except for complete evaporation of the solvent utilized to prepare a drug and polymer solution for electrospinning. However, a short drying time is expected since nanofibers generated by electrospinning would not generally contain much of residual solvent. Moreover, a large area of nanofiber layers have been successfully fabricated with the electrospinning method[109], which would be favorable for coating of multiple stents at once in a scale up production. In this way, the thicker PN layers employed for a prolonged drug release could be obtained simply by a longer collection of PN nanofibers via electrospinning. The stability of 5-FU is expected to be retained during this process since the organic solvents and a high voltage used for electrospinning were reported to have almost no effect on the drug activity [110, 136].

The coating layers that we prepared in this work may need to be improved further to give more mechanical flexibility and pliability needed for a practical use of an esophageal stent. For example, the stent needs to be contracted for insertion, which is then expanded fully after placement in the esophagus [137]. In addition, the stent is usually under repetitive mechanical stress due to the peristalsis of esophagus [136]. To be more acceptable, therefore, the coating layers may need to be composed of more pliant polymers, such as elastomers [138]. Incorporation of a plasticizer, such as

polyurethane and poly (lactic−co− ε −caprolactone) may also help to give more flexibility to the PLGA coating layers[139]. The study is now in progress to develop the esophageal stents coated with the polymeric layers with more flexibility, as well as longer drug release.

5.5 Conclusion

An esophageal stent has been accepted in clinical use for palliative therapy to relieve malignant dysphagia and odynophagia mostly found with the esophageal cancer patients. However, many of the stents are still limited in restenosis due to rapid growth of tumor cells around the stent. To address this obstacle, we developed the esophageal stents enabled with delivery of an anti-cancer drug. For this purpose, the stents were coated with nanofiber layers of a biocompatible polymer, PLGA, containing an anti-cancer drug, 5-FU, via electrospinning. A coating procedure with the electrospinning method is considered to be simple, as compared with some of the previous trials involved with separate fabrication of drug-delivery layers and manual attachment of the layers to a stent.

The stents coated with drug-loaded nanofibers (DPN) can sustain drug release and the period of drug release can be more prolonged by adding nanofiber layers composed of PLGA only (PN), surrounding the DPN layer, as a more resistive diffusion barrier. The stents coated with a 70 μm-thick DPN layer in this work could release the drug for 6 days, which could be extended to up to 21 days when the 122 μm-and 192 μm-thick PN layers were deposited on top and bottom of the DPN layers, respectively. We expect that a longer drug release period can be realized simply by incorporating the thicker PN layers via electrospinning. Therefore, we conclude that a drug-delivery esophageal stent suggested in this work has a

promising potential for a long-term treatment of dysphagia of the esophageal cancer patients.

Chapter 6

Conclusion and Perspective

Effective drug delivery at the desired site of action is essential for the treatment of diseases. However, this is often challenging due to low bioavailability, unwanted systemic exposure and adverse side effects. To address this problem, the author presented newly developed devices for the effective delivery of drugs and, thus, better treatment of diseases by applying nanofiber-structured biopolymers.

In Chapter 2, we provided the main rationale for the biopolymer selection and optimization process for nanofiber-structured biopolymers. We chose PLGA as a biopolymer, due to its excellent biocompatibility, biodegradability and easy tunability. Then, we varied many parameters through electrospinning to find the most optimized nanofiber structures (i.e., those that possess an optimized

high-specificity surface area and micro-porosity).

In Chapter 3, we examined mucoadhesive NM for their extended preocular retention and thus improved drug bioavailability. The NMs were prepared simply by freeze-milling the nanofibrous sheets to create entangled nanofibers in each of the microparticles, which exhibited a more than 10-fold increase in specific surface area compared with conventional MS. The NM with an added mucoadhesion promoter adhered better to the mucus layer of the eye. This interaction can be synergistically enhanced by using a rapidly dissolving dry tablet formulation, which can increase tear viscosity and avoid the rapid clearance of microparticles by not providing additional fluid. Thus, the *in vivo* animal experiment revealed that the best preocular retention could be obtained with the PLGA/PEG NM tablet. Accordingly, when the BRT was delivered via a dry PLGA/PEG NM tablet, the NM delivered the drug in a sustained manner to the surface of the eye. This improved drug bioavailability, hence prolonging the IOP-lowering effect of 13 h, which was more than twice the drug efficacy, as compared with Alphagan-P, a medication already approved for clinical use.

In Chapter 4, we suggested the use of nanofibrous sheets of micro-porosity for the linear delivery of nifedipine. A blend of a model drug, nifedipine, and a solubility enhancer, PVP, was compressed to give a drug tablet, which, in turn, was capped and sealed with nanofibrous sheets made of a biocompatible polymer, PLGA. The capped drug tablets were prepared by a simple multi-

step process of stamping. The capped drug tablets released the drug in a sustained manner, even showing various lag times of drug release depending on the thickness of the nanofibrous sheets. The two tablets capped with nanofibrous sheets of 50 μm- and 75 μm-thickness, respectively, when combined as a single system, exhibited an almost linear release of nifedipine during 24 h. Overall, we concluded that an appropriate combination of the two tablets, each capped with nanofibrous sheets of different thicknesses, is a novel method of linear delivery of oral drugs.

In Chapter 5, we developed the esophageal stent enabled with delivery of anti-cancer drug for the prevention of re-occlusion by esophageal cancer. For this purpose, the stents were coated with nanofiber layers of a biocompatible polymer, PLGA, containing an anti-cancer drug, 5-FU, using electrospinning. The stents coated with drug-loaded PLGA nanofibers (DPN) can sustain drug release, and the drug-release period can be extended by adding nanofiber layers composed of PLGA only (PN), surrounding the DPN layer, as a more resistive diffusion barrier. The stents coated with a 70 μm-thick DPN layer released the drug for 6 days, which could be extended to up to 21 days when the 122 μm- and 192 μm-thick PN layers were deposited on top and bottom of the DPN layers, respectively. We expect that a longer drug-release period could be realized by incorporating thicker PN layers via electrospinning. Therefore, we conclude that the drug-delivery esophageal stent suggested here is promising for the long-term treatment of

dysphagia in esophageal cancer patients.

According to the obtained results, nanofiber-structured biopolymers have many unique features, such as high specific surface area and micro-porosity, which could be used to develop advanced drug-delivery systems that are needed for the treatment of various diseases. Recently, the number of publications on biopolymer nanofibers has been continuously increasing due to their ease of fabrication, remarkably low cost, and the variety of their potential applications in diverse areas. In addition, nanofiber-based products have been commercialized in many fields, including regenerative medicine, and drug delivery systems. In this regard, we hope that this study contributes to the development of an advanced drug delivery system with nanofiber-structured biopolymers for the better treatment of diseases, thereby improving quality of life.

References

[1] O. Pillai, R. Panchagnula, Polymers in drug delivery, Curr. Opin. Chem. Biol., 5 (2001) 447-451.
[2] N. Saito, K. Takaoka, New synthetic biodegradable polymers as BMP carriers for bone tissue engineering, Biomaterials, 24 (2003) 2287-2293.
[3] R. Nayak, R. Padhye, I. Kyratzis, Y.B. Truong, L. Arnold, Recent advances in nanofibre fabrication techniques, Text. Res. J., 82 (2012) 129-147.
[4] C.-L. Zhang, S.-H. Yu, Nanoparticles meet electrospinning: recent advances and future prospects, Chem. Soc. Rev., (2014) 4423-4448.
[5] C.E. Astete, C.M. Sabliov, Synthesis and characterization of PLGA nanoparticles, J. Biomater. Sci. Polym. Ed., 17 (2006) 247-289.
[6] F. Danhier, E. Ansorena, J.M. Silva, R. Coco, A. Le Breton, V. Préat, PLGA-based nanoparticles: an overview of biomedical applications, J. Control. Release, 161 (2012) 505-522.
[7] H.K. Makadia, S.J. Siegel, Poly lactic-co-glycolic acid (PLGA) as biodegradable controlled drug delivery carrier, Polymers-Basel, 3 (2011) 1377-1397.
[8] P.A. Gunatillake, R. Adhikari, Biodegradable synthetic polymers for tissue engineering, Eur. Cell. Mater., 5 (2003) 1-16.
[9] J. Anderson, M. Shive, Biodegradation and biocompatibility of PLA and PLGA microspheres, Adv. Drug Deliv. Rev, 28 (1997) 5-24.
[10] C.G. Park, M.H. Kim, M. Park, J.E. Lee, S.H. Lee, J.H. Park, K.H. Yoon, Y.B. Choy, Polymeric nanofiber coated esophageal stent for sustained delivery of an anticancer drug, Macromol. Res., 19 (2011) 1210-1216.
[11] B. Inanç, Y.E. Arslan, S. Seker, A.E. Elçin, Y.M. Elçin, Periodontal ligament cellular structures engineered with electrospun poly (DL-lactide-co-glycolide) nanofibrous membrane scaffolds, J. Biomed. Mater. Res. A, 90 (2009) 186-195.
[12] D. Ghate, H.F. Edelhauser, Ocular drug delivery, Expert. Opin. Drug Deliv., 3 (2006) 275-287.
[13] G.D. Novack, Ophthalmic drug delivery: development and regulatory considerations, Clin. Pharmacol. Ther., 85 (2009) 539-543.
[14] J.S. Berger, K.R. Head, T.O. Salmon, Comparison of two artificial tear formulations using aberrometry, Clin. Exp. Optom., 92 (2009) 206-211.
[15] H. Zhu, A. Chauhan, Effect of viscosity on tear drainage and ocular residence time, Optom. Vis. Sci., 85 (2008) E715-E725.
[16] M. Casolaro, I. Casolaro, S. Lamponi, Stimuli-responsive hydrogels for controlled pilocarpine ocular delivery, Eur. J. Pharm. Biopharm., 80 (2011) 553-561.
[17] A.H. Krauland, V.M. Leitner, A. Bernkop-Schnürch, Improvement in the in situ gelling properties of deacetylated gellan gum by the immobilization of thiol groups, J. Pharm. Sci., 92 (2003) 1234-1241.
[18] C. Koelwel, S. Rothschenk, B. Fuchs-Koelwel, B. Gabler, C. Lohmann,

A. Göpferich, Alginate inserts loaded with epidermal growth factor for the treatment of keratoconjunctivitis sicca, Pharm. Dev. Technol., 13 (2008) 221-231.
[19] K. Rathore, R. Nema, Review on ocular inserts, Int. J. PharmTech. Res., 1 (2009) 164-169.
[20] S. Ding, Recent developments in ophthalmic drug delivery, Pharm. Sci. Technol. Today, 1 (1998) 328-335.
[21] E. Lavik, M.H. Kuehn, Y.H. Kwon, Novel drug delivery systems for glaucoma, Eye, 25 (2011) 578-586.
[22] Y. Sultana, R. Jain, M. Aqil, A. Ali, Review of ocular drug delivery, Curr. Drug Deliv., 3 (2006) 207-217.
[23] H. Rosen, T. Abribat, The rise and rise of drug delivery, Nat. Rev. Drug Discov., 4 (2005) 381-385.
[24] A. Zimmer, J. Kreuter, Microspheres and nanoparticles used in ocular delivery systems, Adv. Drug Deliver. Rev., 16 (1995) 61-73.
[25] R.C. Nagarwal, S. Kant, P. Singh, P. Maiti, J. Pandit, Polymeric nanoparticulate system: A potential approach for ocular drug delivery, J. Control. Release, 136 (2009) 2-13.
[26] J.K. Vasir, K. Tambwekar, S. Garg, Bioadhesive microspheres as a controlled drug delivery system, Int. J. Pharm., 255 (2003) 13-32.
[27] K.P.R. Chowdary, Y. Srinivasa Rao, Mucoadhesive microspheres for controlled drug delivery, Biol. Pharm. Bull., 27 (2004) 1717-1724.
[28] E. Gavini, P. Chetoni, M. Cossu, M.G. Alvarez, M.F. Saettone, P. Giunchedi, PLGA microspheres for the ocular delivery of a peptide drug, vancomycin using emulsification/spray-drying as the preparation method: in vitro/in vivo studies, Eur. J. Pharm. Biopharm., 57 (2004) 207-212.
[29] Y.B. Choy, J.H. Park, B.E. McCarey, H.F. Edelhauser, M.R. Prausnitz, Mucoadhesive microdiscs engineered for ophthalmic drug delivery: effect of particle geometry and formulation on preocular residence time, Invest. Ophthalmol. Vis. Sci., 49 (2008) 4808-4815.
[30] Y.B. Choy, S.R. Patel, J.H. Park, B.E. McCarey, H.F. Edelhauser, M.R. Prausnitz, Mucoadhesive microparticles in a rapidly dissolving tablet for sustained drug delivery to the eye, Invest. Ophthalmol. Vis. Sci., 52 (2011) 2627-2633.
[31] W.B. Liechty, D.R. Kryscio, B.V. Slaughter, N.A. Peppas, Polymers for drug delivery systems, Annu. Rev. Chem. Biomol., 1 (2010) 149-173.
[32] S. Zalipsky, Chemistry of polyethylene glycol conjugates with biologically active molecules, Adv. Drug Delive.r Rev., 16 (1995) 157-182.
[33] N. Efremova, Y. Huang, N. Peppas, D. Leckband, Direct measurement of interactions between tethered poly (ethylene glycol) chains and adsorbed mucin layers, Langmuir, 18 (2002) 836-845.
[34] J. Shen, Y. Wang, Q. Ping, Y. Xiao, X. Huang, Mucoadhesive effect of thiolated PEG stearate and its modified NLC for ocular drug delivery, J. Control. Release, 137 (2009) 217-223.
[35] T. Tadros, P. Izquierdo, J. Esquena, C. Solans, Formation and stability of nano-emulsions, Adv. Colloid. Interface. Sci., 108-109 (2004) 303-318.
[36] S. van der Graaf, C.G.P.H. Schroen, R.M. Boom, Preparation of double

emulsions by membrane emulsification – a review, J. Membrane. Sci., 251 (2005) 7–15.
[37] R. Vehring, W.R. Foss, D. Lechuga–Ballesteros, Particle formation in spray drying, J. Aerosol. Sci., 38 (2007) 728–746.
[38] M. Ameri, Y.F. Maa, Spray drying of biopharmaceuticals: Stability and process considerations, Dry. Technol., 24 (2006) 763–768.
[39] H. Okochi, M. Nakano, Preparation and evaluation of w/o/w type emulsions containing vancomycin, Adv. Drug Deliver. Rev., 45 (2000) 5–26.
[40] A.C.D. de Medeiros, N.A.B. de Cervantes, A.P.B. Gomes, R.O. Macedo, Thermal stability of prednisone drug and tablets, J. Therm. Anal. Calorim., 64 (2001) 745–750.
[41] A. Greiner, J.H. Wendorff, Electrospinning: A fascinating method for the preparation of ultrathin fibres, Angew. Chem. Int. Edit., 46 (2007) 5670–5703.
[42] I. Pal Kaur, M. Kanwar, Ocular preparations: the formulation approach, Drug Dev. Ind. Pharm., 28 (2002) 473–493.
[43] M.Q. Rahman, K. Ramaesh, D.M.I. Montgomery, Brimonidine for glaucoma, Expert Opin. Drug Saf., 9 (2010) 483–491.
[44] H.V. Danesh–Meyer, Neuroprotection in glaucoma: recent and future directions, Curr. Opin. Ophthal., 22 (2011) 78–86.
[45] C.G. Park, E. Kim, M. Park, J.H. Park, Y.B. Choy, A nanofibrous sheet–based system for linear delivery of nifedipine, J. Control Release., 149 (2011) 250–257.
[46] S. Dhital, A.K. Shrestha, M.J. Gidley, Effect of cryo–milling on starches: Functionality and digestibility, Food Hydrocoll., 24 (2010) 152–163.
[47] R. Sakurovs, Relationships between CO_2 sorption capacity by coals as measured at low and high pressure and their swelling, Int. J. Coal. Geol., 90 (2012) 156–161.
[48] N.N. Nassar, A. Hassan, P. Pereira–Almao, Comparative oxidation of adsorbed asphaltenes onto transition metal oxide nanoparticles, Colloids Surf. A Physicochem. Eng. Asp., 384 (2011) 145–149.
[49] Y.P. Sun, X.Q. Li, J.S. Cao, W.X. Zhang, H.P. Wang, Characterization of zero–valent iron nanoparticles, Adv. Colloid. Interfac., 120 (2006) 47–56.
[50] X. Liu, L. Lei, J.W. Hou, M.F. Tang, S.R. Guo, Z.M. Wang, K.M. Chen, Evaluation of two polymeric blends (EVA/PLA and EVA/PEG) as coating film materials for paclitaxel–eluting stent application, J. Mater. Sci. Mater. Med., 22 (2011) 327–337.
[51] A. Tejado, C. Pena, J. Labidi, J. Echeverria, I. Mondragon, Physico–chemical characterization of lignins from different sources for use in phenol–formaldehyde resin synthesis, Bioresour. Technol., 98 (2007) 1655–1663.
[52] Y.P. Li, Y.Y. Pei, X.Y. Zhang, Z.H. Gu, Z.H. Zhou, W.F. Yuan, J.J. Zhou, J.H. Zhu, X.J. Gao, PEGylated PLGA nanoparticles as protein carriers: synthesis, preparation and biodistribution in rats, J. Control Release., 71 (2001) 203–211.
[53] A.K. Dutta, K. Kamada, K. Ohta, Spectroscopic studies of Nile red in organic solvents and polymers, J. Photochem. Photobiol. A Chem., 93 (1996)

57-64.
[54] J.Q. Dong, D.M. Babusis, D.F. Welty, A.A. Acheampong, D. Tang-Liu, S.M. Whitcup, Effects of the preservative Purite® on the bioavailability of brimonidine in the aqueous humor of rabbits, J. Ocul. Pharmacol. Th., 20 (2004) 285-292.
[55] C. Shasteen, S.M. Kwon, K.Y. Park, S.Y. Jung, S.H. Lee, C.G. Park, M.H. Kim, S. Kim, W.C. Son, T.H. Choi, Biodegradable internal fixation plates enabled with X-ray visibility by a radiopaque layer of β-tricalcium phosphate and poly (lactic-co-glycolic acid), J. Biomed. Mater. Res. Part B: Appl. Biomater., 101 (2013) 320-329.
[56] S. Maiti, S. Paul, R. Mondol, S. Ray, B. Sa, Nanovesicular formulation of brimonidine tartrate for the management of glaucoma: In vitro and In vivo evaluation, AAPS PharmSciTech, 12 (2011) 755-763.
[57] S.Y. Botelho, E.V. Martinez, Electrolytes in lacrimal gland fluid and in tears at various flow rates in the rabbit, Am. J. Physiol., 225 (1973) 606-609.
[58] M.W. Lee, C.L. Hung, J.C. Cheng, Y.J. Wang, A new anti-adhesion film synthesized from polygalacturonic acid with 1-ethyl-3-(3-dimethylaminopropyl) carbodiimide crosslinker, Biomaterials, 26 (2005) 3793-3799.
[59] P. Greenspan, S.D. Fowler, Spectrofluorometric studies of the lipid probe, Nile red, J. Lipid. Res., 26 (1985) 781-789.
[60] S. Grandi, A. Magistris, P. Mustarelli, E. Quartarone, C. Tomasi, L. Meda, Synthesis and characterization of SiO_2–PEG hybrid materials, J. Non. Cryst. Solids., 352 (2006) 273-280.
[61] W.D. Li, E.Y. Ding, Preparation and characterization of cross-linking PEG/MDI/PE copolymer as solid-solid phase change heat storage material, Sol. Energ. Mat. Sol., 91 (2007) 764-768.
[62] M.V. Jose, V. Thomas, D.R. Dean, E. Nyairo, Fabrication and characterization of aligned nanofibrous PLGA/Collagen blends as bone tissue scaffolds, Polymer, 50 (2009) 3778-3785.
[63] J.H. Lee, N.G. Rim, H.S. Jung, H. Shin, Control of osteogenic differentiation and mineralization of human mesenchymal stem cells on composite nanofibers containing poly [lactic-co-(glycolic acid)] and hydroxyapatite, Macromol. Biosci., 10 (2010) 173-182.
[64] J.E. Lee, C.G. Park, B.M. An, M.H. Kim, M. Park, S.H. Lee, Y.B. Choy, Linear delivery of verapamil via nanofibrous sheet-based system, Pharm. Res., 29 (2012) 1787-1796.
[65] E.J. German, M.A. Hurst, D. Wood, Reliability of drop size from multi-dose eye drop bottles: is it cause for concern?, Eye, 13 (1999) 93-100.
[66] J.W. Sieg, J.W. Triplett, Precorneal retention of topically instilled micronized particles, J. Pharm. Sci., 69 (1980) 863-864.
[67] H. Zhu, A. Chauhan, A mathematical model for ocular tear and solute balance, Curr. Eye Res., 30 (2005) 841-854.
[68] K.E. Fischer, B.J. Alemán, S.L. Tao, R.H. Daniels, E.M. Li, M.D. Bünger, G. Nagaraj, P. Singh, A. Zettl, T.A. Desai, Biomimetic nanowire coatings for next generation adhesive drug delivery systems, Nano Lett., 9 (2009) 716-

720.
[69] J. Ceulemans, A. Vermeire, E. Adriaens, J.P. Remon, A. Ludwig, Evaluation of a mucoadhesive tablet for ocular use, J. Control. Release, 77 (2001) 333-344.
[70] A. Ludwig, The use of mucoadhesive polymers in ocular drug delivery, Adv. Drug. Deliver. Rev., 57 (2005) 1595-1639.
[71] K.E. Fischer, G. Nagaraj, R. Hugh Daniels, E. Li, V.E. Cowles, J.L. Miller, M.D. Bunger, T.A. Desai, Hierarchical nanoengineered surfaces for enhanced cytoadhesion and drug delivery, Biomaterials, 32 (2011) 3499-3506.
[72] K.E. Fischer, A. Jayagopal, G. Nagaraj, R.H. Daniels, E.M. Li, M.T. Silvestrini, T.A. Desai, Nanoengineered surfaces enhance drug loading and adhesion, Nano Lett., 11 (2011) 1076-1081.
[73] V. Uskokovic, K. Lee, P.P. Lee, K.E. Fischer, T.A. Desai, Shape Effect in the design of nanowire coated microparticles as transepithelial drug delivery devices, ACS nano, 6 (2012) 7832-7841.
[74] K. H Singh, U. A Shinde, Development and evaluation of novel polymeric nanoparticles of brimonidine tartrate, Curr. Drug Deliv., 7 (2010) 244-251.
[75] K.S. Lim, S.S. Wickremasinghe, M.F. Cordeiro, C. Bunce, P.T. Khaw, Accuracy of intraocular pressure measurements in New Zealand white rabbits, Invest. Ophthalmol. Vis. Sci., 46 (2005) 2419-2423.
[76] P. Vareilles, P. Conquet, J.C. Le Douarec, A method for the routine intraocular pressure (IOP) measurement in the rabbit: range of IOP variations in this species, Exp. Eye Res., 24 (1977) 369-375.
[77] H. Gupta, D. Bhandari, A. Sharma, Recent trends in oral drug delivery: A review, Recent. Pat. Drug Deliv. Formul., 3 (2009) 162-173.
[78] S.V. Sastry, J.R. Nyshadham, J.A. Fix, Recent technological advances in oral drug delivery-a review, Pharm. Sci. Technol. Today, 3 (2000) 138-145.
[79] P. Colombo, F. Sonvico, G. Colombo, R. Bettini, Novel platforms for oral drug delivery, Pharm. Res., 26 (2009) 601-611.
[80] M. Efentakis, C. Peponaki, Formulation study and evaluation of matrix and three-layer tablet sustained drug delivery systems based on carbopols with isosorbite mononitrate, AAPS PharmSciTech, 9 (2008) 917-923.
[81] M. Efentakis, H. Naseef, M. Vlachou, Two-and three-layer tablet drug delivery systems for oral sustained release of soluble and poorly soluble drugs, Drug Dev. Ind. Pharm., 36 (2010) 903-916.
[82] M. Gohel, S. Bariya, Fabrication of triple-layer matrix tablets of venlafaxine hydrochloride using xanthan gum, AAPS PharmSciTech, 10 (2009) 624-630.
[83] Y. Tang, S. Venkatraman, F. Boey, L. Wang, Sustained release of hydrophobic and hydrophilic drugs from a floating dosage form, Int. J. Pharm., 336 (2007) 159-165.
[84] J. Goole, F. Vanderbist, K. Amighi, Development and evaluation of new multiple-unit levodopa sustained-release floating dosage forms, Int. J. Pharm., 334 (2007) 35-41.

[85] R. Lucinda-Silva, R. Evangelista, Microspheres of alginate-chitosan containing isoniazid, J. Microencapsul., 20 (2003) 145-152.
[86] R. Rastogi, Y. Sultana, M. Aqil, A. Ali, S. Kumar, K. Chuttani, A. Mishra, Alginate microspheres of isoniazid for oral sustained drug delivery, Int. J. Pharm., 334 (2007) 71-77.
[87] M. Khan, Recent trends and progress in sustained or controlled oral delivery of some water soluble drugs: morphine salts, diltiazem and captopril, Drug Dev. Ind. Pharm., 21 (1995) 1037-1070.
[88] D. Fleisher, C. Li, Y. Zhou, L. Pao, A. Karim, Drug, meal and formulation interactions influencing drug absorption after oral administration: clinical implications, Clin. Pharmacokinet., 36 (1999) 233-254.
[89] R. Conley, S.K. Gupta, G. Sathyan, Clinical spectrum of the osmotic-controlled release oral delivery system (OROS®), an advanced oral delivery form, Curr. Med. Res. Opin., 22 (2006) 1879-1892.
[90] Q. Liu, R. Fassihi, Zero-order delivery of a highly soluble, low dose drug alfuzosin hydrochloride via gastro-retentive system, Int. J. Pharm., 348 (2008) 27-34.
[91] D. Yu, C. Branford-White, Z. Ma, L. Zhu, X. Li, X. Yang, Novel drug delivery devices for providing linear release profiles fabricated by 3DP, Int. J. Pharm., 370 (2009) 160-166.
[92] D. Yu, X. Yang, W. Huang, J. Liu, Y. Wang, H. Xu, Tablets with material gradients fabricated by three-dimensional printing, J. Pharm. Sci., 96 (2007) 2446-2456.
[93] V. Malaterre, J. Ogorka, N. Loggia, R. Gurny, Oral osmotically driven systems: 30 years of development and clinical use, Eur. J. Pharm. Biopharm., 73 (2009) 311-323.
[94] P. Laidler, S.C. Maslin, R.W. Gilhome, What's new in osmosin and intestinal perforation?, Pathol. Res. Pract., 180 (1985) 74-76.
[95] R. Verma, D. Krishna, S. Garg, Formulation aspects in the development of osmotically controlled oral drug delivery systems, J. Control. Release., 79 (2002) 7-27.
[96] D. Swanson, B. Barclay, P. Wong, F. Theeuwes, Nifedipine gastrointestinal therapeutic system, Am. J. Med., 83 (1987) 3-9.
[97] I. Sugimoto, A. Kuchiki, H. Nakagawa, K. Tohgo, S. Kondo, I. Iwane, K. Takahashi, Dissolution and absorption of nipedipine from nifedipine-polyvinylpyrrolidone coprecipitate, Drug Deve. Ind. Pharm., 6 (1980) 137-160.
[98] B. Inanc, Y. Arslan, S. Seker, A. Elcin, Y. Elcin, Periodontal ligament cellular structures engineered with electrospun poly (DL lactide co glycolide) nanofibrous membrane scaffolds, J. Biomed. Mater. Res. A, 90 (2009) 186-195.
[99] T.H. Kim, T.G. Park, Critical effect of freezing/freeze-drying on sustained release of FITC-dextran encapsulated within PLGA microspheres, Int. J. Pharm., 271 (2004) 207-214.
[100] D. Li, M. Frey, Y. Joo, Characterization of nanofibrous membranes with capillary flow porometry, J. Memb. Sci., 286 (2006) 104-114.
[101] A.A. Deshpande, C.T. Rhodes, N.H. Shah, A.W. Malick, Controlled-

release drug delivery systems for prolonged gastric residence: an overview, Drug Dev. Ind. Pharm., 22 (1996) 531-539.
[102] P.W. Gibson, H.L. Schreuder Gibson, D. Rivin, Electrospun fiber mats: transport properties, AIChE J., 45 (1999) 190-195.
[103] C. Foley, N. Nishimura, K. Neeves, C. Schaffer, W. Olbricht, Flexible microfluidic devices supported by biodegradable insertion scaffolds for convection-enhanced neural drug delivery, Biomed. Microdevices, 11 (2009) 915-924.
[104] S. Davis, N. Washington, G. Parr, A. Short, V. John, P. Lloyd, S. Walker, Relationship between the rate of appearance of oxprenolol in the systemic circulation and the location of an oxprenolol Oros 16/260 drug delivery system within the gastrointestinal tract as determined by scintigraphy, Br. J. Clin. Pharmacol., 26 (1988) 435-443.
[105] K.M. Boje, M. Sak, H.L. Fung, Complexation of nifedipine with substituted phenolic ligands, Pharm. Res., 5 (1988) 655-659.
[106] L. Liu, J. Ku, G. Khang, B. Lee, J. Rhee, H. Lee, Nifedipine controlled delivery by sandwiched osmotic tablet system, J. Control. Release., 68 (2000) 145-156.
[107] V.P. Shah, Y. Tsong, P. Sathe, J.-P. Liu, In vitro dissolution profile comparison—statistics and analysis of the similarity factor, f_2, Pharm. Res., 15 (1998) 889-896.
[108] H. Lieberman, L. Lachman, J. Schwartz, Pharmaceutical dosage forms-tablets, second ed., Marcel Dekker, New York, 1989.
[109] Z.M. Huang, Y.Z. Zhang, M. Kotaki, S. Ramakrishna, A review on polymer nanofibers by electrospinning and their applications in nanocomposites, Compos. Sci. Technol., 63 (2003) 2223-2253.
[110] H. Gao, Y. Gu, Q. Ping, The implantable 5-fluorouracil-loaded poly (L-lactic acid) fibers prepared by wet-spinning from suspension, J. Control. Release., 118 (2007) 325-332.
[111] A. Jemal, R. Siegel, E. Ward, Y. Hao, J. Xu, M. Thun, Cancer statistics, 2009, CA Cancer J. Clin., 59 (2009) 225-249.
[112] J. Muller, H. Erasmi, M. Stelzner, U. Zieren, H. Pichlmaier, Surgical therapy of oesophageal carcinoma, Br. J. Surg., 77 (1990) 845-857.
[113] P. Enzinger, R. Mayer, Esophageal cancer, N. Engl. J. Med., 349 (2003) 2241-2252.
[114] M. Sundelof, D. Ringby, D. Stockeld, L. Granstrom, E. Jonas, J. Freedman, Palliative treatment of malignant dysphagia with self-expanding metal stents: a 12-year experience, Scand. J. Gastroenterol., 42 (2007) 11-16.
[115] D. Xinopoulos, S. Bassioukas, D. Dimitroulopoulos, D. Korkolis, G. Steinhauer, D. Kipraios, E. Paraskevas, Self-expanding plastic stents for inoperable malignant strictures of the cervical esophagus, Dis. Esophagus, 22 (2009) 354-360.
[116] J. Ellul, A. Watkinson, R. Khan, A. Adam, R. Mason, Self-expanding metal stents for the palliation of dysphagia due to inoperable oesophageal carcinoma, Br. J. Surg., 82 (1995) 1678-1681.
[117] R.C. Eberhart, S.H. Su, K.T. Nguyen, M. Zilberman, L. Tang, K.D.

Nelson, P. Frenkel, Review: Bioresorbable polymeric stents: current status and future promise, J. Biomater. Sci. Polym. Ed., 14 (2003) 299-312.
[118] R. Tung, S. Kaul, G.A. Diamond, P.K. Shah, Narrative review: drug-eluting stents for the management of restenosis: a critical appraisal of the evidence, Ann. Intern. Med., 144 (2006) 913-919.
[119] G. Nakazawa, A.V. Finn, F.D. Kolodgie, R. Virmani, A review of current devices and a look at new technology: drug-eluting stents, Expert. Rev. Med. Devices, 6 (2009) 33-42.
[120] S. Jeon, S. Eun, C. Shim, C. Ryu, J. Kim, J. Cho, J. Lee, M. Lee, S. Jin, Effect of drug-eluting metal stents in benign esophageal stricture: an in vivo animal study, Endoscopy, 41 (2009) 449-456.
[121] Q. Guo, S. Guo, Z. Wang, A type of esophageal stent coating composed of one 5-fluorouracil-containing EVA layer and one drug-free protective layer: in vitro release, permeation and mechanical properties, J. Control. Release., 118 (2007) 318-324.
[122] S.R. Guo, Z.M. Wang, Y.Q. Zhang, L. Lei, J.M. Shi, K.M. Chen, Z. Yu, In vivo evaluation of 5-fluorouracil-containing self-expandable nitinol stent in rabbits: Efficiency in long-term local drug delivery, J. Pharm. Sci., 99 (2010) 3009-3018.
[123] K. Kuraishi, H. Iwata, S. Nakano, S. Kubota, H. Tonami, M. Toda, N. Toma, S. Matsushima, K. Hamada, S. Ogawa, Development of nanofiber covered stents using electrospinning: In vitro and acute phase in vivo experiments, J. Biomed. Mater. Res. Part B Appl. Biomater., 88 (2009) 230-239.
[124] J.E. Puskas, L.G. Munoz-Robledo, R.A. Hoerr, J. Foley, S.P. Schmidt, M. Evancho-Chapman, J. Dong, C. Frethem, G. Haugstad, Drug-eluting stent coatings, Wiley Interdiscip. Rev. Nanomed. Nanobiotechnol., 1 (2009) 451-462.
[125] D. Longley, D. Harkin, P. Johnston, 5-fluorouracil: mechanisms of action and clinical strategies, Nat. Rev. Cancer, 3 (2003) 330-338.
[126] X.S. Wu, Synthesis and properties of biodegradable lactic/glycolic acid polymers, Encyclopedic handbook of biomaterials and bioengineering, (1995) 1015-1054.
[127] R. Vasita, K. Shanmugam, D.S. Katti, Degradation behavior of electrospun microfibers of blends of poly (lactide-co-glycolide) and Pluronic® F-108, Polym. Degrad. Stab., 95 (2010) 1605-1613.
[128] S. Cho, H. Lee, Preparation of 5-fluorouracil-loaded poly (l-lactide-co-glycolide) wafer and evaluation of in vitro release behavior, Macromol. Res., 11 (2003) 183-188.
[129] C. Shim, Y. Cho, J. Moon, J. Kim, J. Cho, Y. Kim, J. Lee, M. Lee, Fixation of a modified covered esophageal stent: its clinical usefulness for preventing stent migration, Endoscopy, 33 (2001) 843-848.
[130] C. Berkland, D.W. Pack, K. Kim, Controlling surface nano-structure using flow-limited field-injection electrostatic spraying (FFESS) of poly (d,l-lactide-co-glycolide), Biomaterials, 25 (2004) 5649-5658.
[131] K. Dillen, J. Vandervoort, G. Van den Mooter, L. Verheyden, A. Ludwig, Factorial design, physicochemical characterisation and activity of

ciprofloxacin-PLGA nanoparticles, Int. J. Pharm., 275 (2004) 171-187.
[132] C.E. Wilkes, J.W. Summers, C.A. Daniels, M.T. Berard, PVC handbook, Hanser Gardner Pubns, 2005.
[133] N. Washington, C. Washington, C. Wilson, Physiological pharmaceutics: barriers to drug absorption, CRC Press, 2001.
[134] A. Gennaro, A. Osol, Remington's Pharmaceutical sciences 15th ed. Easton, in, Mack Publishing Company, 1975.
[135] E.M.L. Verschuur, A. Repici, E.J. Kuipers, E.W. Steyerberg, P.D. Siersema, New design esophageal stents for the palliation of dysphagia from esophageal or gastric cardia cancer: a randomized trial, Am. J. Gastroenterol., 103 (2008) 304-312.
[136] J. Fang, H.T. Niu, T. Lin, X.G. Wang, Applications of electrospun nanofibers, Chinese Sci. Bull., 53 (2008) 2265-2286.
[137] R. Jayakumar, M. Prabaharan, S. Nair, H. Tamura, Novel chitin and chitosan nanofibers in biomedical applications, Biotechnol. Adv., 28 (2010) 142-150.
[138] K. Zhu, J. Zhang, C. Wang, H. Yasuda, A. Ichimaru, K. Yamamoto, Preparation and in vitro release behaviour of 5-fluorouracil-loaded microspheres based on poly (L-lactide) and its carbonate copolymers, J. Microencapsul., 20 (2003) 731-743.
[139] Z. Xie, G. Buschle Diller, Electrospun poly (D, L lactide) fibers for drug delivery: The influence of cosolvent and the mechanism of drug release, J. Appl. Polym. Sci., 115 (2010) 1-8.

Abstract in Korean

국문 초록

이 논문은 나노섬유구조의 생체고분자를 이용하여 질병 치료 효과를 극대화시킬 수 있는 차세대 약물 전달장치에 관한 것으로 나노섬유구조가 가지고 있는 넓은 비표면적과 마이크로 공극률의 특징들을 효과적으로 활용하여 다양한 전달경로와 질병에 맞는 약물전달 장치를 개발 하는 것이다.

첫째로, 점안약이 갖는 낮은 생체이용도를 해결하고자, 친점액성 물질이 포함된 표면적이 극대화된 마이크로입자를 제작하고, 녹내장 치료제인 브로모니딘을 탑재시킨 후, 약물정 형태로 눈에 전달하여 생체이용도를 높일 수 있는 약물운반체를 제작하였다. 표면이 거친 나노형상마이크로 입자는 나노형상을 잘 유지하고 있으며 비표면적을 측정하였을 때 기존의 에멀전 방식을 이용하여 제작된 구형 마이크로입자보다 13배 이상의 넓은 표면적을 지니고 있음을 확인하였다. 이를 통해, 눈에서 빠르게 녹아나는 약물정 형태로 전달하였을 때, 구형 마이크로입자에 비해서 전안부에서의 거주시간이 10배이상 증가됨을 확인하였고, 모델 약물인 브리모니딘이 탑재되었을 때, 안압 하강 효과가 기존의 제형인 알파간피 (Alphagan-P)와 비교하여 2배 이상 증가하였음을 확인하였다. 이 연구를 통하여, 친점액성 물질이 포함되고 비표면적이 증가된 나노형상 마이크로입자는 전안부에서의 거주시간이 월등히 증가되고, 그 기간 동안 약물이 서방 방출되어 약물의 생체이용도를 증가시킬 수 있는 유망한 제형임을 확인 하였다.

둘째로, 경구 투여 약물인 니페디핀의 선형전달을 위하여 나노섬유구조 시트기반의 약물전달 제형을 개발하였다. 이를 위하여 생체적합성 고분자인 poly (lactic-co-glycolic acid)(PLGA)를 전기방사 방법을 이용하여 마이크로 공극률을 가지는 나노섬유시트를 제작하였다. 녹내장 치료제인 니페디핀을 모델 약물로 선정하고 용해도 증강제인 polyvinylpyrrolidone와 섞어 약물정으로 제작 후, 위에 제작된 나노섬유시트를 덮어 캐핑하였다. 다양한 약물 방출 형상을 얻기 위하여 다양한 두께의 나노섬유시트를 이용하여 약물정을 캐핑하였고, 약물전달 실험 결과 나노섬유시트의 두께가 두꺼워질수록 약이 보다 서서히 방출되는 결과를 확인하였다. 각각 다른 두께의 나노섬유로 캐핑된 2개의 서로 다른 약물정을 결합하여 24시간동안 선형전달이 가능한 제형을 제작하였다. 이 연구를 통하여, 약물정을 캐핑하는 나노섬유 두께에 따라 약물의 전달형상이 달라짐을 확인하였고, 다른 두께의 나노섬유로 캐핑된 약물정의 결합을 통하여 약물의 선형전달이 가능함을 확인하였다.

마지막으로, 식도스텐트 시술 후, 암세포의 스텐트 주변부로의 빠른 성장으로 인해 스텐트가 막히는 단점을 해결하고자, 항암제 서방 전달 기능성이 부여된 식도스텐트를 개발하였다. PLGA를 약물확산벽 물질로 사용하였고, 대표적인 항암제인 5-FU를 모델 약으로 사용하여 전기방사 방법으로 식도스텐트를 코팅하였다. 그 결과 수용성 약물인 5-FU는 6일만에 모두 용출되었다. 약물의 다량방출을 차단하고 서방전달 기간을 증가시키고자, 약이 들어있지 않은 나노섬유를 약물이 탑재된 코팅면 앞뒤로 추가 코팅하여 약물의 서방 방출 기간을 21일까지 연장시켰다. 이 연구를 통하여 식도스텐트에 약물부가기능성을 부여하여 약물을 서방전달 시킴으로써 스텐트 이식

후에도 장기간 동안 암세포의 증식을 억제하여 스텐트의 다시 막힘 현상을 오랜 기간 막을 수 있는 스텐트를 제작할 수 있었다.

핵심어: 생체고분자, 약물전달시스템, 전기방사, 마이크로 공극, 나노섬유, 비표면적, 코팅

학번: 2009-23194

Acknowledgement

감사의 글

본 박사학위 논문을 마치며 학위 과정 동안 아낌없는 성원과 많은 도움을 주신 모든 분들께 감사의 말씀을 올리고 싶습니다.

가장 먼저, 학부과정 전공도 달랐던 저를 바이오 엔지니어의 길로 인도해주시고 아낌없이 가르쳐 주신, 존경하는 지도 교수님 최영빈 교수님께 고개 숙여 감사 드립니다. 24살에 대학원 입학해 너무나 부족하고 어수룩한 저를 많이 믿어 주셨고, 실험 내외적으로 많은 것을 가르쳐 주셨습니다. 교수님의 가르침 하나하나가 모여서 지금의 제가 되었고, 박사학위라는 소중한 결실을 맺을 수 있었습니다. 귀한 시간을 내주시어 흔쾌히 학위 심사를 맡아주시고 아낌없는 조언을 해 주신 김희찬 교수님, 박기호 교수님, 이정찬 교수님, 박지호 교수님께도 깊은 감사를 드립니다. 뵐 때 마다 항상 좋은 말씀 해주시는 윤형진 교수님, 최진욱 교수님, 김성완 교수님과 이화여자대학 최진호 교수님께도 깊은 감사를 드립니다. 앞으로도 저는 교수님들께서 해주셨던 많은 말씀들을 마음 깊이 새기고, 떠올리며 더 좋은 연구자가 될 수 있도록 성심껏 노력하겠습니다.

지난 5년동안 동거 동락했던 서울대학교 생체재료공정 연구실 동료들에게도 모두 감사의 인사를 전합니다. 항상 형으로써 연구실에서 정신적 지주가 되어준 곧 결혼할 것 같은 민이형, 멀리 떨어져있다가 얼마 전 연구실로 들어온 벌써 애 아빠가 된 명훈이 (그리고 수진이), 요즘 연구 욕심이 부쩍 많아진 승호, 항상 긍정적으로 연구실 사람들 누구나 좋아하는 범강이형 그리고 벌써부터 일이 많아졌지만 잘 해내고

있는 세나누나 모두 정말 고맙습니다. 항상 멀리서 고생하는 분당방장 병휘형, 형의 농담을 잘 받아 치는 원석이, 그리고 역시나 다른 분야에서 넘어와서 고생하는 막내 영빈이까지 정말 고맙습니다. 지금은 졸업해서 보기 힘들지만, 각자의 위치에서 최선을 다하고 있을 졸업생들도 생각이 납니다. 곧 다시 미국으로 넘어 간다던 Katie, 회사생활 열심히 하고 있을 지은이와 성윤이 그리고 미국에서 공부 이어서 하고 있는 수빈이에게도 이 글을 통해 함께 있을 때에는 말을 못했지만 그때 정말 고마웠다고 말하고 싶습니다. 부족한 “사수”밑에서 인턴을 했던, 지은이, 은빛이, 병무, 경선이, 민재, 유정이, 영은이, 민아, 혜림이, 그리고 가령이, 짧은 기간이었지만 다들 너무 고생했고, 잘해줘서 고마웠다.

마음으로는 더 자주 연락 드리고 싶지만, 바쁘다는 핑계로 연락 자주 못 드린 해룡고등학교 김성현 선생님, 은희균 선생님, 이승룡 선생님, 박혁수 선생님 앞으로는 더 자주 연락 드리겠습니다. 캐나다에서 처음 만나서 아직까지도 정말 많은 도움을 주신 쉐리문 집사님, 박사학위 과정 동안 용기를 많이 주시고 조언을 아끼지 않으셨던 재수형님을 포함한 정석이형, 근형이형, 형철이형, 그리고 완전히 다른 분야지만 사업에 성공하셔서 모범을 보여주신 종섭형님께도 감사의 인사를 전합니다. 해룡고-한양대 모임 꾸준히 유지 시켜주시는 희석이형, 판홍이형 포함한 많은 선후배님들도 감사 드리며, 은호형, 형근이형도 보고 싶습니다.

힘들다고, 즐겁다고, 주말이라고, 연말이라고, 이유 불문하고 나와서 나와 술잔을 기울여준 대진이, 연상이, 형대, 원균이를 비롯한 해벗 친구들에게도 정말 고맙다는 말을 전하고 싶다. 특히 고등학교 때부터 지금까지 우정 변치 않고 한결같이 곁에서 힘이되 주는 대진이에게 고맙고, 부산에서 열심히 사업하는 상범아, 너는 나에게 자랑스러운 친구다. 또 대학원 들어가고 나서 알게 됐지만 최근에 가장 많이 만난

현성이는 짧은 기간이지만 정말 많은 이야기를 한 친구라서 마치 오래된 친구 같다. 이제 이사를 가지만 앞으로도 자주 보면 좋겠다. 역시나 오랜 시간은 아니지만 친해진 석진철 사장님, 사업 번창하시길 바라고, 동생들에게 맛있는 것 많이 사주는 지영이형도 정말 고맙습니다. 대학교 2학년 때부터 같이 전공을 바꿔서 내내 붙어 다녔던 이젠 애 아빠가 된 상균이, 중학교 때부터 대학교까지 같은 학교를 다닌 유일한 친구이자 형인 선휘형, 우리 조만간 봅시다. 말 많은 영화, 세정이, 해외에 있는 배영, 그리고 정수빈, 연락하자. 또, 대전에서 열심히 연구중인 성훈이, 대정이, 현준이, 서울에서 열심히 하고 있는 윤표, 달콤이 빨리 만나자. 할 이야기가 많을 것 같다.

미국에 있어서 자주보지는 못하지만, 곧 결혼하는 나의 멘토 보나 누나, 얼마 전에 결혼한 소영누나 너무너무 고맙고, 더 행복하길 바랄게. 바쁜 거 뻔히 알지만 항상 잘 챙겨주시는 박대환 박사님도 매우 감사 드립니다. 요즘은 서로 바빠서 명절 때만 만나게 되는 진석이형, 혁이형, 수경누나, 동수형을 포함한 친척들도 앞으로는 더욱 자주 보면 좋겠습니다.

대학원 생활 내내 도움을 주신 김행순 선생님, 김희자 선생님, 김화룡 선생님, 최은경 선생님, 최양선 선생님, 정희원 선생님, 김사훈 선생님, 오은석 선생님, 김영국 선생님, 김미정 선생님, 이재용 선생님, 박선후 선생님, 신라현 선생님, 심재희 선생님, 조은수 선생님께 이 글을 통해 감사의 인사를 전합니다. 또, 대학원 들어와서 친해진 상경이형, 민혜, 원규, 성준이형, 수환이형, 수영이, 홍지, 보림이 (그리고 설희), 명선이, 치원이, 가람이, 병욱이, 지흠이, 돈 많이 버시는 이충희 박사님 그리고 이번에 같이 졸업하는 승우형, 형선이 모두 감사합니다.

마지막으로 어떠한 글로도 어떠한 표현으로도 지금껏 받은 사랑을 표현할 수 조차 없는, 저를 키워주신 사랑하는 엄마, 무뚝뚝한 척하지만

누구보다 걱정 많이 해주고 도움을 많이 주는 존경하는 아빠에게도 무한한 감사를 올립니다. 어릴 때 참 많이 싸웠지만, 지금은 서로를 너무 잘 알기에 10년째 최고의 동거인이 되어준 누나에게도 무한한 감사를 드리며, 바쁘다는 핑계로 자주 만나지 못하는 우리 형도 이 글을 통해서 더 자주 만나자는 약속을 해봅니다.

제가 사랑하는 그리고 저를 사랑해주시는 많은 분들께도 표현하진 않지만 마음속으로 항상 감사하고 모든 일이 잘 풀리길, 그리고 항상 건강하시길 기도하고 있다는 점을 말씀 드리고 싶습니다.

시간이 지나면 지날수록 한걸음씩 더 앞으로 나아가는 자랑스러운 박천권이 되도록 오늘도 노력하겠습니다. 감사합니다.

2014년 7월 비가 많이 오는 날에……

박 천 권

APPENDIX

EDUCATION

☐ Ph. D. Sep. 2009–Aug. 2014

Interdisciplinary Program in Bioengineering,
College of Engineering, Seoul National University
Supervisor: Professor Young Bin Choy
Dissertation Topic: A NANOFIBER–STRUCTURED BIOPOLYMER FOR ADVANCED DRUG DELIVERY SYSTEMS

☐ B. S. Mar. 2005–Sep. 2009

Media Communications Engineering
College of Engineering, Hanyang University

PUBLICATIONS

1. Choi, S. Y., Hur, W. J., Kim, B. K., Shasteen, C., Kim, M. H., Choi, L., M., Lee, S. H, Park C. G, Park M., Min, H. S, Kim, S.W, Choi, T.H.*, Choy, Y. B.* , Bioabsorbable bone fixation plates for X–ray imaging diagnosis by a radiopaque layer of barium sulfate and poly (lactic–co–glycolic acid), Journal of Biomedical Materials Research: Part B – Applied Biomaterials, in press, 2014
2. Park, C. G., Kim, M. J., Park, M., Choi, S. Y., Lee, S. H., Lee, J. E., Shin, G. –S., Park, K. H., Choy, Y. B.*, Nanostructured Mucoadhesive Microparticles for Enhanced Preocular Retention, Acta Biomaterialia, 10(1), 77–86, 2014
3. Lee, J. E., Park, S., Park, M., Kim, M. H., Park, C. G., Lee, S. H., Choi, S. Y., Kim, B. H., Park, H. J., Park, J. –H., Heo, C. Y.*, Choy, Y. B.*, Surgical Suture assembled with Polymeric Drug–Delivery Sheet for Sustained, Local Pain–relief, Acta Biomaterialia, 9(9), 8318–8327, 2013
4. Park, M., Lee, J. E., Park, C. G., Lee, S. H., Seok, H. –K., Choy, Y. B.*, Polycaprolactone Coating with Varying Thicknesses for Controlled Corrosion of Magnesium, Journal of Coatings

Technology and Research, 10(5), 695-706, 2013

5. Shasteen, C., Kwon, S. M., Park, K. Y., Jung, S. Y., Lee, S. H., Park, C. G., Kim, M. H., Kim, S., Son, W.- C., Choi, T. H.*, Choy, Y. -B.*, Biodegradable Polymer Fixation Plates Enabled with X-ray Visibility, Journal of Biomedical Materials Research: Part B - Applied Biomaterials, 101(2), 320-329, 2013
6. Lee, J. E.†, Park, C. G.†, An, B. M., Kim, M. H., Park, M., Lee, S. H., Choy, Y. B.*, Linear Delivery of Verapamil via Nanofibrous Sheet-Based System, Pharmaceutical Research, 29(7), 1787-1796, 2012.
   †These authors contributed equally to this work.
7. Park, M., Park, C. G., Lee, S. H., Lee, J. E., Cho, E., Prausnitz, M. R., Choy, Y. B.*, Polymeric Tube-shaped Devices with Controlled Geometry for Programmed Drug Delivery, Macromolecular Research, 20(9), 960-967, 2012.
8. Lee, S. H., Park, M., Park, C. G., Lee, J. E., Prausnitz, M. R., Choy, Y. B.*, Microchip for Sustained Drug Delivery by Diffusion Through Microchannels, AAPS PharmSciTech, 13(1), 211-217, 2012.
9. Park, C. G., Kim, M. H., Park, M., Lee, J. E., Lee, S. H., Park, J. -H., Yoon, K.-H., Choy, Y. B.*, Polymeric Nanofiber Coated Esophageal Stent for Sustained Delivery of an Anticancer Drug, Macromolecular Research, 19(11), 1210-1216, 2011
10. Park, C. G., Kim, E., Park, M., Park, J.-H., Choy, Y. B.*, A nanofibrous sheet based system for linear delivery of nifedipine, Journal of Controlled Release, 149(3), 250-257, 2011

PATENTS

- International Patents (PCT)

1. Mucoadhesive nano-structured microparticles
   Young Bin Choy, Chun Gwon Park
   2013. 05. 14 (PCT/KR2013/004252)
2. Code-mark and manufacturing method, cognition system, cognition method thereof
   Young Bin Choy, Chun Gwon Park
   2013. 05. 28 (PCT/KR2013/004649)

- Domestic Patents (대한민국)

□ 등록 특허

1. 나노섬유시트 기재의 경구용 약물의 제어 전달을 위한 시스템
   최영빈, **박천권**, 이지은
   2013. 07. 03 (등록번호 10-1284368)
2. 약물의 제어 전달이 가능한 식도 스텐트 및 이의 제조방법
   최영빈, **박천권**
   2013. 10. 28 (등록번호 10-1324772)
3. 코드마크 및 이의 제조방법, 인식시스템, 인식 방법
   최영빈, **박천권**
   2014. 04. 07 (등록번호 10-1384612)

□ 출원 특허

1. 점막부착성 나노형상 마이크로입자
   최영빈, **박천권**
   2013. 05. 15 (출원번호 10-2013-0053851)

HONORS and AWARDS

1. Best Paper Award
   3rd Conference on Bioengineering, Seoul National University, Seoul, Korea (2011)
   Paper entitled with "A Nanofibrous Sheet-based System for Linear Delivery of Nifedipine"
2. Best Paper Award/Grants
   Annual Conference, Biomedical Research Institute, Seoul National University Hospital, Seoul, Korea (2011)
   Paper entitled with "A Nanofibrous Sheet-based System for Linear Delivery of Nifedipine"
3. Best Paper Award/Grants
   Annual Conference, Biomedical Research Institute, Seoul National University Hospital, Seoul, Korea (2012)
   Paper entitled with "Linear Delivery of Verapamil via Nanofibrous Sheet-Based System"
4. Best Presentation Award/Grants
   Annual Conference, the Korean Ophthalmological Society (2014)
   Presentation entitled with "Nanostructured Mucoadhesive Microparticles for Enhanced Bioavailability of Brimonidine"

CONFERENCE PROCEEDINGS

□ INTERNATIONAL CONFERENCE

1. S. H. Lee, M. Park, B. H. Kim, C. G. Park, Y. B. Choy*, Implantable Pump Actuated by Static Magnetic Field for On-demand Drug Delivery, Abstract & Poster Presentation, 2014, CRS 41th Annual Meeting, Chicago, Illinois, USA
2. Park, C. G., Choi, S. Y., Park, M., Lee, S. H., Chung, Y. J., Jung, Y. E., Choy, Y. B.*, Nanostructured Mucoadhesive Microparticles for Enhanced Bioavailability of Brimonidine, Abstract & Poster Presentation, 2013, BMES Annual Meeting, Seattle, USA
3. Park, S. B., Lee, J. E., Park, M., Kim, M. H., Park, C. G., Lee, S. H., Heo, C. Y.*, Choy, Y. B.*, Drug Delivery Surgical Sutures for Pain Relief, Abstract & Poster Presentation, 2012, BMES Annual Meeting, Atlanta, USA
4. Park, M., Lee, J. E., Park, C. G., Lee, S. H, Seok, H. K., Choy, Y. B.*, Polycaprolactone Coating with Varying Thickness for Controlled Corrosion of Magnesium, Abstract & Poster Presentation, 2012, BMES Annual Meeting, Atlanta, USA
5. Lee, S. H., Park, M., Park, C. G., Lee, J. E., Choy, Y. B.*, Implantable Microchip for Long-term Sustained Drug Delivery, Abstract & Poster Presentation, 2012, BMES Annual Meeting, Atlanta, USA
6. Choi, S. Y., Shasteen, C., Kim, M. H., Park, C. G., Lee, J. E., Park, M., Lee, S. H., Choi, T. H., Choy, Y. B.*, Barium Sulfate Layer Coating on Bioabsorbable Bone Fixation Plate for X-ray imaging, Abstract & Poster Presentation, 2012, SPIE Nanosystems in Engineering + Medicine, Incheon, Republic of Korea
7. Park, M., Lee, J. E., Park, C. G., Cho, S. Y., Seok, H. K., Choy, Y. B.*, Titanium Implants enabled with Vancomycin Delivery for Inhibition of Infection, Abstract & Poster Presentation, 2012, SPIE Nanosystems in Engineering + Medicine, Incheon, Republic of Korea
8. Park, C. G., Park, M., Choi, S. Y., Lee, J. E., Lee, S. H., Shin, G. -S., Choy, Y. B.*, Nano-structured Microparticles for Prolonged Residence Time on Preocular Surface, Abstract & Poster

Presentation, 2012, SPIE Nanosystems in Engineering + Medicine, Incheon, Republic of Korea

9. Lee, J. E., Park, S., Park, C. G., Kim, M. H., Park, M., Lee, S. H., Heo, C. Y.*, Choy, Y. B.*, Drug-delivery Surgical Sutures for Post-Surgical Pain Relief, Abstract & Poster Presentation, 2012, SPIE Nanosystems in Engineering + Medicine, Incheon, Republic of Korea
10. Lee, S. H., Park, M., Park, C. G., Lee, J. E., Choy, Y. B.*, Drug Delivery Microchip for Potential Application to Chronic Pain Relief, Abstract & Oral Presentation, 2012, SPIE Nanosystems in Engineering + Medicine, Incheon, Korea
11. Lee, J. E., Park, S., Park, C. G., Kim, M. H., Park, M., Lee, S. H., Heo, C. Y.*, Choy, Y. B.*, Drug-delivery Surgical Sutures for Post-Surgical Pain Relief, Abstract & Poster Presentation, 2012, The 39th Annual Meeting & Eexposition of the Controlled Release Society, Quebec City, Canada
12. Park, C. G., Park, M., Lee, J. E., Lee, S. H., Shin, G. -S., Choy, Y. B.*, Nano-structured Microparticles for Prolonged Residence Time on Preocular Surface, Abstract & Podium Presentation, 2012, The 39th Annual Meeting & Exposition of the Controlled Release Society, Quebec City, Canada
13. Park, C. G., Choy, Y. B.*, A Nanofibrous Sheet-based System for Linear Delivery of Oral Drug, Abstract & Poster Presentation, 2012, SNU-KAIST-ETHZ-EPFL Joint Symposium on "Engineering for Biomedical Applications", Seoul, Korea
14. Shasteen, C., Kwon, S.M., Park, K.Y., Lee, S. H., Park, C. G., Kim, M.H., Choi, T. H.*, Choy, Y. B.*, X-ray Visible Coating for Bioabsorbable Polymer Fixation Plates, Abstract & Poster, 2011, The 3rd Asian Biomaterials Congress, Busan, Korea
15. Lee, J. E., Park, S., Park, C. G., Park, M., Lee, S. H., Choy, Y. B.*, Drug-delivery Surgical Sutures for Post-Surgical Pain Relief, Abstract & Oral Presentation, 2011, The 3rd Asian Biomaterials Congress, Busan, Korea
16. Park, C. G., Kim, M. H., Park, M., Lee, J. E., Lee, S. H., Park, J. -H., Choy, Y. B.*, Esophageal Stent Coated with Biocompatible Polymeric Nanofibers for Sustained Delivery of an Anticancer

Agent, Abstract & Poster, 2011, The 38th Annual Meeting & Exposition of the Controlled Release Society, Maryland, USA

17. Lee, J. E. †, **Park, C. G.** †, Park, M., Lee, S. H., Choy, Y. B.*, Controlled Delivery of Verapamil through a Nanofibrous Sheet Barrier, Abstract & Poster, 2011, The 38th Annual Meeting & Exposition of the Controlled Release Society, Maryland, USA

†These authors contributed equally to this work.

18. Lee, S. H., Park, M., **Park, C. G.**, Lee, J. E., Choy, Y. B.*, Microchip for Sustained Drug Delivery by Diffusion through Microchannels, Abstract & Podium, 2011, The 38th Annual Meeting & Exposition of the Controlled Release Society, Maryland, USA.
19. Park, M., **Park, C. G.**, Lee, S. H., Prausnitz, M. R.*, Choy, Y. B.*, Tube-shaped Devices with Controlled Geometry for Programmed Drug Delivery, Abstract & Poster, 2011, Annual Meeting & Exposition of Society for Biomaterials, Orlando, USA
20. **Park, C. G.,** Choy, Y. B.*, Controlled Delivery of Nifedipine via Nanofibrous Sheet Based System, Abstract & Podium, 2010, the 37th Annual Meeting & Exposition of the Controlled Release Society, Portland, USA

□ DOMESTIC CONFERENCE

1. 김병휘, 박민, 박효진, 이승호, 최성윤, **박천권**, 정웅, 한수민, 허찬영*, 최영빈*, 실리콘 임플란트 주변 피막구축 억제를 위한 Cysteinyl Leukotrienes 장기간 국소억제, 제 49 회 대한의용생체공학회 춘계학술대회, 2014
2. 이승호, 박민, 김병휘, 임병윤, **박천권**, 최영빈*, Implantable, Drug-delivery Pump Actuated by Static Magnetic Field for Treatment of Chronic Diseases, 제 49 회 대한의용생체공학회 춘계학술대회, 2014
3. **박천권**, 박민, 이승호, 최성윤, 이원석, 최영빈*, Nanostructured Mucoadhesive Microparticles for Enhanced Bioavailability of Brimonidine, 한국 고분자학회 춘계학술대회, 2014

4. 허범강, 최성윤, **박천권**, 김병휘, 박민, 허찬영*, 최영빈*, A Biodegradable Suture Enabled with Local Delivery of Diclofenac Sodium for Pain Relief, 한국 고분자학회 춘계학술대회, 2014
5. 허우준, 박민, 김명훈, 이승호, **박천권**, 최태현, 최영빈*, Bioabsorabable Bone Plates Enabled with Local, Sustained Delivery of Alendronate, 한국 고분자학회 춘계학술대회, 2014
6. 최성윤, 김병휘, 박민, **박천권**, 이승호, 허찬영*, 최영빈*, 반흔 형성 억제 기능성 봉합사의 개발 및 효용성 평가, 한국 고분자학회 춘계학술대회, 2014
7. 이원석, 박민, **박천권**, 이승호, 예성준*, 최영빈*, Surface Modification of Metallic Brachytherapy Seed for Prevention of Migration, 한국 고분자학회 춘계학술대회, 2014
8. **박천권**, 김영국, 김미정, 박민, 김명훈, 이승호, 최성윤, 이원석, 정유정, 정영은, 박기호*, 최영빈*, Nanostructured Mucoadhesive Microparticles for Enhanced Bioavailability of Brimonidine, 제 9 차 한국생체재료학회 춘계학술대회, 2014
9. 허범강, 김병휘, 최성윤, **박천권**, 박민, 이승호, 허찬영*, 최영빈* 통증완화 기능성 디클로페낙 서방전달 봉합사 개발, 제 9 차 한국생체재료학회 춘계학술대회, 2014
10. **박천권**, 김영국, 김미정, 박민, 김명훈, 이승호, 최성윤, 정유정, 정영은, 박기호*, 최영빈*, 브리모니딘 생체이용도 향상을 위한 나노구조 친점액성 마이크로입자, 대한안과학회 제 110 회 학술대회, 2013
11. 최성윤, 김병휘, 정웅, 박민, **박천권**, 허찬영*, 최영빈* 흉터 형성 억제를 위한 약물전달기능 생체흡수성 외과용 봉합사, 48 회 대한의용생체공학회 추계학술대회, 2013
12. 이승호, 박민, **박천권**, 김병휘, 최영빈* 디클로페넥 서방 전달을 위한 체내 이식형마이크로칩, 8 회 대한의용생체공학회 추계학술대회, 2013
13. **박천권**, 김영국, 김미정, 박민, 김명훈, 이승호, 최성윤, 정유정, 정영은, 박기호, 최영빈* 브로모니딘 생체이용도 향상을 위한 나노구조 친점액성 마이크로입자, 8 회 대한의용생체공학회 추계학술대회, 2013
14. 박수빈, 박민, 이지은, 박효진, 이승호, **박천권**, 허찬영*, 최영빈* 실리콘 임플란트 주변 피막구축 억제를 위한 TGF-β 장기간, 국소억제, 48 회 대한의용생체공학회 추계학술대회, 2013

15. 허범강, 최성윤, **박천권**, 김병휘, 박민, 허찬영*, 최영빈* 통증 완화를 위헌 다클로페낙의 국소전달이 가능한 생분해성 봉합사, 48 회 대한의용생체공학회 추계학술대회, 2013
16. 이승호, 박민, **박천권**, 김병휘, 이지은, 최성윤, 최영빈* "Implantable Microchip for Controlled Delivery of Diclofenac Sodium", 제 9 회 생체재료 아카데미, 2013
17. 최성윤, Chatherine Shasteen, 김명훈, 박민, 이승호, **박천권**, 최태현*, 최영빈* 흡수성 골고정용 플레이트의 X-선 진단을 위한 황산바륨 레이어 코팅, 47 회 대한의용생체공학회 춘계학술대회, 2013
18. **박천권**, 박민, 최성윤, 이승호, 이지은, 박민, 최영빈* 점안부 거주시간 향상을 위한 나노형상 친점액성 마이크로입자, 47 회 대한의용생체공학회 춘계학술대회, 2013
19. 박수빈, 박민, 이지은, 이승호, **박천권**, 허찬영*, 최영빈* 약물의 국소, 서방전달에 의한 실리콘 임플란트 주변 피막구축 억제, 47 회 대한의용생체공학회 춘계학술대회, 2013
20. 이승호, 박민, **박천권**, 최성윤, 최영빈*, 디클로페넥 제어 전달을 위한 체내 이식형 마이크로칩, 47 회 대한의용생체공학회 춘계학술대회, 2013
21. 이승호, 박민, **박천권**, 최성윤, 최영빈*, 디클로페넥 제어 전달을 위한 마이크로칩 디바이스, 한국고분자학회 2013 년도 춘계총회, 2013
22. 박민, 최성윤, **박천권**, 이승호, 최영빈*, Patterned polymeric coating on titanium bone plate for local, sustained release of vancomycin, 한국고분자학회 2013 년도 춘계총회, 2013
23. **박천권**, 박민, 최성윤, 이승호, 최영빈*, Nanostructured Muco adhesive Microparticles for Enhanced Preocular Retention, 한국고분자학회 2013 년도 춘계총회, 2013
24. 최성윤, 김병휘, 박민, **박천권**, 이승호, 허찬영*, 최영빈*, 흉터 형성 억제를 위한 약물전달기능 생체흡수성 외과용 봉합사, 제 8 회 생체재료 아카데미, 2013
25. **박천권**, 박민, 최성윤, 이승호, 이지은, 최영빈*, 점안부 거주시간 향상을 위한 나노형상 친점액성 마이크로입자", 제 8 회 생체재료 아카데미, 2013

26. Catherine Shasteen, 권석민, 박근영, 이승호, **박천권**, 김명훈, 최태현*, 최영빈*, X-ray 조영효과를 위한 흡수성 골고정용 플레이트, 45 회 대한의용생체공학회 춘계 학술대회, 2012
27. 이지은†, **박천권**†, 안병무, 김명훈, 박민, 이승호, 최영빈*, 나노섬유시트를 통한 베라파밀의 선형전달, 45 회 대한의용생체공학회 춘계 학술대회, 2012

†These authors contributed equally to this work

28. 최성윤, Catherine Shasteen, 김명훈, **박천권**, 이지은, 박민, 이승호, 최영빈*, Barium Sulfate Film Coating on Bioabsorbable Fixation Plate for X-ray Visibility, 44 회 대한의용생체공학회 추계 학술대회, 2011
29. 박민, 이승호, **박천권**, 최영빈*, Implantable Perforated Tubular Devices, 44 회 대한의용생체공학회 추계 학술대회, 2011
30. 이승호, 박민, **박천권**, 이지은, 최영빈*, Microchip Embedded with Diffusion-Channels and Drug-Wells for Sustained Drug Delivery, 43 회 대한의용생체공학회 춘계 학술대회, 2011
31. 박민, 이승호, **박천권**, 최영빈*, Programmable Tubular Devices for Treatment of Parkinson's disease, 43 회 대한의용생체공학회 춘계 학술대회, 2011
32. 이승호, 박민, **박천권**, 이지은, 최영빈*, Implantable Microchip for Continuous Drug Delivery, 42 회 대한의용생체공학회 추계 학술대회, 2010
33. 이지은, **박천권**, 김명훈, 박민, 조은빛, 이승호, 허찬영*, 최영빈*, Development of Ibuprofen-delivery Biodegradable Sutures for Pain Relief to the Surgical Wound, 42 회 대한의용생체공학회 추계 학술대회, 2010
34. 박민, **박천권**, 이승호, 최영빈*, Implantable Tubular Devices for Pulsatile Drug Delivery, 42 회 대한의용생체공학회 추계 학술대회, 2010 <우수 논문상 선정>
35. **박천권**, 김은지, 박민, 박정환, 최영빈*, Controlled Delivery of Nifedipine via Nanofibrous Sheet Based System, 42 회 대한의용생체공학회 추계 학술대회, 2010

36. **박천권**, 김명훈, 김은지, 조은빛, 박민, 박정환, 최영빈*, 5-FU 서방전달을 위한 의용고분자 나노섬유로 코팅된 식도 스텐트, 제 18 차 한국생체재료학회 학술대회, 2010
37. 박민, **박천권**, 김은지, 최영빈*, 프로그램형 약물전달을 위한 조립형 튜브 디바이스, 41 회 대한의용생체공학회 춘계 학술대회, 2010
38. **박천권**, 김은지, 박민, 박정환, 최영빈*, 항암제 서방전달을 위한 의용고분자 나노섬유로 코팅된 식도 스텐트, 41 회 대한의용생체공학회 춘계 학술 대회, 2010